2006

Computational fluid dynamic modeling of acoustic liquid manipulation

Nicholus Ryan Clinkinbeard
Iowa State University

i

Computational fluid dynamic modeling of acoustic liquid manipulation

by

Nicholus Ryan Clinkinbeard

A thesis submitted to the graduate faculty

in partial fulfillment of the requirements for the degree of

MASTER OF SCIENCE

Major: Mechanical Engineering

Program of Study Committee:
J. Adin Mann III, Major Professor
Shankar Subramaniam
Partha Sarkar

Iowa State University
Ames, Iowa
2006

UMI Number: 1439847

Copyright 2006 by

Clinkinbeard, Nicholus Ryan

All rights reserved.

UMI®

DEDICATION

This thesis work is dedicated to my wife, Kristin, who has stuck with me through all my endeavors, educational or otherwise. She has continually taught and reminded me that no matter how important this or any other work I will perform in my life may seem, nothing comes close to the love of God in our lives and the saving power of Christ Jesus.

TABLE OF CONTENTS

LIST OF FIGURES

LIST OF TABLES

LIST OF SYMBOLS AND NOMENCLATURE

Symbol or Nomenclature	Definition
a	Transducer Element x-Division
ADI	Alternating Direction Implicit
ALM	Acoustic Liquid Manipulation
b	Transducer Element y-Division
c	Speed of Sound Through Fluid (General Notation)
c_b	Speed of Sound in Bubble
c_f	Speed of Sound in Fluid
CFD	Computational Fluid Dynamics
C_T	Isothermal Specific Heat of Fluid
dB	Decibels
$\dfrac{D}{Dt}$	Material Derivative
dx	Infinitesimal x-Spacing
dy	Infinitesimal y-Spacing
dz	Infinitesimal z-Spacing
$\hat{e}$	Unit Normal Vector
$\mathbf{f}$	Body Force Vector
f	Arbitrary Function
$\bar{f}(\bar{r})$	Bubble Force
f_x	Body Force in x-Direction
f_z	Body Force in z-Direction
g	Arbitrary Function
$G(\bar{r}|\bar{r}_0)$	Green's Function
GUI	Graphical User Interface
H	Transducer Height
Hz	Hertz
I	Sound Intensity Magnitude
$\mathbf{I}$	Sound Intensity Vector
$\hat{i}$	x-Direction Vector Indicator
I_2	Second Order Sound Intensity
I_x	x-Direction Sound Intensity
I_z	z-Direction Sound Intensity
J	Imaginary Number
k	Acoustic Wave Number
$\mathbf{k}$	Acoustic Wave Number Vector
$\hat{k}$	z-Direction Vector Indicator
L	Fluid Tank Length
L	Transducer Length
$\dot{m}$	Mass Flow Rate of Fluid
MHz	Megahertz

Symbol or Nomenclature	Definition
NASA	
N_x	Number of Transducer Elements in x-Direction
N_y	Number of Transducer Elements in y-Direction
p	Fluid Pressure, Sound Pressure
p_0	Zeroth Order Fluid Pressure
p_1	First Order Fluid Pressure
p_2	Second Order Fluid Pressure
$p(\bar{r})$	Sound Pressure
$p_{ij}(\bar{r} - \bar{r}_{ij})$	Sound Pressure Calculated at Position $\bar{r}$ for Arrayed Transducer Element $\bar{r}_{ij}$
Pr	Prandtl Number
q	Heat Load
R	Bubble Radius
$\bar{r}$	Observation Position
$\bar{r}_{ij}$	Position of Array Element i,j
$\bar{r}_0$	Transducer Position
RF	Radio Frequency
SOR	Successive Overrelaxation
$S_{transducer}$	Surface of Sound Source (Transducer)
T	Temperature
$T(\bar{r})$	Temperature as a Function of Radial Distance, r
T_{WALL}	Temperature at Boundary Wall
u	x-Velocity
U	x-Directional Velocity Amplitude
$\mathbf{u}$	Fluid Velocity Vector
$\mathbf{u_1}$	First Order Fluid Velocity Vector
$\mathbf{u_2}$	Second Order Fluid Velocity Vector
$\overline{u}_{transducer}$	Velocity at Transducer Surface
w	z-Velocity
W	Fluid Tank Width
W	z-Directional Velocity Amplitude
$\mathbf{x}$	x-Displacement Vector
$\mathbf{z}$	z-Displacement Vector
α	Attenuation Coefficient
Δ	Denotes a Change in Quantity
δ	Diffusivity of Sound
δ_{ij}	Kronecker Delta
ε_1	Stream Function Error
ε_2	Vorticity Error
ε_3	Temperature Error
γ	Specific Heat Ratio

Symbol or Nomenclature	Definition
λ	Thermal Conductivity
μ	Dynamic Viscosity of Fluid
ν	Kinematic Viscosity of Fluid
ρ	Fluid Density
ρ_0	Zeroth Order Fluid Density
ρ_1	First Order Fluid Density
ρ_2	Second Order Fluid Density
ρ_b	Density of Bubble
ρ_f	Density of Fluid (for Bubble Force Calculation)
ϖ	Fluid Angular Velocity
ω	Sound Transducer Circular Frequency
ψ	Stream Function
ψ_2	Second-Order Stream Function
ζ	Vorticity
ζ_2	Second Order Vorticity
$\langle \ \rangle$	Time Average Operator
$\times$	Cross Product Operator
$\cdot$	Dot Product Operator
$\dfrac{\partial}{\partial t}$	Partial Time Derivative
$\dfrac{\partial}{\partial x}$	Partial Spatial Derivative with Respect to x
$\dfrac{\partial}{\partial z}$	Partial Spatial Derivative with Respect to z
∇	Del Operator $\dfrac{\partial}{\partial x}\hat{i} + \dfrac{\partial}{\partial z}\hat{k}$

.

ACKNOWLEDGEMENTS

I would like to take this opportunity to show my deep appreciation to a number of key individuals for their contribution to this work and my higher education. First of all, I would like to show my appreciation to my advisor, Dr. Adin Mann, for enduring my long-lived pursuit of obtaining a graduate degree in Mechanical Engineering. He has provided much-needed guidance and this thesis could not have been successful without his advice and direction. Also, I would like to thank the following for spending their valuable time evaluating me and my research: Dr. Partha Sarkar, who has also taught me a great deal about mechanical vibrations through his undergraduate and graduate courses, and Dr. Shankar Subramaniam, who directed me toward finding a suitable CFD methodology for acoustic streaming.

Mr. John Laage performed the PIV tests which were critical to the evaluation of the code I worked to develop—as well as the conclusions drawn near the end of this thesis—and I much appreciate his work and the availability of his data for evaluation.

Although I never got to meet him or work directly with him, Mr. Richard Oeftering of NASA Glenn Research Center provided much of the inspiration and ground work for my thesis through his collaboration with Dr. Adin Mann and prior graduate studies at Iowa State University.

Next, I would like to thank my current employer—Rockwell Collins—for its support of my pursuit for a Master's degree in Mechanical Engineering. My initial desire to pursue graduate studies was motivated by my first exposure to real engineering work, which occurred in the Environmental Effects Engineering Vibration Lab (where I now serve as dynamicist) during my first month at Rockwell Collins as a cooperative

education student. In particular, I would like to thank my former manager and mentor—Wes Lucken—first for hiring me on full-time, but also for allowing me the freedom to work around my class schedule and—most importantly—teaching me self- and others-management skills by continually "throwing me into the fire."

I would like to give a special *thank you* (not *thank-you*) to my high school English instructor, Mr. Steven Sales, for two lessons he taught me. First of all, without his noble attempt to instruct me in the proper usage of my native tongue, imperfect as it is, the writing of this thesis would have been an utter failure. Secondly—although not directly related to the writing portion of this thesis—he taught me a hard lesson in integrity during my junior year which I have yet to forget.

Finally, I would like to thank my family—particularly my wife Kristin, parents David and Julie, sisters Tara and Tyann, and my grandparents June, Sam, and Joan (the latter two who have sadly passed on)—for giving me the extra push I have so desperately needed to succeed in life. They endured my start as a lazy, whiny little kid, and I hope my completion of this research has made up for some of the lost ground. I know I have a hard time showing my appreciation, but you all have really taught me to believe that I can accomplish most endeavors I set my mind to.

ABSTRACT

Acoustic liquid manipulation, or ALM, is a term used to qualify three effects of nonlinear sound transmitted through fluid: radiation pressure, streaming, and heating. ALM is harnessed for a number of uses, such as the creation of fountains, formation of jets, and the destruction of cancerous tumors. As with any physical phenomenon, a computational model is desired to allow prediction of ALM.

Since prior work associated with this study produced a model for nonlinear sound, this thesis focused on developing computational fluid dynamic code to predict fluid velocity and heating. The model was compared with experimental data for water at room temperature and found to produce similar flow paths, although the code produced velocities orders of magnitude below the empirical setup. A number of cases were also examined to determine effects of fluid property variation. The conclusions discuss the merits of the model, as well as improvements for future work.

CHAPTER 1. INTRODUCTION

1.1 Acoustic Liquid Manipulation

As stated by Richard Oeftering (1999) of the NASA Glenn Research Center, "Acoustic Liquid Manipulation (ALM) is a term coined to describe the use of non-linear acoustics to move liquid, manipulate liquid surfaces, and propel buoyant objects." In essence, ALM is the management of fluid and buoyant object motion within fluids using the nonlinear effects of high-frequency, high-power sound. ALM phenomena are created using focused and directed sound beams at radio frequency (RF) levels using burst modulation (Oeftering, 1999). Sound levels to create the nonlinear sound are typically above 130 dB (Faidley, 2001) and may be in excess of 200 dB for frequencies above 1 MHz (Mann et al., 2003). Two major physical effects are typically considered to be ALM phenomena: radiation pressure and acoustic streaming (Oeftering, 1999). A third—fluid heating—was cited by Faidley (2001) and is an integral part of the research at hand. These three phenomena may be described as follows.

1. *Radiation Pressure:* Radiation pressure may be described as a pressure or force on an object in the direction of sound wave propagation (WordReference.com).

2. *Acoustic Streaming:* Acoustic streaming is the bulk motion of a fluid due to sound wave attenuation by the fluid (Nightingale, 2000). This bulk motion is described as the non-zero time-average of a fluctuating flow (Riley, 1998 and 2001). Although pressure and velocity vary with time in a sound field, their temporal averages are non-zero.

3. *Fluid Heating:* Fluid heating within the context of ALM is the conversion of
absorbed acoustic energy to heat (Faidley, 2001).

1.2 ALM Applications

Acoustic Liquid Manipulation phenomena have relevance in many research and
practical applications. Radiation pressure and streaming, particularly, show great
potential in such areas as aerospace and manufacturing, offering benefits over traditional
fluid and buoyant object management techniques, as well as process improvements.
These prospective fields of utilization have resulted in a great deal of research interest—
particularly in the domains of model generation and empirical testing.

1.2.1 Radiation Pressure/Force Applications

As alluded to in section 1.1, radiation pressure is created in the presence of
nonlinear sound. This pressure results in forces on bodies within a fluid, such as bubbles
and other buoyant objects. As can be seen through the literature research process, many
applications exist or have the potential to exist due to the phenomenon of radiation
pressure. Although the focus of this thesis is not on this force creation phenomenon per
se, it is an integral part of ALM. As such, this section addresses a small subset of the
applications of radiation pressure within the boundaries of the definition for ALM set in
section 1.1.

1.2.1.1 Fluid Surface Manipulation

Mitome (1990) demonstrated through a series of visualization experiments that a
result of radiation pressure when a transducer is placed below the surface of a liquid
facing upward is the creation of an ultrasonic fountain. He showed that this phenomenon

is independent of streaming flow by placing a film over the transducer, which resulted in

little to no degradation of the fountain itself (see Figure 1.1).
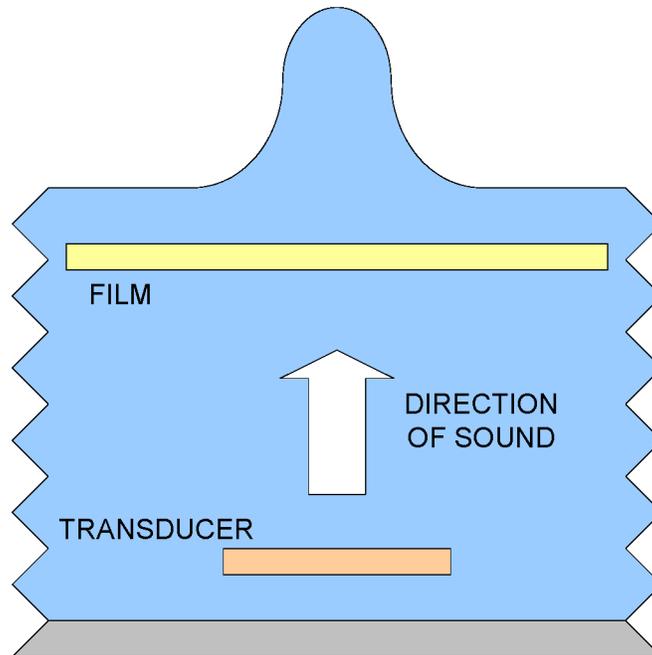
Figure 1.1 Depiction of Ultrasonic Fountain

Such fountains may be used in maskless plating and etching applications by forcing the

fluid to contact a component suspended over the fluid bath.

1.2.1.2 Small Particle Collection

Anderson et al. (2002) verified experimentally that radiation pressure can be used

to co-locate small particles within a localized portion of a fluid for the purpose of

removal from the fluid. The particles collected in this study were water in an air channel.

This process has application in both static and moving fluids.

1.2.1.3 Microgravity

Rich Oeftering of NASA is investigating the use of radiation pressure to control

the position of gas bubbles in liquid propellant, as well as manipulate liquid-gas surfaces

(Oeftering, 2003). This work is being performed using high-intensity directed acoustic beams.

Another application of radiation pressure in microgravity is the control of gaseous bubbles within fuel lines (Mann et al., 2000). Unlike significant gravity environments, which for the large part allow bubbles to rise to the surface in a liquid fuel tank due to buoyant forces, microgravity environments lack the acceleration to cause this movement. As a result, transducer arrays may be employed where needed (likely near the outlet of the fuel tank) in order to create a radiation pressure force on the gas bubbles and thus direct their movement out of the fuel lines. This application has the potential to reduce or eliminate the negative effects of current methods, which oftentimes disrupt microgravity experiments within the shuttle or space station or even limit the amount of available fuel.

1.2.2 Acoustic Streaming Applications

Since Raleigh observed streaming caused by standing sound waves between plane walls (Riley, 1998), a number of researchers have investigated the effects of acoustic streaming in an effort to characterize and utilize its effects. For the past few years, this interest has been focused in large part on streaming caused by ultrasonics. A small subset of past and current work in the area of acoustic streaming—covering both the theoretical and experimental—is presented in this section.

1.2.2.1 Streaming Jets

In addition to his work with the surface manipulation effects of radiation pressure, Mitome (1990) studied jets created through streaming. He explained that unlike conventional jets, streaming jets do not have resultant spreading. In fact, a streaming jet

will continue to accelerate away from the transducer, resulting in the recruitment of surrounding fluid into the jet.

Yu and Kim (2003) at the University of Southern California investigated using acoustic streaming to create atomization of liquid or air. For their application, they demonstrated the use of microfabricated liquid atomizer using both singular and arrayed ultrasonic transducers. Potential benefits of such an acoustically-enabled device are enhanced delivery of drugs, vapor production, and chemical reaction acceleration benefiting from an increase in surface area.

1.2.2.2 Medical Applications

In medical applications, acoustic streaming has the potential for many useful purposes. As Zauhar, Starritt, and Duck (1998) explain, one of the promising uses for streaming is in diagnostics. In addition to safety improvements, streaming within cells has been detected.

One particularly interesting medical application of ultrasonic streaming is the prediction of streaming velocity in cystic breast lesions (Nightengale and Trahey, 2000). Streaming detection is employed to find cystic breast lesions using ultrasonic pulses in a patient when sonographs present indeterminate results. The goal of this application is to determine methods of increasing streaming velocity within the lesion to improve detection while at the same time decreasing the exposure a patient has to high intensity ultrasound during streaming detection. In their study, Nightengale and Trahey developed a finite element model to make streaming predictions.

Another usage of acoustic streaming lies within the realm of nebulisers, which are used to deliver drugs into lungs via fine mist (Jenkins, 2003). An oscillatory

piezoelectronic crystal can be designed to generate a liquid fountain. This fountain is created with the ultrasound produced by the crystal.

1.2.2.3 Microgravity

Quite a bit of research into acoustic streaming effects in near-zero gravity has been performed as of late. In microgravity environments, the lack of buoyancy practically eliminates natural convection heat transfer within fluids (Trinh, 1998). This results in a need for artificially-produced flows, which historically have required significant mechanical mechanisms. Oftentimes, though, these mechanical systems are quite large or unreliable. Acoustic streaming can be employed to create fluid motion in precise locations in order to enhance convection and thus improve heat transfer.

Another use of acoustic streaming is in the area of propellant mixing for space applications. Unlike current methods which utilize mechanisms (i.e., moving parts), which can be unreliable, acoustic streaming has the potential to allow the mixing of propellants with no intrusion into the fluid (Oeftering, Chato, and Mann, 2003). Acoustic streaming can be employed within liquid propellant to induce currents without the use of nozzles or mechanical propellers.

1.2.2.4 Manufacturing Processes

Acoustic streaming holds the potential to improve a number of commonly-used manufacturing processes. Various research studies have shown that acoustic streaming can be used for both maskless etching and maskless electroplating processes (Oeftering, 1999). Masking of components prior to plating is oftentimes a primary cost driver for the completed component. Eliminating these steps would certainly reduce costs of plating and etching, as well as possibly increasing the accuracy of the process.

1.2.3 Heating Applications

As mentioned previously, ALM can result in the localized heating of a fluid. This heating may be beneficial or detrimental, depending on the application. Some examples of heating due to ALM are discussed in this section.

Huang et al. (2004) discuss the creation of high intensity focused ultrasound for the controlling of bleeding. In addition, they explain that ultrasound is useful for the gentle heating of tumors. Their research included a presentation of a model and numerical simulation, which included a demonstration of convective heat transfer due to acoustic streaming. Additionally, ultrasound is used for the precise destruction of cancerous cells while allowing for nearby healthy cells to remain unscathed (Mann et al., 2000).

1.3 Importance of a CFD Model for ALM

As discussed in the previous section, ALM phenomena provide the potential for a variety of useful research and practical applications in industry, government, and academia. As with any physical process, an accurate model describing ALM is desired to reduce both the cost and the time required for analyzing an ALM application. A simple yet concise model provides the benefit of cost savings over the design and purchase of experimental equipment and setups and allows the investigator to consider multiple use cases and scenarios rather speedily. Previous work undertaken by Faidley and Mann resulted in such a model being developed for radiation pressure, radiation force on a buoyant object, fluid body force divided by density, and rate of temperature increase due to high-powered, high-frequency sound. An attempt was made by Faidley to develop an appropriately simplified form of the Navier-Stokes and energy equations and solve for

the streaming velocity and temperature field using finite element code available in Matlab®. However, since the primary work was focused on the acoustic aspects rather than the fluid dynamic and heat generation aspects of ALM, not much time or effort was expended to create a CFD model. Therefore, the next step is to develop such a model for the streaming velocity and temperature profile of a fluid experiencing ALM effects based on (and to complement) their works. A number of researchers using a variety of numerical techniques have attempted to create models with varying degrees of success— these methodologies include CFD methods (Wan and Kuznetsov and Amari, Joly, and Gusev, 2003), finite element methods (Nightengale and Trahey, 2000). However, much work is yet to be completed or even undertaken in this important field.

1.4 Outline of Thesis

This thesis primarily presents the development of a numerical model of the fluid streaming and heating facets of ALM. A detailed derivation and development of the fundamental equations for acoustic streaming and heating is given in CHAPTER 2. This chapter presents the development and simplification (due to various assumptions) and subsequent expansion of forms of the Navier-Stokes and energy equations useful for evaluation of two-dimensional flow and heat transfer, along with boundary conditions. CHAPTER 3 details the discretization of the derived Navier-Stokes and heat transfer equations using a finite differencing method. The chosen scheme, along with the corresponding solution algorithm for solving the discretized equations through iteration techniques, is explained in detail. The development and function of a Matlab® graphical user interface (GUI) called simply "ALM Program" is discussed in CHAPTER 4. This program was originally designed for use by Rich Oeftering at NASA and allows the

ALM investigator to select and/or specify parameters such as fluid field, fluid properties, transducer geometry and frequency, and transducer heat dissipation in order to calculate the radiation pressure, fluid acceleration, force on a bubble, rate of change of temperature, and the velocity and temperature fields for the chosen tank. CHAPTER 5 is dedicated to the analysis and comparison of simulation and experimental results for the case of water at room temperature. Additional simulations for non-aqueous, cryogenic fluids—along with evaluations of property variation effects for water at room temperature—are also presented. Finally, the thesis closes with CHAPTER 6 in a brief discussion of the conclusions drawn from the comparisons between the simulation and experimental results. Interpretations of model and experimental data, as well as recommendations for future work in light of conclusions drawn, are posited for evaluation by the reader and are intended to inspire future research and development work.

CHAPTER 2. THEORETICAL DEVELOPMENT

This chapter presents—in detail—the theoretical development of the fundamental fluid and energy equations undertaken as a first step to establishing a model of temperature and velocity behavior of a fluid due to ALM phenomena. The chapter begins in section 2.1 with a brief discussion of a fluid tank model setup and assumptions levied on it. In section 2.2, the critical ALM equations are briefly presented and discussed (but not fully developed). Four primary terms are shown: nonlinear sound pressure, force on a spherical object in a fluid due to the nonlinear sound, fluid acceleration due to the nonlinear sound, and heating rate of the fluid. Emphasis in section 2.3 is placed on the development of useful but simple and appropriate forms of the Navier-Stokes and energy equations. Elements of this section which are of particular interest include the integration of ALM effects to formulate the streaming solution and the presentation of a vorticity-stream function approach to the Navier-Stokes equations to simplify the CFD calculation process. The former is accomplished using two methods—herein referred to as the Nyborg streaming formulation and the Lighthill streaming formulation, the details of which will be discussed later in the chapter. The final section of this chapter—2.4—is dedicated to a derivation and discussion of the heating equation. In sections 2.2, 2.3, and 2.4, the basic equations are given, transformation of the equations into a form conducive to the CFD environment is performed, the streaming body force is applied, and boundary conditions are developed.

The ultimate goal of this chapter is to lay the analytical foundation for a numerical model which will calculate the velocity at which streaming occurs due to nonlinear sound determine heating effects caused by the streaming.

2.1 Model Setup

The ALM model used for this thesis work was chosen to facilitate design of an experimental fluid tank setup which could be constructed and utilized for code validation. (The realization of this setup is described in CHAPTER 5.) The ALM model was set up to calculate fluid flow and temperature in the two-dimensional regime. The model was devised in such a manner to allow use of results taken from the nonlinear sound model developed by Faidley (2001) and Mann, Faidley, Morfeld, & Kopp (2000).

2.1.1 Modeling Process

As a prelude to a thorough discussion of the theory and numerical modeling of ALM acoustic streaming and heating phenomena, a high-level view of the modeling process is presented. This process begins with a selection of fluid properties, specification of the external environment, sizing of the tank, and selection of the sound transducer type and dimensions. Next, the acoustic solution is obtained, resulting in field information for fluid pressure, temperature fluctuation (over time), body force, and force on a bubble. The body force output is then input (along with property values, external environment, and tank geometry) into the streaming solution solver. The streaming velocity field, vorticity, and stream function are output. Finally, the heating solver is called upon to produce the fluid temperature field. A graphical illustration of the process is shown in Figure 2.1.
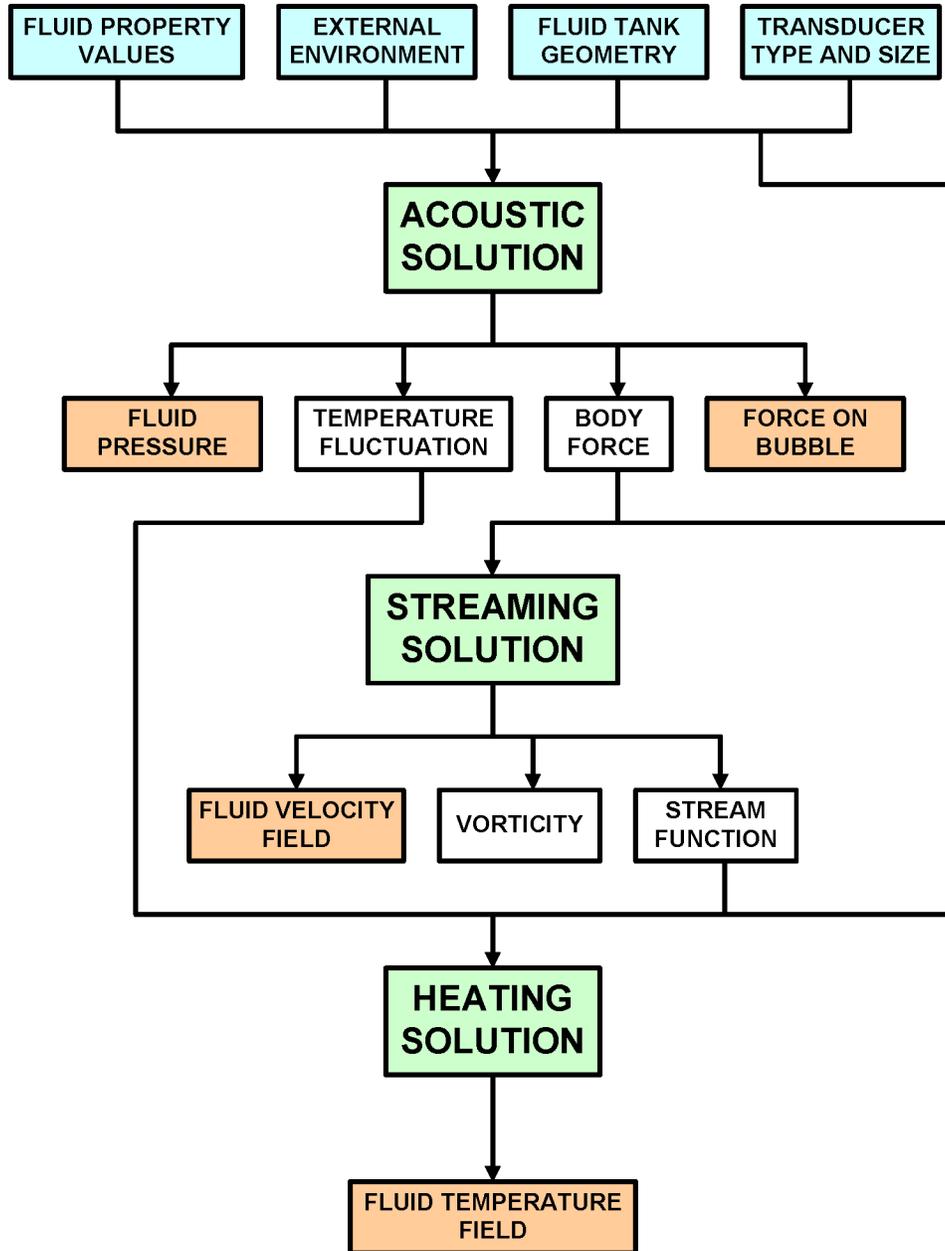
Figure 2.1 Block Diagram of ALM Calculation Process

As can be seen, feedback from one solution to another does not occur, rather the entire

calculation methodology builds entirely upon previous computations. For example, the

streaming solution is in no way influenced by the heating solution. The philosophies of

theoretical derivation, numerical simulation, and data postprocessing detailed in this

thesis follow the process explained in this section.

2.1.2 Assumptions

A number of assumptions were decided upon in order to simplify the equation development process. These were based on the physical properties and constraints of the planned test setup which was eventually constructed to validate the computational fluid dynamic code developed. The assumptions driving the analysis of this system are listed as follows.

1. The fluid medium is homogeneous.

2. The fluid medium is incompressible.

3. The fluid viscosity is constant over time and space.

4. Fluid flow is steady-state.

5. Fluid flow is laminar.[1]

6. Fluid flow is two-dimensional.

7. The fluid is Newtonian.

8. Gravity has no effect on fluid flow.

Although the above assumptions should pertain to a number of fluids investigated for ALM, they were verified experimentally for the specific case of water in a tank at room temperature since this was deemed to be the most practical method of validating the streaming results (again, see CHAPTER 5). In the remaining sections of this chapter, these assumptions are applied to the Navier-Stokes equations and energy equations to simplify the computational process.

---

[1] During development of the Navier-Stokes equations, a time-averaged Reynolds stress is called upon, although this is for the streaming body force. No attempt is made at turbulence modeling. The assumption of non-turbulence is not claimed to be necessarily correct, rather just a simplifying assumption.

2.1.3 Tank Model

The theory and boundary conditions for this study of acoustic streaming were

formulated for a two-dimensional tank filled with a fluid to simplify the system such that

an experiment could be developed for which gravity would be perpendicular to the $W \times L$

(width and length) plane of the tank. Although not completely necessary, the goal was to

remove gravity as a parameter of the Navier-Stokes and energy equations in order to

isolate the nonlinear sound as the sole source of fluid motion. A simple diagram of the

tank is shown in Figure 2.2.
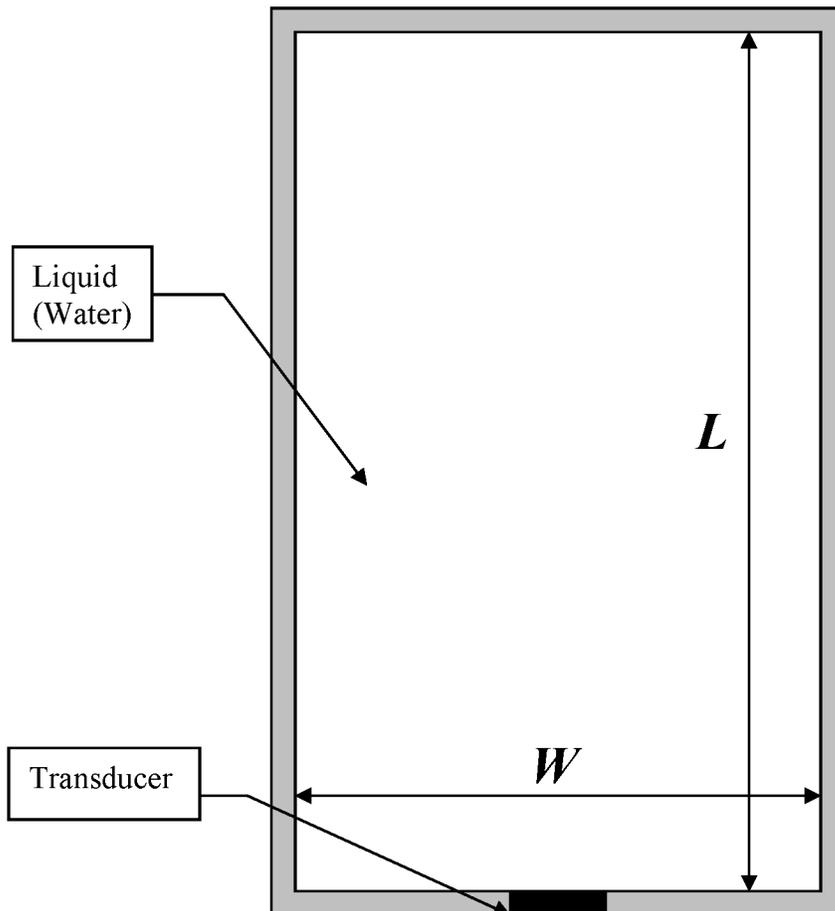
Figure 2.2 Tank for which streaming model was developed.

The model was designed such that any combination of L and W could be investigated by simply changing their values.

2.2 Acoustic Model

As a prerequisite for the study of ALM effects, the underlying influences involved—namely radiation pressure, streaming, and heating—must be discussed. This section gives a brief description of the acoustic theory important to—but not developed by—this study of streaming due to ALM.

The foundation of this thesis lies in the development of a nonlinear acoustic model previously undertaken by Faidley (2001) and Mann et al. (2000). Of particular importance to the development of a CFD model of the fluid streaming and heating is the existence of the nonlinear sound pressure field. Although none of the theory presented in this section was developed during this study or is expounded upon in great detail during the course of this thesis, it is presented as an essential component of the development of a CFD model of ultrasonic acoustic streaming. This section begins with a discussion of the foundation of ALM—the linear approximation model of nonlinear sound radiation.

2.2.1 Sound Pressure

Two sound pressure models are presented in this section—acoustic model for a single transducer and acoustic model for a transducer array.

2.2.1.1 Acoustic Model for a Single Transducer

For a single transducer, Faidley (2001) models the generated sound (pressure, $p(\bar{r})$) field in a fluid using the Helmholtz integral:

$$p(\bar{r}) = \frac{j\omega\rho}{2\pi} \int\int G(\bar{r}|\bar{r}_0)\bar{u}_{transducer}dS_{transducer} \, , \tag{2.1}$$

where ρ is the fluid density, ω is the transducer circular frequency, $\bar{r}_0$ is the position on

the transducer (in radial coordinates), $\bar{r}$ is the observation position, $G(\bar{r}|\bar{r}_0)$ is Green's

function, $\bar{u}_{transducer}$ is the velocity at the surface of the transducer, and $S_{transducer}$

represents the surface of the sound source which—in this case—is the transducer itself.

2.2.1.2 Acoustic Model for an Transducer Array

Mann, Clinkinbeard, Laage, Olsen, & Subramaniam (2005) present a model for a

rectangular array composed of rectangular sound transducer source elements. Figure 2.3

gives a simplified view of such an array, along with element x- and y-dimensions (a and b,

respectively), x- and y-spacing (dx and dy, respectively), and number of elements in the x-

and y-directions (N_x and N_y, respectively).
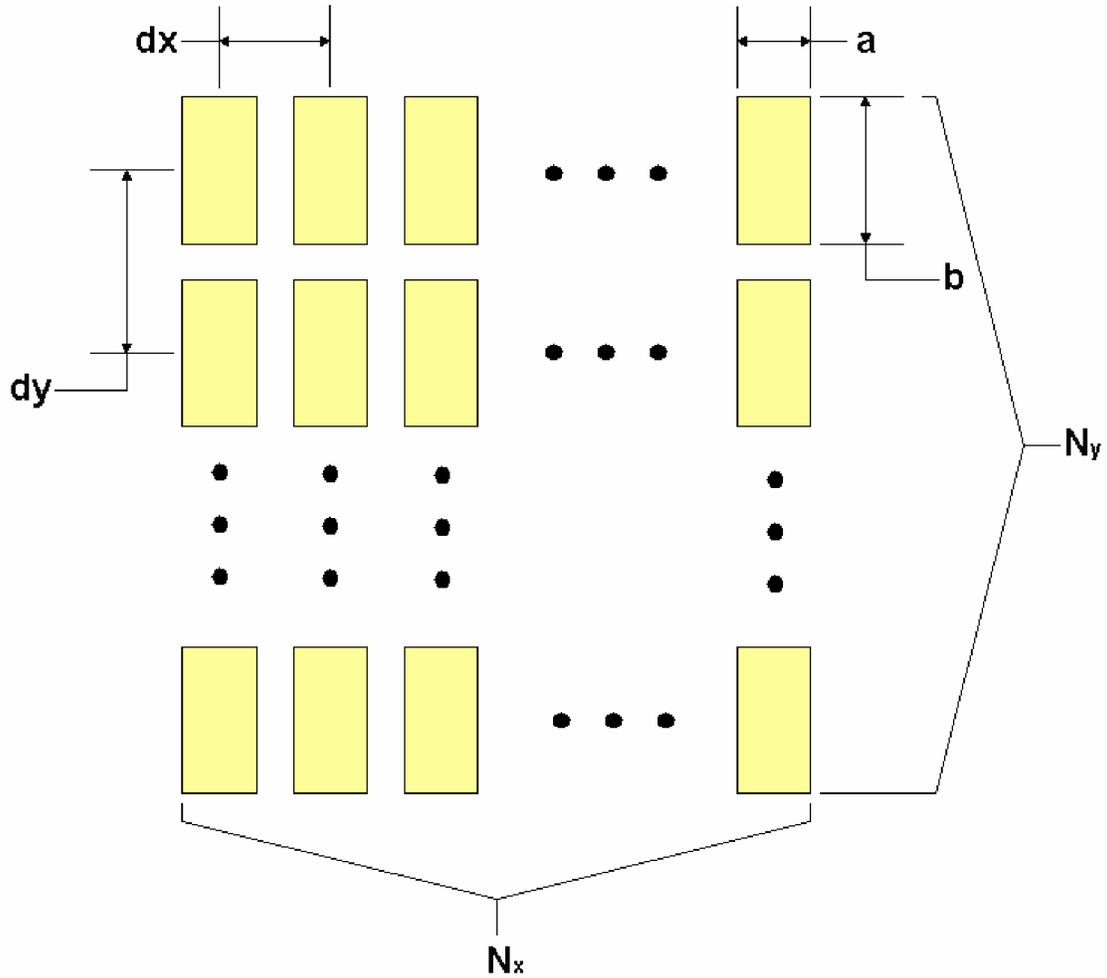
Figure 2.3 Schematic of an Array with Parameters

As a result, Mann et al. (2005) show that the sound radiation pressure, $p(\bar{r})$, can be

represented as a superposition—or sum—of the radiation pressures for all transducers in

the array:

$$p(\bar{r}) = \sum_{i=1}^{N_x} \sum_{j=1}^{N_y} p_{ij}(\bar{r} - \bar{r}_{ij}), \qquad (2.2)$$

where $\bar{r}_{ij}$ is the position of array element i,j, $\bar{r}$ is the point from at which the sound

radiation pressure is calculated, $p_{ij}(\bar{r} - \bar{r}_{ij})$ is the sound pressure calculated at position $\bar{r}$

for the transducer located at position $\bar{r}_{ij}$, and N_x and N_y are the number of transducers in the x- and y-directions, respectively.

2.2.2 Force Due to Nonlinear Sound

Although not an essential component of the fluid streaming or heating effects discussion of ALM in this thesis, the force on a gaseous sphere in a liquid medium (i.e., bubble) due to nonlinear sound is presented here. This term is calculated using a linear model. The resulting linear approximation was developed by Wang (1998), as modified by Faidley (2001), to be

$$\bar{f}(\bar{r}) = \frac{2\pi \langle p(\bar{r}) \rangle^2 k^4 R^4}{\rho_f c_f{}^2 \left\{ \dfrac{c_f{}^4}{c_b{}^4} k^6 R^6 + \left[\dfrac{3\rho_b}{\rho_f} - \left(\dfrac{kR\rho_f}{\rho_b} \right)^2 \right]^2 \right\}}, \qquad (2.3)$$

where $p(\bar{r})$ is the sound pressure, $\bar{r}$ is the position of the bubble, R is the bubble radius, ρ_f is the density of the fluid medium, c_f is the speed of sound through the fluid medium, ρ_b is the density of the bubble gas, c_b is the speed of sound through the bubble gas, and k is the acoustic wave number. The acoustic wave number is calculated as

$$k = \frac{2\pi f}{c_f}. \qquad (2.4)$$

2.2.3 Streaming Body Force

Perhaps the most important term for a direct analysis and discussion of acoustic streaming—the fluid streaming body force—is presented in this section. Although two philosophies for calculating acoustic streaming motion are shown in this thesis, both rely

on the existence of a time-averaged Reynolds stress, which is essentially the streaming

body force. Although presented with a fair amount of detail by Faidley (2001),

manipulation of equations to derive the streaming body force is shown in this section due

to its criticality with subsequent model development.

2.2.3.1 Euler's Equation

To begin the discussion and derivation of the streaming force, Euler's equation is

invoked:

$$\frac{\partial(\rho \mathbf{u})}{\partial t} = -\nabla p \,, \tag{2.5}$$

where $\mathbf{u}$ is the velocity vector, ρ is the fluid density, p is the acoustic pressure, and t

represents time. Written in vector form, this becomes

$$\frac{\partial(\rho u)}{\partial t}\hat{i} + \frac{\partial(\rho w)}{\partial t}\hat{k} = -\frac{\partial p}{\partial x}\hat{i} - \frac{\partial p}{\partial z}\hat{k} \,, \tag{2.6}$$

where u is the x-component of velocity and w is the z-component of velocity. Since

density is assumed to be constant, separating Euler's equation out into its separate

components gives

$$\rho \frac{\partial u}{\partial t} = -\frac{\partial p}{\partial x} \tag{2.7}$$

and

$$\rho \frac{\partial w}{\partial t} = -\frac{\partial p}{\partial z} \,. \tag{2.8}$$

Faidley (2001) shows that the values for pressure and velocity take the following form

assuming ∂x and ∂z are small and can be approximated as plane waves, resulting in

$$p(x,z,t) = Pe^{j(\omega t - \mathbf{k} \cdot \mathbf{x})}, \tag{2.9}$$

$$u(x,z,t) = Ue^{j(\omega t - \mathbf{k} \cdot \mathbf{x})}, \tag{2.10}$$

and

$$w(x,z,t) = We^{j(\omega t - \mathbf{k} \cdot \mathbf{x})}. \tag{2.11}$$

where P is the pressure amplitude, U is the x-component velocity amplitude, W is the z-component velocity amplitude, ω is the circular frequency of the sound, $\mathbf{k}$ is the acoustic wave number vector defined as $k_x\hat{i} + k_z\hat{k}$ (where k_x is the x-component of the wave number and k_z is the z-component), and $\mathbf{x}$ is the displacement vector $x\hat{i} + z\hat{k}$. As a result, the first derivatives of the pressure term with respect to the x- and z-directions are

$$\frac{\partial p}{\partial x} = -jk_x Pe^{j(\omega t - \mathbf{k} \cdot \mathbf{x})} = -jkp \tag{2.12}$$

and

$$\frac{\partial p}{\partial z} = -jk_z Pe^{j(\omega t - \mathbf{k} \cdot \mathbf{x})} = -jkp. \tag{2.13}$$

Likewise, the first derivatives of the velocity terms with respect to time are written as

$$\frac{\partial u}{\partial t} = j\omega Ue^{j(\omega t - \mathbf{k} \cdot \mathbf{x})} = j\omega u \tag{2.14}$$

and

$$\frac{\partial w}{\partial t} = j\omega We^{j(\omega t - \mathbf{k} \cdot \mathbf{x})} = j\omega w. \tag{2.15}$$

Replacing equations 2.12, 2.13, 2.14, and 2.15 into the x- and z-components of Euler equation (i.e., equations 2.7 and 2.8) gives the following relationships between velocity and pressure:

$$u = \left(\frac{k}{\rho\omega}\right)p,$$

(2.16)

and

$$w = \left(\frac{k}{\rho\omega}\right)p.$$

(2.17)

2.2.3.2 Time-Averaged Reynolds Stress

A body force due to a time-averaged Reynolds stress can be found to satisfy the equation

$$\mathbf{f} = \rho\big\langle(\mathbf{u}\cdot\nabla)\mathbf{u}\big\rangle.$$

(2.18)

Assuming that the fluid is incompressible with constant density, (i.e., the divergence of velocity is equivalent to zero—shown to be true in section 2.3.1.1 but assumed as fact for this portion of the analysis), the body force can be written as

$$\mathbf{f} = \rho\big\langle(\mathbf{u}\cdot\nabla)\mathbf{u} + \mathbf{u}(\nabla\cdot\mathbf{u})\big\rangle.$$

(2.19)

Expanded into its vector terms, the body force is

$$\mathbf{f} = \rho\Bigg\langle \left(u\frac{\partial u}{\partial x} + w\frac{\partial u}{\partial z}\right)\hat{i} + \left(u\frac{\partial w}{\partial x} + w\frac{\partial w}{\partial z}\right)\hat{k} \\ + \left(u\frac{\partial u}{\partial x} + u\frac{\partial w}{\partial z}\right)\hat{i} + \left(w\frac{\partial u}{\partial x} + w\frac{\partial w}{\partial z}\right)\hat{k} \Bigg\rangle,$$

(2.20)

which simplifies to

$$\mathbf{f} = \rho \left\langle \left(2u \frac{\partial u}{\partial x} + w \frac{\partial u}{\partial z} + u \frac{\partial w}{\partial z} \right) \hat{i} + \left(u \frac{\partial w}{\partial x} + 2w \frac{\partial w}{\partial z} + w \frac{\partial u}{\partial x} \right) \hat{k} \right\rangle. \qquad (2.21)$$

Using the multiplicative property of derivatives which states that for two functions, f and g, the derivative of the product of these functions with respect to variable a is

$$\frac{\partial (fg)}{\partial a} = g \frac{\partial (f)}{\partial a} + f \frac{\partial (g)}{\partial a}, \qquad (2.22)$$

the body force becomes

$$\mathbf{f} = \rho \left\langle \left(\frac{\partial (u^2)}{\partial x} + \frac{\partial (uw)}{\partial z} \right) \hat{i} + \left(\frac{\partial (uw)}{\partial x} + \frac{\partial (w^2)}{\partial z} \right) \hat{k} \right\rangle. \qquad (2.23)$$

Substituting pressure, p, for the velocity terms u in the x-component of the forcing term and w in the z-component gives the following representation of the body force:

$$\mathbf{f} = \rho \left\langle \left(\left\{ \frac{k}{\rho \omega} \right\} \frac{\partial (pu)}{\partial x} + \left\{ \frac{k}{\rho \omega} \right\} \frac{\partial (pw)}{\partial z} \right) \hat{i} + \left(\left\{ \frac{k}{\rho \omega} \right\} \frac{\partial (pu)}{\partial x} + \left\{ \frac{k}{\rho \omega} \right\} \frac{\partial (pw)}{\partial z} \right) \hat{k} \right\rangle, \qquad (2.24)$$

which simplifies to

$$\mathbf{f} = \left\{ \frac{k}{\omega} \right\} \left\langle \left(\frac{\partial (pu)}{\partial x} + \frac{\partial (pw)}{\partial z} \right) \hat{i} + \left(\frac{\partial (pu)}{\partial x} + \frac{\partial (pw)}{\partial z} \right) \hat{k} \right\rangle. \qquad (2.25)$$

The x- and z-component terms of sound intensity are defined as $pu = I_x$ and $pw = I_z$, causing the forcing term to become

$$\mathbf{f} = \left\{ \frac{k}{\omega} \right\} \left\langle \left(\frac{\partial I_x}{\partial x} + \frac{\partial I_z}{\partial z} \right) \hat{i} + \left(\frac{\partial I_x}{\partial x} + \frac{\partial I_z}{\partial z} \right) \hat{k} \right\rangle. \qquad (2.26)$$

Further simplification results in

$$\mathbf{f} = \left\{ \frac{k}{\omega} \right\} \left\langle \left(\frac{\partial I_x}{\partial x} + \frac{\partial I_z}{\partial z} \right) (1\hat{i} + 1\hat{k}) \right\rangle. \qquad (2.27)$$

Given that the term $k/\omega = 1/c$ (equation 2.4) and the bracketed value containing the

intensity terms is the dot product of the del operator, ∇, with the intensity vector, the

forcing term is written as

$$\mathbf{f} = \left(\frac{1}{c}\right)\langle\nabla \cdot \mathbf{I}\hat{\mathbf{e}}\rangle,$$ (2.28)

where $\mathbf{I}$ is the intensity vector and $\hat{\mathbf{e}}$ is the unit normal vector $1\hat{i} + 1\hat{k}$.

The existence of the sound intensity term presents an intriguing, yet

desirable simplifying consequence. According to Lighthill (1978) and Pierce (1981),

when sound waves are unattenuated, the following holds true for the divergence of

intensity:

$$\nabla \cdot \mathbf{I} = 0.$$ (2.29)

However, in the presence of attenuation, this divergence has a non-zero value and can be

written as

$$\nabla \cdot \mathbf{I} = -\alpha I,$$ (2.30)

where I is the magnitude of intensity and α is an attenuation coefficient, which is "the

proportional loss of acoustic energy per unit distance covered by a traveling wave,"

(Lighthill, 1978). Therefore, the body force becomes

$$\mathbf{f} = -\left(\frac{\alpha}{c}\right)I\hat{\mathbf{e}}$$ (2.31)

Thus, the body force used in this study of acoustic streaming takes the form of

$$\mathbf{f} = \rho\langle(\mathbf{u} \cdot \nabla)\mathbf{u}\rangle = -\left(\frac{\alpha}{c}\right)I\hat{\mathbf{e}}.$$ (2.32)

The attenuation coefficient is presented in the next section.

2.2.3.3 Attenuation Coefficient

According to Pierce (1981), the classical form of the attenuation coefficient is

represented as

$$\alpha = \left(\frac{\delta \omega^2}{c^3} \right),$$
(2.33)

where ω is the circular frequency of the sound source, c is the speed of sound through the

fluid medium, and δ is a proportional ratio of the fluid viscosity and density known as the

diffusivity of sound. The sound diffusivity can take one of a number of forms, including

the following common version:

$$\delta = -\frac{\mu}{2\rho} \left(\frac{4}{3} + \frac{\gamma - 1}{\text{Pr}} \right),$$
(2.34)

where μ is the dynamic viscosity, γ is the specific heat ratio, and Pr is the Prandtl number

of the fluid (Pierce, 1981). Evident from equations 2.33 and 2.34 is the fact that the

attenuation coefficient takes on dimensions of the inverse of length.

2.2.4 Fluid Heating

One final effect discussed in this study of ALM is the heating of a fluid. Mann et

al. (2005) give the rate in temperature change in a fluid undergoing ALM as

$$\frac{dT(\bar{r})}{dt} = \frac{\omega^2 \mu \left(\frac{4}{3} + \frac{1 - \gamma}{\text{Pr}} \right)}{2\rho^3 c_f^4 C_T} \langle p(\bar{r}) \rangle^2,$$
(2.35)

where μ is the fluid dynamic viscosity, γ is the specific heat ratio, Pr is the fluid Prandtl number, and C_T is the isothermal specific heat of the fluid. The extent of this equation's purposefulness is evident in section 2.4.

2.3 Streaming Velocity

As stated in the introduction, an important facet of ALM (and one verifiable through experiments) is acoustic streaming. The purpose of focusing this study on streaming is to develop—beginning with the Navier-Stokes equations—computational fluid dynamic code that will be used to determine the velocity, pressure, and acceleration fields. Later in the study, the calculated velocity is compared with the experimental data and the values of computational parameters (such as viscosity, density, and attenuation coefficient) adjusted to determine the effects of their variation on the flow fields.

This section is devoted to the development of equations that will be used in following chapters to determine the flow field due to the acoustic streaming phenomenon.

2.3.1 Navier-Stokes Equations

To facilitate a numerical solution to the velocity flow field for acoustic streaming due to ALM (and any fluid mechanics problem, for that matter), the necessity arrives to first derive the correct form of the Navier-Stokes equations. This is comprised of the development of both the continuity equation (otherwise known as conservation of mass) and the conservation of momentum relations. Although derivations of fundamentals are left to the reader, the development of both sets of equations (based on the fundamental forms) is shown in detail for the remainder of this section.

2.3.1.1 Continuity Equation

In order to do justice to the development of the streaming equations, the basic equations of motion are presented beginning with their most raw forms. The development originates with the idea of continuity, otherwise known as conservation of mass. As Tannehill, Anderson, & Pletcher (1990) explain, the two-dimensional form of the continuity equation can be written as

$$\frac{\partial \rho}{\partial t} + \nabla \cdot (\rho \mathbf{u}) = 0, \tag{2.36}$$

where $\mathbf{u}$ is the particle velocity vector. This equation is expanded to separate its density-variant and velocity-variant terms:

$$\frac{\partial \rho}{\partial t} + \mathbf{u}\nabla\rho + \rho\nabla\mathbf{u} = 0, \tag{2.37}$$

where $d\rho/dt + \mathbf{u}\,\nabla\rho$ is defined as the material derivative $D\rho/Dt$. Since one of the driving assumptions is that the ALM phenomenon under study is for an incompressible fluid, the material derivative is presumed to be zero over time and space (essentially, the fluid density is constant over x, z, and t), and the conservation of mass equation simply becomes the divergence of velocity,

$$\nabla \cdot \mathbf{u} = 0, \tag{2.38}$$

which, considering its x- and z-components of velocity, can also be represented as

$$\frac{\partial u}{\partial x} + \frac{\partial w}{\partial z} = 0. \tag{2.39}$$

Based on the assumptions given, this is the simplest and perhaps most useful form of the continuity equation for the problem at hand and will be later used to simplify the conservation of momentum and energy equations numerous times.

2.3.1.2 Conservation of Momentum

For the conservation of momentum equation, Tannehill et al. (1997) give the following Cartesian form (in mixed vector and Einstein summation notation):

$$\rho \frac{D\mathbf{u}}{Dt} = \mathbf{f} - \nabla p + \frac{\partial}{\partial x_i}\left[\mu\left(\frac{\partial u_i}{\partial x_j} + \frac{\partial u_j}{\partial x_i} \right) - \frac{2}{3}\delta_{ij}\mu\frac{\partial u_k}{\partial x_k} \right], \qquad (2.40)$$

where $\mathbf{f}$ is a body force per unit volume, p is the particle pressure, μ is the dynamic viscosity of the fluid, and $\delta_{i,j}$ is the Kronecker delta function, where $\delta = 1$ if $i = j$ and $\delta = 0$ if $i \neq j$. The body force, $\mathbf{f}$, is typically due to gravity. However, as mentioned in section 2.1.3 of this thesis, the model and experiments were set up to remove gravity from the equation. This was accomplished by orienting the fluid tank such that the gravity vector was normal to the plane on which ALM effects were being recorded. As will be seen with further development of the Navier-Stokes equations, the body force in equation 2.40 is used to represent the streaming body force.

Similar to the case with density in the previous section, the material derivative for the fluid velocity—$D\mathbf{u}/Dt$—is defined as

$$\frac{D\mathbf{u}}{Dt} = \frac{\partial \mathbf{u}}{\partial t} + \left(\mathbf{u}\cdot\nabla\right)\mathbf{u}. \qquad (2.41)$$

In order to simplify the calculation process, more of the assumptions driving this study—that fluid viscosity is constant in space and time and over the temperature ranges

studied and that fluid motion is at steady-state and is incompressible—are called upon.

As a direct result of the underlying assumptions, the conservation of momentum equation

takes the following simplified form:

$$\rho\left[\frac{\partial \mathbf{u}}{\partial t} + (\mathbf{u} \cdot \nabla)\mathbf{u}\right] = \mathbf{f} - \nabla p + \frac{\partial}{\partial x_i}\left[\mu\left(\frac{\partial u_i}{\partial x_j} + \frac{\partial u_j}{\partial x_i}\right) - \frac{2}{3}\delta_{ij}\mu\frac{\partial u_k}{\partial x_k}\right]. \qquad (2.42)$$

The following relations are formed when this equation is split into its x- and z-

directional components. (To save time and space, only x-direction equation derivation is

shown.)

The x-component of the conservation of momentum relation is

$$\rho\left(\frac{\partial u}{\partial t} + u\frac{\partial u}{\partial x} + w\frac{\partial u}{\partial z}\right) = f_x - \frac{\partial p}{\partial x} + \frac{\partial}{\partial x}\left[\mu\left(2\frac{\partial u}{\partial x} - \frac{2}{3}\nabla \cdot \mathbf{u}\right)\right] + \frac{\partial}{\partial z}\left[\mu\left(\frac{\partial w}{\partial x} + \frac{\partial u}{\partial z}\right)\right] \qquad (2.43)$$

where f_x is the x-component of the body force. This equation is further expanded to give

the following:

$$\rho\left(\frac{\partial u}{\partial t} + u\frac{\partial u}{\partial x} + w\frac{\partial u}{\partial z}\right) = f_x - \frac{\partial p}{\partial x}$$
$$+ \mu\left[2\frac{\partial^2 u}{\partial x^2} - \frac{2}{3}\left(\frac{\partial u}{\partial x} + \frac{\partial w}{\partial z}\right)\right] + \left[\mu\left(\frac{\partial^2 w}{\partial x\partial z} + \frac{\partial^2 u}{\partial z^2}\right)\right] \qquad (2.44)$$

Finally, after making use of the continuity relation, equation 2.44 is simplified into the

following form:

$$\rho\left(\frac{\partial u}{\partial t} + u\frac{\partial u}{\partial x} + w\frac{\partial u}{\partial z}\right) = f_x - \frac{\partial p}{\partial x} + \mu\left(\frac{\partial^2 u}{\partial x^2} + \frac{\partial^2 u}{\partial z^2}\right). \qquad (2.45)$$

Developed in a similar manner, the z-directional component of the conservation of

momentum equation is written as

$$\rho\left(\frac{\partial w}{\partial t} + u\frac{\partial w}{\partial x} + w\frac{\partial w}{\partial z}\right) = f_z - \frac{\partial p}{\partial x} + \mu\left(\frac{\partial^2 w}{\partial x^2} + \frac{\partial^2 w}{\partial z^2}\right), \qquad (2.46)$$

where f_z is the streaming body force in the z-direction. Recombining the x- and z-directional components into vector notation results in

$$\rho\left[\frac{\partial \mathbf{u}}{\partial t} + (\mathbf{u}\cdot\nabla)\mathbf{u}\right] = \mathbf{f} - \nabla p + \mu\nabla^2\mathbf{u}. \qquad (2.47)$$

One last assumption must be accounted for to give the basic model of the Navier-Stokes equation as used in this study, which is the idea that the streaming is a steady-state process. Therefore, $\frac{\partial \mathbf{u}}{\partial t}$ is set equivalent to zero and the fundamental steady-state Navier-Stokes equation for acoustic streaming is

$$\rho(\mathbf{u}\cdot\nabla)\mathbf{u} = \mathbf{f} - \nabla p + \mu\nabla^2\mathbf{u}. \qquad (2.48)$$

This is the simplest form of the Navier-Stokes equation which can be used to develop the streaming solution.

2.3.2 Navier-Stokes Equations using the Vortcity-Stream Function Methodology

Evident from equation 2.48 is that the Navier-Stokes relation developed in section 2.3.1.2 actually represents two equations (in the x- and z-directions). When numerically approximating this expression, two equations are actually required and are interlaced during calculations, drastically complicating the computational process. Thus, a simplification which would result in their consolidation into one equation is desired for ease of developing the CFD code. This becomes possible with the consideration of one of the driving assumptions in this analysis of ALM, which is that the fluid is

incompressible. This incompressibility state allows the vorticity-stream function approach to serve in solving the Navier-Stokes equations, which is the process developed and presented in this section. This is accomplished by first defining vorticity, next developing a stream function, and finally integrating the terms into the Navier-Stokes equations to form the vorticity transport equation. As concluded in this section, development of the vorticity transport equation—based on the assumptions that flow is incompressible and viscosity is constant—allows the simplification of the two components of the conservation of momentum relation into one equation.

Development of the vorticity-transport form of the Navier-Stokes equations was inspired through an early study by the author to calculate the lid-driven cavity flow problem. Tannehill et al. (1997) present a detailed solution to lid-driven cavity flow utilizing the vorticity transport concept, which was drawn upon for the development of the streaming equations shown here.

2.3.2.1 Vorticity Development

The vorticity function, ζ, defined by Tannehill et al. (1997) as twice the value of the fluid angular velocity (ϖ), is represented for the two-dimensional flow under study as

$$\zeta = \nabla \times \mathbf{u} = \left(\frac{\partial w}{\partial x} - \frac{\partial u}{\partial z} \right) \hat{j} = 2\varpi , \qquad (2.49)$$

where the magnitude of vorticity is written as

$$\zeta = \frac{\partial w}{\partial x} - \frac{\partial u}{\partial z} . \qquad (2.50)$$

The first and second spatial derivatives of vorticity in the x-direction are as follows:

$$\frac{\partial \zeta}{\partial x} = \frac{\partial^2 w}{\partial x^2} - \frac{\partial^2 u}{\partial x \partial z},$$ (2.51)

$$\frac{\partial^2 \zeta}{\partial x^2} = \frac{\partial^3 w}{\partial x^3} - \frac{\partial^3 u}{\partial x^2 \partial z}.$$ (2.52)

Likewise, the first and second order derivatives with respect to the z-direction are written as

$$\frac{\partial \zeta}{\partial z} = \frac{\partial^2 w}{\partial x \partial z} - \frac{\partial^2 u}{\partial z^2},$$ (2.53)

and

$$\frac{\partial^2 \zeta}{\partial z^2} = \frac{\partial^3 w}{\partial x \partial z^2} - \frac{\partial^3 u}{\partial z^3}.$$ (2.54)

These derivatives will prove quite useful in the following section.

2.3.2.2 Stream Function Development

In addition to the vorticity concept, a stream function which satisfies the continuity condition is introduced. However, the form of the stream function is dependent on whether or not density is treated as a constant. This results in the presentation of two stream function derivations, one of which will be used in the final CFD code generation.

2.3.2.2.1 Vorticity for Constant Density

For a fluid with constant density, a stream function $\psi(x,z)$ can be found which is related to the x- and z-components of velocity in the following way:

$$u = \frac{\partial \psi}{\partial z} \qquad\qquad (2.55)$$

and

$$w = -\frac{\partial \psi}{\partial x}. \qquad\qquad (2.56)$$

As mentioned by Tannehill et al. (1997), the change in the stream function is related to the change in flow rate of the fluid as

$$\rho \Delta \psi = \rho \frac{\partial \psi}{\partial x} \Delta x + \rho \frac{\partial \psi}{\partial z} \Delta z. \qquad\qquad (2.57)$$

Using the definition for stream function recently derived, this relation becomes

$$\rho \Delta \psi = \rho u \Delta x + \rho w \Delta z \qquad\qquad (2.58)$$

$$\rho \Delta \psi = \rho \overline{u} \cdot \Delta \mathbf{A} \qquad\qquad (2.59)$$

$$\rho \Delta \psi = \Delta \dot{m}. \qquad\qquad (2.60)$$

An obvious result of equation 2.60 is that the stream function term has units of length cubed per unit time, which equates it—in essence—to volumetric flow rate.

The first derivatives of the x-component of velocity with respect to the x- and z-axes are

$$\frac{\partial u}{\partial x} = \frac{\partial^2 \psi}{\partial x \partial z} \qquad\qquad (2.61)$$

and

$$\frac{\partial u}{\partial z} = \frac{\partial^2 \psi}{\partial z^2}. \qquad\qquad (2.62)$$

Likewise, the first derivatives of the z-component of velocity with respect to the x- and z-axes are

$$\frac{\partial w}{\partial x} = -\frac{\partial^2 \psi}{\partial x^2}$$

(2.63)

and

$$\frac{\partial w}{\partial z} = \frac{\partial^2 \psi}{\partial x \partial z}.$$

(2.64)

As a result of the above derivations, the stream function can be related to vorticity in the following manner:

$$\zeta = -\left[\frac{\partial^2 \psi}{\partial x^2} + \frac{\partial^2 \psi}{\partial z^2} \right].$$

(2.65)

Note that this is the elliptical Poisson's equation, where $f(x, z) = -\zeta$.

2.3.2.2.2 Vorticity for Variable Density

If the fluid density is <u>not</u> constant, then a stream function term is derived in the following manner (Tannehill et al., 1997). The steady-state form of the continuity equation from section 2.3.1.1 is

$$\frac{\partial(\rho u)}{\partial x} + \frac{\partial(\rho w)}{\partial z} = 0.$$

(2.66)

The stream function term is then defined as

$$\rho u = \frac{\partial \psi}{\partial z}$$

(2.67)

$$\rho w = -\frac{\partial \psi}{\partial x}$$

(2.68)

To satisfy the vorticity equation, the first spatial derivatives of x- and z-velocity with respect to the z- and x- directions, respectively, are

$$\frac{\partial u}{\partial z} = \frac{\partial}{\partial z}\left(\frac{1}{\rho}\frac{\partial \psi}{\partial z}\right) \qquad (\ 2.69\ )$$

and

$$\frac{\partial w}{\partial x} = -\frac{\partial}{\partial x}\left(\frac{1}{\rho}\frac{\partial \psi}{\partial x}\right) \qquad (\ 2.70\ )$$

Therefore, the vorticity term becomes

$$\zeta = -\left[\frac{\partial}{\partial x}\left(\frac{1}{\rho}\frac{\partial \psi}{\partial x}\right) + \frac{\partial}{\partial z}\left(\frac{1}{\rho}\frac{\partial \psi}{\partial z}\right)\right]. \qquad (\ 2.71\ )$$

Note the complexity in the vorticity equation which is added due to the lack of the constant density assumption. Also evident is the fact that holding the density constant in equation 2.71 gives a similar form to the vorticity of equation 2.65, separated only by a proportional factor of $1/\rho$. Therefore, the stream function used for the ALM calculations is the constant density version developed in section 2.3.2.2.1.

2.3.2.3 Vorticity Transport Equation Development

In this section, the Navier-Stokes (continuity and conservation of momentum), vorticity, and stream function relations are combined to give the vorticity transport equation. This form of the Navier-Stokes equations is that for which the CFD code is developed in CHAPTER 3.

To begin the analysis, the curl is taken on both sides of the conservation of momentum equation developed in section 2.3.1.2 (equation 2.48):

$$\nabla \times [\rho(\mathbf{u} \cdot \nabla)\mathbf{u}] = \nabla \times [\mathbf{f} - \nabla p + \mu \nabla^2 \mathbf{u}].$$ (2.72)

To further expand this equation, each term is developed separately. The convection expression is expanded to give

$$\nabla \times [\rho(\mathbf{u} \cdot \nabla)\mathbf{u}] = \nabla \times \left\{ \rho \left[\left(u\frac{\partial u}{\partial x} + w\frac{\partial u}{\partial z} \right)\hat{i} + \left(u\frac{\partial w}{\partial x} + w\frac{\partial w}{\partial z} \right)\hat{k} \right] \right\}$$

$$= \rho \left[\frac{\partial}{\partial x}\left(u\frac{\partial w}{\partial x} + w\frac{\partial w}{\partial z} \right) - \frac{\partial}{\partial z}\left(u\frac{\partial u}{\partial x} + w\frac{\partial u}{\partial z} \right) \right]$$ (2.73)

$$= \rho \left[u\frac{\partial}{\partial x}\left(\frac{\partial w}{\partial x} - \frac{\partial u}{\partial z} \right) + w\frac{\partial}{\partial z}\left(\frac{\partial w}{\partial x} - \frac{\partial u}{\partial z} \right) \right]$$

Using the definition of vorticity, the convection becomes

$$\nabla \times [\rho(\mathbf{u} \cdot \nabla)\mathbf{u}] = \rho \left[u\frac{\partial \zeta}{\partial x} + w\frac{\partial \zeta}{\partial z} \right].$$ (2.74)

The forcing term—$\nabla \times \mathbf{f}$—is left for section 2.3.3.

The pressure term—$-\nabla \times \nabla p$—is eliminated:

$$-\nabla \times \nabla p = \left(\frac{\partial(\ )}{\partial x}\hat{i} + \frac{\partial(\ )}{\partial x}\hat{k} \right) \times \left(\frac{\partial p}{\partial x}\hat{i} + \frac{\partial p}{\partial x}\hat{k} \right)$$

$$= \frac{\partial^2 p}{\partial x \partial z} - \frac{\partial^2 p}{\partial x \partial z}$$ (2.75)

$$= 0$$

The viscous term is written as

$$\nabla \times \mu \nabla^2 \mathbf{u} = \mu \nabla \times \left[\left(\frac{\partial^2 u}{\partial x^2} + \frac{\partial^2 u}{\partial z^2} \right)\hat{i} + \left(\frac{\partial^2 w}{\partial x^2} + \frac{\partial^2 w}{\partial z^2} \right)\hat{k} \right]$$

$$= \mu \left[\frac{\partial^3 w}{\partial x^3} + \frac{\partial^3 w}{\partial x \partial z} - \frac{\partial^3 u}{\partial x \partial z} - \frac{\partial^3 w}{\partial z^3} \right]$$ (2.76)

$$= \mu \left[\frac{\partial^2}{\partial x^2}\left(\frac{\partial w}{\partial x} - \frac{\partial u}{\partial z} \right) + \frac{\partial^2}{\partial z^2}\left(\frac{\partial w}{\partial x} - \frac{\partial u}{\partial z} \right) \right]$$

Taking the second derivative relations for vorticity, equation 2.76 becomes

$$\nabla \times \mu \nabla^2 \mathbf{u} = \mu \left[\frac{\partial^2 \zeta}{\partial x^2} + \frac{\partial^2 \zeta}{\partial z^2} \right],$$

(2.77)

which is again elliptical. Thus, the Navier-Stokes relations as put into vorticity-stream function transport form are rendered as:

$$\rho \left[u \left(\frac{\partial \zeta}{\partial x} \right) - w \left(\frac{\partial \zeta}{\partial z} \right) \right] = \nabla \times \mathbf{f} + \mu \left(\frac{\partial^2 \zeta}{\partial x^2} + \frac{\partial^2 \zeta}{\partial z^2} \right).$$

(2.78)

The vorticity transport equation can also be written as

$$\rho \left[\left(\frac{\partial \psi}{\partial z} \right) \left(\frac{\partial \zeta}{\partial x} \right) - \left(\frac{\partial \psi}{\partial x} \right) \left(\frac{\partial \zeta}{\partial z} \right) \right] = \nabla \times \mathbf{f} + \mu \left(\frac{\partial^2 \zeta}{\partial x^2} + \frac{\partial^2 \zeta}{\partial z^2} \right).$$

(2.79)

The development of the forcing term, **f**, is somewhat unique to the philosophy through which it is employed in the vorticity transport equation, i.e., whether the Nyborg (section 2.3.3.1) or Lighthill (2.3.3.2) streaming formulation—alluded to in the opening paragraph of this chapter—is employed. Therefore, derivation of the vorticity transport form of the forcing is left to these sections.

2.3.3 Streaming Equations

The primary goal of the Navier-Stokes derivation process is to develop the simplest form of an acoustic streaming equation or equations which will enable computation fluid dynamic modeling of the sound transducer-induced flow field. However, a number of different models exist for describing this flow. For this thesis, two primary formulations are first explored before developing the numerical code—herein named the Nyborg streaming formulation and the Lighthill streaming formulation. Both

formulations basically develop a body force term within the Navier-Stokes equations, which is the mechanism by which acoustic streaming occurs.

2.3.3.1 Nyborg Streaming

Nyborg (1998) developed an acoustic streaming model based on the separation of Navier-Stokes terms of different orders. The derivation of the Nyborg streaming model is presented in detail in this section.

2.3.3.1.1 Navier-Stokes Approximation

Nyborg (1998) derived the streaming force term by separating the Navier-Stokes equation into summations of terms of increasingly higher order. He then set the terms of like order equal to each other in order to develop the final form of the Navier-Stokes equations used for analysis. In order to accomplish this separation of different-order terms, pressure, density, and velocity values (in consecutive order) are approximated as infinite summations of increasing order:

$$p = p_0 + p_1 + p_2 + \cdots$$

$$\rho = \rho_0 + \rho_1 + \rho_2 + \cdots \qquad\qquad (\mathbf{2.80})$$

$$\mathbf{u} = \mathbf{u}_1 + \mathbf{u}_2 + \cdots,$$

where the subscripts "0," "1," and "2," indicate the zeroth order (constant), first order (periodic), and second order (fluctuating) terms, respectively, of the variables. The major assumption driving this particular simplification of the Navier-Stokes equation (and one argued against by Lighthill (1978)) is that terms of order higher than second order are

significantly smaller than lower order terms. Therefore, given that individual third order

and higher terms are ignored, the Navier-Stokes equation becomes

$$\left(\rho_0 + \rho_1 + \rho_2\right)\left[\left(\mathbf{u}_1 + \mathbf{u}_2\right)\cdot\nabla\right]\left(\mathbf{u}_1 + \mathbf{u}_2\right) = -\nabla\left(p_0 + p_1 + p_2\right) + \mu\nabla^2\left(\mathbf{u}_1 + \mathbf{u}_2\right). \qquad (2.81)$$

Since density is considered as constant in this analysis, only its zeroth order term remains,

resulting in the following simplification:

$$\rho_0\left[\left(\mathbf{u}_1\cdot\nabla\right)\mathbf{u}_1 + \left(\mathbf{u}_2\cdot\nabla\right)\mathbf{u}_2\right] = -\nabla\left(p_0 + p_1 + p_2\right) + \mu\nabla^2\left(\mathbf{u}_1 + \mathbf{u}_2\right). \qquad (2.82)$$

As Nyborg discusses, the order of a term of the form $a_l\left(\mathbf{x}_m\cdot\nabla\right)\mathbf{x}_n$ is $l + m + n$, where l, m,

and n represent the order of each individual component of the term. Following from this,

terms of the same order in the derived Navier-Stokes equation can be set equal. Thus, the

partial derivative of the zeroth order of pressure (the constant pressure value) equals zero:

$$\nabla p_0 = 0. \qquad (2.83)$$

Likewise, a conglomeration of first order terms yields the following equation:

$$-\nabla p_1 + \mu\nabla^2\mathbf{u}_1 = 0 \qquad (2.84)$$

The second order relations give the form of the Navier-Stokes equation useful for the

Nyborg formulation:

$$\rho_0\left(\mathbf{u}_1\cdot\nabla\right)\mathbf{u}_1 = -\nabla p_2 + \mu\nabla^2\mathbf{u}_2 \qquad (2.85)$$

Finally, as is evident from the form of the Navier-Stokes equation (2.81), the fourth-order

convection term is zero:

$$\left(\mathbf{u}_2\cdot\nabla\right)\mathbf{u}_2 = 0 \qquad (2.86)$$

In order to simplify the derivation process, the x-component of the Navier-Stokes

equation is now considered with relation to equation 2.85 and is represented as

$$\rho_0 \left[u_1 \frac{\partial u_1}{\partial x} + w_1 \frac{\partial u_1}{\partial z} \right] = -\frac{\partial p_2}{\partial x} + \mu \left[\frac{\partial^2 (u_1 + u_2)}{\partial z^2} + \frac{\partial^2 (u_1 + u_2)}{\partial z^2} \right] \qquad (\,2.87\,)$$

Since the body force developed in section 2.2.3 is a temporal average, the necessity

arrives for taking the time average of the Navier-Stokes relation. This is accomplished

by taking the average of both sides of equation 2.87:

$$\rho_0 \left\langle u_1 \frac{\partial u_1}{\partial x} + w_1 \frac{\partial u_1}{\partial z} \right\rangle = \left\langle -\frac{\partial p_2}{\partial x} + \mu \left[\frac{\partial^2 u_2}{\partial z^2} + \frac{\partial^2 u_2}{\partial z^2} \right] \right\rangle, \qquad (\,2.88\,)$$

where $\langle\ \rangle$ indicates that the time average value of the terms is being calculated. Since the

density term is constant, its average is equal to its zeroth order term. Therefore, it is

removed from the averaging brackets for simplification. Thus, the following simplified

form of the x-component of the Navier-Stokes equation is derived:

$$\rho_0 \left\langle u_1 \frac{\partial u_1}{\partial x} + w_1 \frac{\partial u_1}{\partial z} \right\rangle = -\frac{\partial \langle p_2 \rangle}{\partial x} + \mu \left[\frac{\partial^2 \langle u_2 \rangle}{\partial z^2} + \frac{\partial^2 \langle u_2 \rangle}{\partial z^2} \right]. \qquad (\,2.89\,)$$

Likewise, the z-component is

$$\rho_0 \left\langle u_1 \frac{\partial w_1}{\partial x} + w_1 \frac{\partial w_1}{\partial z} \right\rangle = -\frac{\partial \langle p_2 \rangle}{\partial z} + \mu \left[\frac{\partial^2 \langle w_2 \rangle}{\partial z^2} + \frac{\partial^2 \langle w_2 \rangle}{\partial z^2} \right] \qquad (\,2.90\,)$$

Finally, the vector form of the Navier-Stokes equation is written as

$$\rho_0 \left\langle (\mathbf{u}_1 \cdot \nabla) \mathbf{u}_1 \right\rangle = -\nabla \langle p_2 \rangle + \mu \nabla^2 \langle \mathbf{u}_2 \rangle. \qquad (\,2.91\,)$$

This is the basic form of the Navier-stokes equation used to calculate streaming effects

using the Nyborg formulation. The term $\mathbf{u}_2$ is the streaming velocity of interest. The

$\rho_0 \langle (\mathbf{u}_1 \cdot \nabla)\mathbf{u}_1 \rangle$ term is the convective term due to nonlinear sound and is further

developed in the next section.

2.3.3.1.2 Forcing Term

Evident from the final form of equation 2.91 is the following body force within

the fluid of interest:

$$\mathbf{f} = \rho_0 \langle (\mathbf{u}_1 \cdot \nabla)\mathbf{u}_1 \rangle, \qquad (2.92)$$

where $\mathbf{f}$ is a second-order body force which acts on the fluid due to first-order convection.

Since the individual velocity terms involved in this expression are of first order and can

thus be considered as periodic, this force can actually be represented as the Reynolds

stress term discussed in section 2.2.3.2. Therefore,

$$\mathbf{f} = \rho_0 \langle (\mathbf{u}_1 \cdot \nabla)\mathbf{u}_1 \rangle = -\left(\frac{\alpha}{c}\right)\langle I_2 \rangle \hat{\mathbf{e}}, \qquad (2.93)$$

where $\langle I_2 \rangle$ is the time-averaged acoustic intensity. Finally, the fundamental Nyborg

formulation of the Navier-Stokes equation is

$$-\left(\frac{\alpha}{c}\right)\langle I_2 \rangle \hat{\mathbf{e}} = -\nabla \langle p_2 \rangle + \mu \nabla^2 \langle \mathbf{u}_2 \rangle. \qquad (2.94)$$

2.3.3.1.3 Nyborg Streaming in Vorticity Transport Form

In this section, the Navier-Stokes equations (continuity and conservation of

momentum) and vorticity and stream function relations are combined to give the vorticity

transport form of the Nyborg streaming equation. To begin the analysis, the curl is taken

on both sides of the conservation of momentum equation:

$$\nabla \times \left[-\left(\frac{\alpha}{c}\right)\langle I_2 \rangle \hat{\mathbf{e}} \right] = \nabla \times \left(-\nabla \langle p_2 \rangle + \mu \nabla^2 \langle \mathbf{u}_2 \rangle \right). \tag{2.95}$$

This results in

$$-\left(\frac{\alpha}{c}\right)\left[\nabla \times \langle I_2 \rangle \hat{\mathbf{e}} \right] = -\langle \nabla \times \nabla p_2 \rangle + \mu \nabla \times \nabla^2 \langle \mathbf{u}_2 \rangle. \tag{2.96}$$

The curl of the body force term is

$$
\begin{aligned}
-\left(\frac{\alpha}{c}\right)\left[\nabla \times \langle I_2 \rangle \hat{\mathbf{e}} \right] &= -\left(\frac{\alpha}{c}\right)\left[\nabla \times \left(\langle I_2 \rangle \hat{i} + \langle I_2 \rangle \hat{k} \right) \right] \\
&= -\left(\frac{\alpha}{c}\right)\left(\frac{\partial \langle I_2 \rangle}{\partial x} - \frac{\partial \langle I_2 \rangle}{\partial z} \right)
\end{aligned}
\tag{2.97}
$$

As derived in section 2.3.2.3, the pressure term is

$$\nabla \times \nabla \langle p_2 \rangle = 0, \tag{2.98}$$

while the viscous term becomes

$$\nabla \times \mu \nabla^2 \langle \mathbf{u} \rangle = -\mu \left(\frac{\partial^2 \langle \varsigma_2 \rangle}{\partial x^2} + \frac{\partial^2 \langle \varsigma_2 \rangle}{\partial z^2} \right). \tag{2.99}$$

Thus, the Navier-Stokes relations are now put into vorticity-stream function transport form:

$$-\left(\frac{\alpha}{c}\right)\left(\frac{\partial \langle I_2 \rangle}{\partial x} - \frac{\partial \langle I_2 \rangle}{\partial z} \right) = \mu \left(\frac{\partial^2 \langle \varsigma_2 \rangle}{\partial x^2} + \frac{\partial^2 \langle \varsigma_2 \rangle}{\partial z^2} \right), \tag{2.100}$$

which is an elliptical equation.

2.3.3.2 Lighthill Streaming

Sir James Lighthill (1978) took a different approach to acoustic streaming from Nyborg. He explained that approximating terms above second order to be significantly smaller than terms at or below second order may be detrimental to correct development of the Navier-Stokes equations. Lighthill contended that streaming is due to and should be modeled using a body force which acts on the fluid subjected to a nonlinear sound field. This body force is also actually a time-averaged Reynolds stress.

2.3.3.2.1 Streaming Force Development

Once again, as shown in section 2.3.1.2, the fundamental Navier-Stokes equation is

$$\rho(\mathbf{u} \cdot \nabla)\mathbf{u} = \mathbf{f} - \nabla p + \mu \nabla^2 \mathbf{u}. \qquad (2.101)$$

Lighthill (1978) explained that the forcing term in the Navier-Stokes equation due to acoustic streaming is the spatial derivative of the time average of the Reynolds stress term (in the direction of sound propagation):

$$f_i = -\frac{\partial \langle \rho u_i u_j \rangle}{\partial x_i}. \qquad (2.102)$$

In vector notation, this becomes

$$\mathbf{f} = -\langle \rho[(\mathbf{u} \cdot \nabla)\mathbf{u} + \mathbf{u}(\nabla \cdot \mathbf{u})] \rangle \qquad (2.103)$$

As previously, conservation of mass is held. Thus,

$$\mathbf{u}(\nabla \cdot \mathbf{u}) = 0. \qquad (2.104)$$

Consequently, the forcing function (with constant density) now becomes

$$\mathbf{f} = -\rho\langle(\mathbf{u}\cdot\nabla)\mathbf{u}\rangle,$$

(2.105)

which is strikingly similar to that developed using the Nyborg formulation of the previous section. In fact, it is also of the same form as the streaming body force previously developed. Therefore, the following equation holds true for Lighthill streaming:

$$\mathbf{f} = -\rho\langle(\mathbf{u}\cdot\nabla)\mathbf{u}\rangle = \left(\frac{\alpha}{c}\right)\langle I\rangle\hat{\mathbf{e}}.$$

(2.106)

As a result, the Lighthill streaming form of the Navier-Stokes equations become

$$\rho(\mathbf{u}\cdot\nabla)\mathbf{u} = \left(\frac{\alpha}{c}\right)\langle I\rangle\hat{\mathbf{e}} - \nabla p + \mu\nabla^2\mathbf{u}.$$

(2.107)

2.3.3.2.2 Lighthill Streaming in Vorticity Transport Form

Since the Lighthill streaming formulation utilizes the basic form of the Navier-Stokes equation, it takes the form of

$$\rho\left[\left(\frac{\partial\psi}{\partial z}\right)\left(\frac{\partial\zeta}{\partial x}\right) - \left(\frac{\partial\psi}{\partial x}\right)\left(\frac{\partial\zeta}{\partial z}\right)\right] = \nabla\times\mathbf{f} + \mu\left(\frac{\partial^2\zeta}{\partial x^2} + \frac{\partial^2\zeta}{\partial z^2}\right)$$

(2.108)

as presented in section 2.3.2.3. Therefore, only the forcing term $\nabla\times\mathbf{f}$ needs to be expounded upon here.

Because the force is developed for the Navier-Stokes equations in primitive form, for the streaming force to be in a consistent form with the vorticity-stream function transport equation, it is necessary to develop the force in a consistent structure. This is accomplished by taking the negative of the curl of the forcing function:

$$\nabla \times \mathbf{f} = \left(\frac{\alpha}{c}\right)\begin{vmatrix} \dfrac{\partial}{\partial x} & \dfrac{\partial}{\partial z} \\ \langle I \rangle & \langle I \rangle \end{vmatrix} = \left(\frac{\alpha}{c}\right)\left(\frac{\partial \langle I \rangle}{\partial x} - \frac{\partial \langle I \rangle}{\partial z}\right).$$

(2.109)

Combining this forcing function with the vorticity-stream function form of the Navier-Stokes equation gives its final form:

$$\rho\left[\left(\frac{\partial \psi}{\partial z}\right)\left(\frac{\partial \zeta}{\partial x}\right) - \left(\frac{\partial \psi}{\partial x}\right)\left(\frac{\partial \zeta}{\partial z}\right)\right] = \left(\frac{\alpha}{c}\right)\left(\frac{\partial \langle I \rangle}{\partial x} - \frac{\partial \langle I \rangle}{\partial z}\right) + \mu\left(\frac{\partial^2 \zeta}{\partial x^2} + \frac{\partial^2 \zeta}{\partial z^2}\right).$$

(2.110)

2.3.3.3 Boundary Conditions

An important (and absolutely necessary) consideration in computing the streaming solution is the development of correct boundary conditions of the tank. Although for the acoustic solution the problem is considered to be unbounded, this does not hold be true for the streaming solution (velocity profile). For example, recirculation may occur in the tank while it is subjected to acoustic streaming. The boundaries of the tank would act to route the recirculation paths. As a result, the streaming solution for this study is formulated for a two-dimensional tank with solid boundaries.

2.3.3.3.1 Primitive Variable Boundary Conditions

From the no-slip condition imposed on the solid boundaries, the velocity components along the tank walls are found to be

$$u(0, z) = u(W, z) = u(x, 0) = u(x, L) = 0$$

(2.111)

and

$$w(0, z) = w(W, z) = w(x, 0) = w(x, L) = 0,$$

(2.112)

where L and W represent the tank length and width, respectively. In addition, the following relation holds true at the left and right tank walls, respectively:

$$\left.\frac{\partial w}{\partial x}\right|_{x=0,z} = \left.\frac{\partial w}{\partial x}\right|_{x=W,z} = 0.$$

(2.113)

Likewise, the following relation holds true at the front and rear tank walls, respectively:

$$\left.\frac{\partial u}{\partial z}\right|_{x,z=0} = \left.\frac{\partial u}{\partial z}\right|_{x,z=L} = 0.$$

(2.114)

2.3.3.3.2 *Vorticity Transport Equation Boundary Conditions*

Finally, the stream function term—$\psi(x,z)$—has a value of zero at the tank boundaries (Tannehill et al., 1997). In the next chapter, the discretized forms of these relations are combined using a Taylor series expansion of the stream function to represent the boundary conditions using vorticity terms.

Following from equations 2.111 and 2.112 in the previous section and equations 2.55 and 2.56 in section 2.3.2.2.1,

$$\left.\frac{\partial \psi}{\partial x}\right|_{x=0,z} = \left.\frac{\partial \psi}{\partial x}\right|_{x=W,z} = \left.\frac{\partial \psi}{\partial x}\right|_{x,z=0} = \left.\frac{\partial \psi}{\partial x}\right|_{x,z=W} = 0$$

(2.115)

and

$$\left.\frac{\partial \psi}{\partial z}\right|_{x=0,z} = \left.\frac{\partial \psi}{\partial z}\right|_{x=W,z} = \left.\frac{\partial \psi}{\partial z}\right|_{x,z=0} = \left.\frac{\partial \psi}{\partial z}\right|_{x,z=W} = 0$$

(2.116)

A Taylor series expansion of the stream function term with respect to z at the tank front wall boundary is represented as

$$\psi(x,\Delta z) = \psi(x,0) + \frac{\partial \psi}{\partial z}\bigg|_{x,z=0} \Delta z + \frac{1}{2}\frac{\partial^2 \psi}{\partial z^2}\bigg|_{x,z=0} (\Delta z)^2 + \ldots + \frac{1}{n}\frac{\partial^n \psi}{\partial z^n}\bigg|_{x,z=0} (\Delta z)^n. \qquad (2.117)$$

Since

$$\frac{\partial \psi}{\partial z}\bigg|_{x,0} = u(x,0) = 0, \qquad (2.118)$$

if terms higher than second order are approximated to be negligible, the equation can be rewritten as

$$\frac{\partial^2 \psi}{\partial z^2}\bigg|_{x,z=0} = \frac{2[\psi(x,\Delta z) - \psi(x,0)]}{(\Delta z)^2} \qquad (2.119)$$

Using similar representations of Taylor series expansion for the other three wall locations, the following expressions at wall boundaries are determined:

$$\frac{\partial^2 \psi}{\partial z^2}\bigg|_{x,z=L} = \frac{2[\psi(x,L-\Delta z) - \psi(x,L)]}{(\Delta z)^2}, \qquad (2.120)$$

$$\frac{\partial^2 \psi}{\partial x^2}\bigg|_{x=0,z} = \frac{2[\psi(\Delta x,z) - \psi(0,z)]}{(\Delta x)^2}, \qquad (2.121)$$

and

$$\frac{\partial^2 \psi}{\partial x^2}\bigg|_{x=W,z} = \frac{2[\psi(W-\Delta x,z) - \psi(W,z)]}{(\Delta x)^2}. \qquad (2.122)$$

Finally, the vorticity term at the walls is evaluated. At the front wall, the vorticity magnitude is written as

$$\zeta(x,0) = -\left(\frac{\partial^2 \psi}{\partial x^2}\bigg|_{x,z=0} + \frac{\partial^2 \psi}{\partial z^2}\bigg|_{x,z=0}\right) \qquad (2.123)$$

The first term on the right hand is found to be zero. This is due to the fact that

$$\left.\frac{\partial^2 \psi}{\partial x^2}\right|_{x,z=0} = -\left.\frac{\partial w}{\partial x}\right|_{x,z=0} = 0 , \qquad (2.124)$$

which falls from developments in the previous section. Therefore, after substituting for

the second right-side term, the vorticity at the front wall becomes

$$\zeta(x,0) = -\frac{2[\psi(x,\Delta z) - \psi(x,0)]}{\Delta z^2} \qquad (2.125)$$

Since the stream function is a constant at the boundaries (Tannehill et al., 1997), an

assumption can be made which allows the stream function at the boundaries to be set to

zero. Therefore, equation 2.125 becomes

$$\zeta(x,0) = -\frac{2\psi(x,\Delta z)}{\Delta z^2} \qquad (2.126)$$

Likewise, the following are found to be true at the remaining tank walls:

$$\zeta(x,L) = -\frac{2\psi(x,L - \Delta z)}{\Delta z^2} , \qquad (2.127)$$

$$\zeta(0,z) = -\frac{2\psi(\Delta x,z)}{\Delta x^2} , \qquad (2.128)$$

and

$$\zeta(W,z) = -\frac{2\psi(W - \Delta x,z)}{\Delta x^2} . \qquad (2.129)$$

As will be shown in CHAPTER 3, these boundary conditions will be called upon for the

numerical computation of the vorticity transport equations prior to retransformation of

the stream function into the primitive velocity terms.

2.4 Heating Effects

An additional effect of ALM is heating of the fluid due to nonlinear sound. This section shows the methodology used to calculate the temperature profile of the tank while the transducer was excited. As will be presented, the temperature profile is only achieved after derivation of the energy equation.

2.4.1 Theoretical Development

The following two-dimensional representation of the energy equation was given by Incropera and DeWitt (2002) and is modified here to account for the time rate of temperature change within a fluid:

$$\rho c_p \left(\frac{\partial T}{\partial t} + u \frac{\partial T}{\partial x} + w \frac{\partial T}{\partial z} \right) =$$

$$\lambda \left(\frac{\partial^2 T}{\partial x^2} + \frac{\partial^2 T}{\partial z^2} \right) + \mu \left[2 \left(\frac{\partial u}{\partial x} \right)^2 + 2 \left(\frac{\partial w}{\partial z} \right)^2 + \left(\frac{\partial u}{\partial z} + \frac{\partial w}{\partial x} \right)^2 - \frac{2}{3} \left(\frac{\partial u}{\partial x} + \frac{\partial w}{\partial z} \right)^2 \right], \qquad (2.130)$$

where T is the fluid temperature, c_p is the specific heat of the fluid, λ is the thermal conductivity of the fluid, ρ is the fluid density, and μ is the viscosity of the fluid. However, after considering the form of continuity previously developed in section 2.3.1.1, specifically $\dfrac{\partial u}{\partial x} + \dfrac{\partial w}{\partial z} = 0$, the energy relation reduces to

$$\rho c_p \left(\frac{\partial T}{\partial t} + u \frac{\partial T}{\partial x} + w \frac{\partial T}{\partial z} \right) =$$

$$\lambda \left(\frac{\partial^2 T}{\partial x^2} + \frac{\partial^2 T}{\partial z^2} \right) + \mu \left[2 \left(\frac{\partial u}{\partial x} \right)^2 + 2 \left(\frac{\partial w}{\partial z} \right)^2 + \left(\frac{\partial u}{\partial z} + \frac{\partial w}{\partial x} \right)^2 \right]. \qquad (2.131)$$

Using the stream function, this becomes

$$-\left(\frac{\partial^2 T}{\partial x^2}+\frac{\partial^2 T}{\partial z^2}\right)=-\left(\frac{\rho c_p}{\lambda}\right)\left[\frac{\partial T}{\partial t}+\left(\frac{\partial \psi}{\partial z}\right)\left(\frac{\partial T}{\partial x}\right)-\left(\frac{\partial \psi}{\partial z}\right)\left(\frac{\partial T}{\partial z}\right)\right]+$$
$$+\left(\frac{\mu}{\lambda}\right)\left[2\left(\frac{\partial^2 \psi}{\partial x\partial z}\right)^2+2\left(-\frac{\partial^2 \psi}{\partial x\partial z}\right)^2+\left(\frac{\partial^2 \psi}{\partial z^2}-\frac{\partial^2 \psi}{\partial x^2}\right)^2\right]. \qquad (2.132)$$

Equation 2.132 is the basic form of the energy equivalence and is discretized in the next chapter in order to allow the temperature profile of the fluid tank to be calculated.

2.4.2 Time-Varying Temperature Term

Although the time-dependent terms were ignored for the Navier-Stokes equations, they are considered when dealing with the temperature equation. As seen in section 2.2.4, Mann et al. (2005) show that the time rate of change in fluid temperature term due to the nonlinear sound is

$$\frac{dT(\vec{r})}{dt}=\frac{\omega^2\mu\left(\frac{4}{3}+\frac{1-\gamma}{\text{Pr}}\right)}{2\rho^3 c_f{}^4 C_T}\langle p(\vec{r})\rangle^2, \qquad (2.133)$$

where ω is the sound frequency in radians per second, $p(\vec{r})$ is the time-averaged sound pressure, k is the acoustic wave number, ρ is the density of the fluid, c_f is the specific heat of the fluid, μ is the fluid viscosity, γ is the specific heat ratio, Pr is the fluid Prandtl number, and C_T is the isothermal specific heat of the fluid.

The term developed above acts as the thermal "forcing," or heat generation, that drives temperature differences in the fluid caused by the nonlinear sound. However, it does not serve as the only possible mechanism for heat generation. Dissipation within the fluid due to viscous motion is a major contributor. Additionally, heat dissipated by

the sound transducer itself could be considered as a boundary condition and is developed in the next section.

2.4.3 Boundary Conditions

The tank model was investigated for two boundary condition sets. The first is simply for a tank with sidewalls held at a constant temperature. For this set, heat dissipated by the transducer is considered to be negligible. The purpose of this particular set of boundary conditions is to observe the extent of any heat that would be dissipated within the fluid itself. The idea is to determine the magnitude of heating effects caused by the nonlinear acoustics of the transducer and the fluid motion itself.

The second set of boundary conditions is identical to the first, with the exception that a uniform heat load is assumed at the tank boundary where the transducer is located. This heat load is due to inefficiencies within the transducer itself. The assumption of a uniform heat load is considered by the author to be a conservative estimate of heating within the tank since the only heat dissipation path will be for heat to spread within the fluid itself. This would potentially give a maximum temperature differential within the fluid.

The boundary along the wall with the transducer is developed using the one-dimensional form of Fourier's equation (Incropera & DeWitt, 2002):

$$-\lambda A \frac{dT}{dz}\bigg|_{z=0} = q \,, \qquad (\,2.134\,)$$

where q is the power dissipated by the transducer transformed into heat and A is the area of the transducer. This condition is only valid in the transducer location along the wall of the tank at $z = 0$ and over the surface of the heat source.

2.5 General Comments

This chapter presented an overview of the required theory for full development of an acoustic streaming and heating model. Although general in nature, the concepts explained in this chapter lays the foundation for the computational fluid dynamic formulation presented in CHAPTER 3. However, the theory must be evaluated with respect to the assumptions levied upon it, which come into play during the closing chapters of this thesis.

CHAPTER 3. NUMERICAL DEVELOPMENT

With the goal of computing the tank fluid velocity and temperature fields due to the acoustic streaming effects of ALM, utilizing a finite difference scheme, the fundamental fluid dynamics and heat transfer equations developed in CHAPTER 2 were discretized over a grid of nodes and spacing identical to that established for the acoustic solution. This chapter describes the development of the discrete form of the fundamental fluid and energy equations. However, prior to presenting the numerical approximations to the Navier-Stokes and heat transfer relations, general terms using an arbitrary function, $g(x,z)$, are investigated in order to fully describe the necessary expressions for obtaining a solution. The study of this dependent variable results in discrete terms for the first, second, and mixed partial derivatives, which are subsequently applied to the fundamental fluid and heat transfer equations.

3.1 Generalized Discretization

Discretization of the continuity, conservation of momentum, and conservation of energy equations was conducted using a mixture of finite difference relations. The discrete form for each of these relations was derived using a combination of terms derived from a number of forms of Taylor series. The methodologies and philosophies drawn on to eventually create a CFD model are presented in this section, beginning with an analysis based on various forms of Taylor series.

3.1.1 Using a Taylor Series for Discretization

The basis of the grid used for the ALM investigation is a five-point grid formula (see Figure 3.1). The foundation for this model may be found from various sources, including Tannehill et al. (1997).
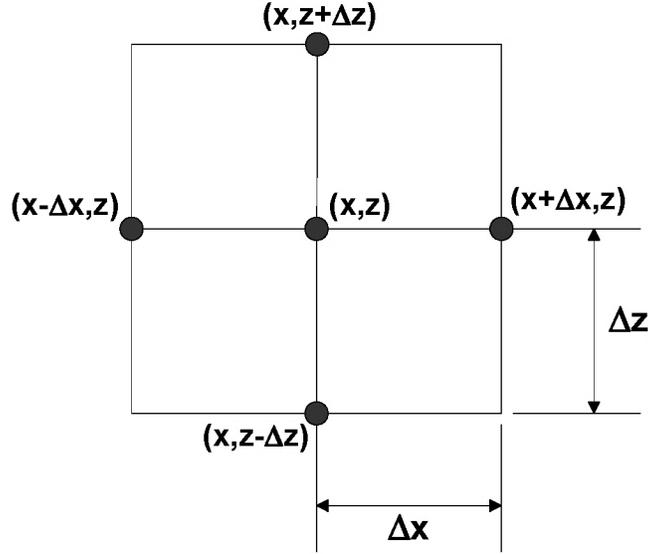
Figure 3.1 Grid for Five-Point Formulation

The forward Taylor series for an arbitrary function $g(x,z)$ with respect to the x-axis is defined as

$$g(x + \Delta x, z) - g(x, z) = \frac{\partial g(x, z)}{\partial x} \Delta x + \frac{\partial^2 g(x, z)}{\partial x^2} \frac{(\Delta x)^2}{2} + \ldots + \frac{\partial^n g(x, z)}{\partial x^n} \frac{(\Delta x)^n}{n}. \quad (3.1)$$

Likewise, the backward Taylor series for the same function is found to be of the following form:

$$g(x - \Delta x, z) - g(x, z) = \frac{\partial g(x, z)}{\partial x} (-\Delta x) + \frac{\partial^2 g(x, z)}{\partial x^2} \frac{(\Delta x)^2}{2} + \ldots + \frac{\partial^n g(x, z)}{\partial x^n} \frac{(-\Delta x)^n}{n}. \quad (3.2)$$

To extract an approximation of the first derivative of the generic function $g(x,z)$ with respect to the x-direction, the forward and backward Taylor series are subtracted and terms higher than second order are eliminated to get

$$g(x + \Delta x, z) - g(x - \Delta x, z) = 2 \frac{\partial g(x, z)}{\partial x} \Delta x.$$
(3.3)

The equation is rearranged as

$$\frac{\partial g(x, z)}{\partial x} = \frac{g(x + \Delta x, z) - g(x - \Delta x, z)}{2 \Delta x}.$$
(3.4)

Next, the addition of the forward and backward equations and elimination of terms beyond second order is performed to achieve the second derivative of $g(x,z)$ with respect to the x-direction:

$$g(x + \Delta x, z) + g(x - \Delta x, z) = 2g(x, z) + \frac{\partial^2 g(x, z)}{\partial x^2} (\Delta x)^2,$$
(3.5)

which is rearranged for simplification:

$$\frac{\partial^2 g(x, z)}{\partial x^2} = \frac{g(x + \Delta x, z) - 2g(x, z) + g(x - \Delta x, z)}{(\Delta x)^2}.$$
(3.6)

Following the same line of reasoning, the first and second derivatives approximations of $g(x,z)$ with respect to z are established:

$$\frac{\partial g(x, z)}{\partial z} = \frac{g(x, z + \Delta z) - g(x, z - \Delta z)}{2 \Delta z}$$
(3.7)

and

$$\frac{\partial g^2(x, z)}{\partial z^2} = \frac{g(x, z + \Delta z) - 2g(x, z) + g(x, z - \Delta z)}{(\Delta z)^2}.$$
(3.8)

When reflecting back on equation 2.132, one notices that in addition to the partial

derivatives found in during the derivation of the fluid motion and energy equations,

mixed partial derivatives are present and therefore must be approximated for

completeness. In order to find a mixed partial derivative, $\dfrac{\partial^2 g(x,z)}{\partial x \partial z}$, one must

necessarily evaluate the function $g(x,y)$ at the coordinates $(x + \Delta x, y + \Delta y)$, $(x - \Delta x, y + \Delta y)$, $(x + \Delta x, y - \Delta y)$, and $(x - \Delta x, y - \Delta y)$. The following succession of equations shows

the form of the Taylor series for each coordinate point required:

$$g(x + \Delta x, z + \Delta z) - g(x, z) =$$

$$\left(\Delta x \frac{\partial}{\partial x} + \Delta z \frac{\partial}{\partial z} \right) g(x, z) + \frac{1}{2} \left(\Delta x \frac{\partial}{\partial x} + \Delta z \frac{\partial}{\partial z} \right)^2 g(x, z) + \ldots, \qquad (3.9)$$

$$g(x - \Delta x, z + \Delta z) - g(x, z) =$$

$$\left(-\Delta x \frac{\partial}{\partial x} + \Delta z \frac{\partial}{\partial z} \right) g(x, z) + \frac{1}{2} \left(-\Delta x \frac{\partial}{\partial x} + \Delta z \frac{\partial}{\partial z} \right)^2 g(x, z) + \ldots, \qquad (3.10)$$

$$g(x + \Delta x, z - \Delta z) - g(x, z) =$$

$$\left(\Delta x \frac{\partial}{\partial x} - \Delta z \frac{\partial}{\partial z} \right) g(x, z) + \frac{1}{2} \left(\Delta x \frac{\partial}{\partial x} - \Delta z \frac{\partial}{\partial z} \right)^2 g(x, z), \qquad (3.11)$$

and

$$g(x - \Delta x, z - \Delta z) g(x, z) =$$

$$\left(-\Delta x \frac{\partial}{\partial x} + -\Delta z \frac{\partial}{\partial z} \right) g(x, z) + \frac{1}{2} \left(-\Delta x \frac{\partial}{\partial x} - \Delta z \frac{\partial}{\partial z} \right)^2 g(x, z). \qquad (3.12)$$

Now that the previous four relations have been derived, equations 3.9 and 3.12 are added.

Subtracted from the sum of these two equations are equations 3.10 and 3.11. The

combination of these relations results in the following second-order approximation:

$$g(x + \Delta x, z + \Delta z) - g(x - \Delta x, z + \Delta z) -$$

$$g(x + \Delta x, z - \Delta z) + g(x - \Delta x, z - \Delta z) = 4\Delta x \Delta z \frac{\partial^2 g(x, z)}{\partial x \partial z}. \tag{3.13}$$

Solving for the mixed partial derivative term $\dfrac{\partial^2 g(x, z)}{\partial x \partial z}$ gives the final expression:

$$\frac{\partial^2 g(x, z)}{\partial x \partial z} = \frac{1}{4\Delta x \Delta z} [g(x + \Delta x, z + \Delta z) - g(x - \Delta x, z + \Delta z)$$
$$- g(x + \Delta x, z - \Delta z) + g(x - \Delta x, z - \Delta z)] \tag{3.14}$$

In addition to this numerical treatment of the mixed partial derivative, Tannehill et al.

(1997) explains a number of other representations that are possible. However, these

alternative representations are deemed unnecessary and contrary to the desired

methodology at hand and are neither presented nor discussed during this study.

3.1.2 Discretized Terms in Subscript Form

With the intention of shortening the form of the above equations and provide

continuity between "pen and paper" representation and symbolization within the

Matlab® code environment, the functional $g(x,z)$ rendering is dropped in favor of a

subscript notation. Thus, the function $g(x,z)$ is represented as

$$g(x, z) = g_{i,k}. \tag{3.15}$$

The first and second derivatives are likewise shown to be

$$\frac{\partial g(x,z)}{\partial x} = \frac{\partial g}{\partial x}\bigg|_{i,k} = \frac{g_{i+1,k} - g_{i-1,k}}{2\Delta x}, \tag{3.16}$$

$$\frac{\partial g^2(x,z)}{\partial x^2} = \frac{\partial^2 g}{\partial x^2}\bigg|_{i,k} = \frac{g_{i+1,k} - 2g_{i,k} + g_{i+1,k}}{(\Delta x)^2}, \tag{3.17}$$

$$\frac{\partial g(x,z)}{\partial z} = \frac{\partial g}{\partial z}\bigg|_{i,k} = \frac{g_{i,k+1} - g_{i,k-1}}{2\Delta z}, \tag{3.18}$$

and

$$\frac{\partial g^2(x,z)}{\partial z^2} = \frac{\partial^2 g}{\partial z^2}\bigg|_{i,k} = \frac{g_{i,k+1} - 2g_{i,k} + g_{i,k-1}}{(\Delta z)^2}. \tag{3.19}$$

which—in subscript notation—is represented as

$$\frac{\partial g^2(x,z)}{\partial x \partial z} = \frac{\partial^2 g}{\partial x \partial z}\bigg|_{i,k} = \frac{g_{i+1,k+1} - g_{i-1,k+1} - g_{i+1,k-1} + g_{i-1,k-1}}{4\Delta x \Delta z}. \tag{3.20}$$

While x and z insinuate continuity, the subscripts i and k indicate a particular (discrete) x- and z-coordinate point. Specifically, the subscripts represent the nodal coordinates on the (i,k) plane. The analogue to the five-point grid shown in Figure 3.1 is apparent in Figure 3.2.
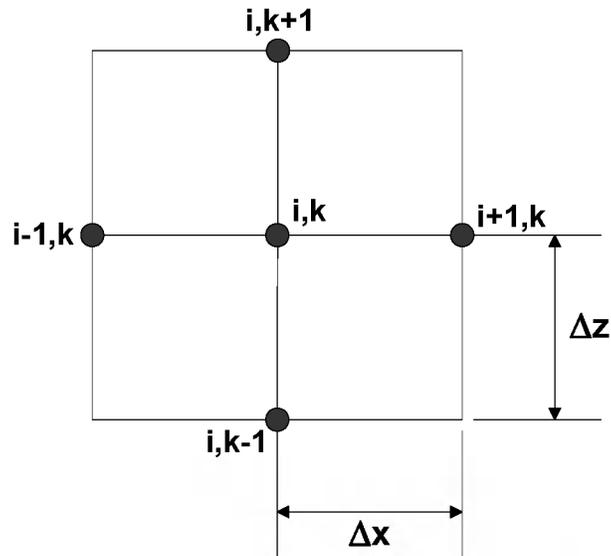
Figure 3.2 Grid for Five-Point Formulation Using Subscript Notation

3.1.3 Summary of Discretized Terms

The following is a summary of discretized terms for the five-point grid model shown in this chapter, which includes basic dependent variables, first partial derivatives, second partial derivatives, and mixed partial derivatives.

- **Basic Dependent Variable**

$$g(x, z) = g_{i,k} \tag{3.21}$$

- **First Partial Derivatives**

$$\left. \frac{\partial g}{\partial x} \right|_{i,k} = \frac{g_{i+1,k} - g_{i-1,k}}{2\Delta x} \tag{3.22}$$

$$\left. \frac{\partial g}{\partial z} \right|_{i,k} = \frac{g_{i,k+1} - g_{i,k-1}}{2\Delta z} \tag{3.23}$$

- **Second Partial Derivatives**

$$\left.\frac{\partial^2 g}{\partial x^2}\right|_{i,k} = \frac{g_{i+1,k} - 2g_{i,k} + g_{i+1,k}}{(\Delta x)^2} \qquad (3.24)$$

$$\left.\frac{\partial^2 g}{\partial z^2}\right|_{i,k} = \frac{g_{i,k+1} - 2g_{i,k} + g_{i,k-1}}{(\Delta z)^2} \qquad (3.25)$$

- **Mixed Partial Derivative**

$$\left.\frac{\partial^2 g}{\partial x \partial z}\right|_{i,k} = \frac{g_{i+1,k+1} - g_{i-1,k+1} - g_{i+1,k-1} + g_{i-1,k-1}}{4\Delta x \Delta z} \qquad (3.26)$$

These six discretized terms lay the foundation for the discretization of the Navier-Stokes and energy equations.

3.1.4 Comments on Discretization Methods

As with most numerical approximation methodologies, numerous methods for discretizing the Navier-Stokes and energy equations are available and each is valid in its own right. For example, rather than choosing to transform the expressions into an approximate form which contains a solution only at discrete points (using a Taylor series or integral method), one might opt instead to model the equations using a finite volume philosophy and perform an energy balance on each element. Or, one may utilize decide to adopt a finite element approach and utilize polynomial relations to approximate the fluid flow. As alluded to in the previous paragraphs, the above derivations by no means serve as a "standard" or "all-inclusive" method of obtaining an approximation of the dependent variables. However, this methodology proved to the author to be very straightforward and simple in its implementation.

3.2 Streaming Velocity Field Discretization

The streaming velocity as developed in CHAPTER 2 using two methods—

Nyborg streaming formulation and Lighthill streaming formulation—is further developed

in this section to facilitate computation of the streaming velocity fields using CFD code.

Results of the discretized equation derivation shown in the previous section are

substituted into vorticity-stream function form of the Navier-Stokes expressions.

3.2.1 Nyborg Streaming Discretization

As developed in section 2.3.3.1, the Nyborg streaming equation is

$$-\left(\frac{\alpha}{c}\right)\left(\frac{\partial\langle I_2\rangle}{\partial z} - \frac{\partial\langle I_2\rangle}{\partial x}\right) = \mu\left(\frac{\partial^2\langle \varsigma_2\rangle}{\partial x^2} + \frac{\partial^2\langle \varsigma_2\rangle}{\partial z^2}\right),$$

$$(3.27)$$

where the right side of the expression is elliptic and thus amenable to the five point

solution. The form of the left side of the equation is irrelevant due to the fact that it was

determined from the acoustic solution and is thus a known value at each grid point (i,k)

for this study.

Using the discretization methods developed in section 3.1, the equation is

approximated as

$$-\left(\frac{\alpha}{c}\right)\left(\frac{\langle I_2\rangle_{i+1,k} - \langle I_2\rangle_{i-1,k}}{2\Delta x} - \frac{\langle I_2\rangle_{i,k+1} - \langle I_2\rangle_{i,k-1}}{2\Delta z}\right)$$
$$= \mu\left(\frac{\langle \varsigma_2\rangle_{i+1,k} - 2\langle \varsigma_2\rangle_{i,k} + \langle \varsigma_2\rangle_{i-1,k}}{(\Delta x)^2} + \frac{\langle \varsigma_2\rangle_{i,k+1} - 2\langle \varsigma_2\rangle_{i,k} + \langle \varsigma_2\rangle_{i,k-1}}{(\Delta z)^2}\right).$$

$$(3.28)$$

Solving for the vorticity term gives

$$\langle \zeta_2 \rangle_{i,k} = \frac{1}{2\mu} \left(\frac{1}{(\Delta x)^2} + \frac{1}{(\Delta z)^2} \right)^{-1} \left[\mu \left(\frac{\langle \zeta_2 \rangle_{i+1,k} + \langle \zeta_2 \rangle_{i-1,k}}{(\Delta x)^2} + \frac{\langle \zeta_2 \rangle_{i,k+1} + \langle \zeta_2 \rangle_{i,k-1}}{(\Delta z)^2} \right) \right.$$
$$\left. + \left(\frac{\alpha}{c} \right) \left(\frac{\langle I_2 \rangle_{i+1,k} - \langle I_2 \rangle_{i-1,k}}{2\Delta x} - \frac{\langle I_2 \rangle_{i,k+1} - \langle I_2 \rangle_{i,k-1}}{2\Delta z} \right) \right] \quad . \quad (3.29)$$

As presented in section 2.3.3.1.3, vorticity transport equation is

$$\langle \zeta_2 \rangle = -\left[\frac{\partial^2 \langle \psi_2 \rangle}{\partial x^2} + \frac{\partial^2 \langle \psi_2 \rangle}{\partial z^2} \right] , \quad (3.30)$$

which is also an elliptic partial differential equation. In discretized form, this equation is approximated as

$$\langle \zeta_2 \rangle_{i,k} = -\left[\frac{\langle \psi_2 \rangle_{i+1,k} - 2\langle \psi_2 \rangle_{i,k} + \langle \psi_2 \rangle_{i-1,k}}{(\Delta x)^2} + \frac{\langle \psi_2 \rangle_{i,k+1} - 2\langle \psi_2 \rangle_{i,k} + \langle \psi_2 \rangle_{i,k-1}}{(\Delta z)^2} \right] . \quad (3.31)$$

Finally, solving for the stream function term at the point of interest results in

$$\langle \psi_2 \rangle_{i,k} = \frac{1}{2} \left[\frac{1}{(\Delta x)^2} + \frac{1}{(\Delta z)^2} \right]^{-1} \left[\langle \zeta_2 \rangle_{i,k} \right.$$
$$\left. + \frac{\langle \psi_2 \rangle_{i+1,k} + \langle \psi_2 \rangle_{i-1,k}}{(\Delta x)^2} + \frac{\langle \psi_2 \rangle_{i,k+1} + \langle \psi_2 \rangle_{i,k-1}}{(\Delta z)^2} \right] . \quad (3.32)$$

One last step is required in order to achieve the necessary terms for characterization of the velocity field. Similar to that shown in section 2.3.2.2.1, the stream function used in this analysis is described by the following two equations:

$$\langle u_2 \rangle = \frac{\partial \langle \psi_2 \rangle}{\partial z} \quad (3.33)$$

and

$$\langle w_2 \rangle = -\frac{\partial \langle \psi_2 \rangle}{\partial x}. \qquad (3.34)$$

Using the first-order finite difference relations derived in the previous section, the discretized versions of these equations are

$$\langle u_2 \rangle_{i,k} = \frac{\langle \psi_2 \rangle_{i,k+1} - \langle \psi_2 \rangle_{i,k-1}}{2\Delta z} \qquad (3.35)$$

and

$$\langle w_2 \rangle_{i,k} = -\frac{\langle \psi_2 \rangle_{i+1,k} - \langle \psi_2 \rangle_{i-1,k}}{2\Delta z}. \qquad (3.36)$$

These two equations can subsequently be used to plot the velocity field of the tank since the terms $\langle u_2 \rangle_{i,k}$ and $\langle w_2 \rangle_{i,k}$ are the velocities at each node point on the grid.

Another useful value is the scalar velocity at each point. This is calculated simply as

$$\langle U_2 \rangle_{i,k} = \sqrt{\left(\langle u_2 \rangle_{i,k}\right)^2 + \left(\langle w_2 \rangle_{i,k}\right)^2}. \qquad (3.37)$$

3.2.2 Lighthill Streaming Discretization

In order to determine the streaming velocity using the Lighthill streaming formulation, discretization is initially performed for the modified vorticity-stream function method of the Navier-Stokes equations. Using relations previously developed, the equation for vorticity is represented as

$$\zeta = -\left[\frac{\partial^2 \psi}{\partial x^2} + \frac{\partial^2 \psi}{\partial z^2}\right]. \qquad (3.38)$$

Using the finite difference method of discretization presented in section 3.1, the

discretized version of this equation (using the finite difference method) is found to be the

following:

$$\zeta_{i,k} = -\left[\frac{\psi_{i+1,k} - 2\psi_{i,k} + \psi_{i-1,k}}{(\Delta x)^2} + \frac{\psi_{i,k+1} - 2\psi_{i,k} + \psi_{i,k-1}}{(\Delta z)^2}\right].$$ (3.39)

This equation is solved for the stream function at location (i,k):

$$\psi_{i,k} = \frac{1}{2}\left[\frac{1}{(\Delta x)^2} + \frac{1}{(\Delta z)^2}\right]^{-1}\left[\zeta_{i,k}\right.$$
$$\left. + \frac{\psi_{i+1,k} + \psi_{i-1,k}}{(\Delta x)^2} + \frac{\psi_{i,k+1} + \psi_{i,k-1}}{(\Delta z)^2}\right].$$ (3.40)

In addition, as developed in sections 2.3.1 and 2.3.3.2.2, the vorticity transport

equation is defined as

$$u\frac{\partial \zeta}{\partial x} + w\frac{\partial \zeta}{\partial z} = \left(\frac{\mu}{\rho}\right)\left(\frac{\partial^2 \zeta}{\partial x^2} + \frac{\partial^2 \zeta}{\partial z^2}\right) + \left(\frac{\alpha}{\rho c}\right)\left(\frac{\partial \langle I\rangle}{\partial z} - \frac{\partial \langle I\rangle}{\partial x}\right).$$ (3.41)

When approximated using the finite difference method, the vorticity transport equation is

found to be

$$\left(\frac{\psi_{i,k+1} - \psi_{i,k-1}}{2\Delta z}\right)\left(\frac{\zeta_{i+1,k} - \zeta_{i-1,k}}{2\Delta x}\right) - \left(\frac{\psi_{i+1,k} - \psi_{i-1,k}}{2\Delta x}\right)\left(\frac{\zeta_{i,k+1} - \zeta_{i,k-1}}{2\Delta z}\right)$$
$$= \frac{\mu}{\rho}\left(\frac{\zeta_{i+1,k} - 2\zeta_{i,k} + \zeta_{i-1,k}}{(\Delta x)^2} + \frac{\zeta_{i,k+1} - 2\zeta_{i,k} + \zeta_{i,k-1}}{(\Delta z)^2}\right)$$ (3.42)
$$+ \left(\frac{\alpha}{\rho c}\right)\left(\frac{\langle I\rangle_{i,k+1} - \langle I\rangle_{i,k-1}}{2\Delta z} - \frac{\langle I\rangle_{i+1,k} - \langle I\rangle_{i-1,k}}{2\Delta x}\right)$$

In order for this approximation to prove useful, the equation is solved for the vorticity

term, $\zeta_{i,k}$:

$$\zeta_{i,k}$$

$$
= \frac{1}{2\upsilon}\left[\frac{1}{(\Delta x)^2}+\frac{1}{(\Delta z)^2}\right]^{-1}\left\{-\left(\frac{\psi_{i,k+1}-\psi_{i,k-1}}{2\Delta z}\right)\left(\frac{\zeta_{i+1,k}-\zeta_{i-1,k}}{2\Delta x}\right)\right.
$$

$$
+\left(\frac{\psi_{i+1,k}-\psi_{i-1,k}}{2\Delta x}\right)\left(\frac{\zeta_{i,k+1}-\zeta_{i,k-1}}{2\Delta z}\right) \qquad (3.43)
$$

$$
+\upsilon\left(\frac{\zeta_{i+1,k}+\zeta_{i-1,k}}{(\Delta x)^2}+\frac{\zeta_{i,k+1}+\zeta_{i,k-1}}{(\Delta z)^2}\right)
$$

$$
\left.-\left(\frac{\alpha}{\rho c}\right)\left(\frac{\langle I_2\rangle_{i+1,k}-\langle I_2\rangle_{i-1,k}}{2\Delta x}-\frac{\langle I_2\rangle_{i,k+1}-\langle I_2\rangle_{i,k-1}}{2\Delta z}\right)\right\}
$$

Similar to the Nyborg streaming formulation, the velocity terms are calculated as

$$
u_{i,k}=\frac{\psi_{i,k+1}-\psi_{i,k-1}}{2\Delta z}, \qquad (3.44)
$$

$$
w_{i,k}=-\frac{\psi_{i+1,k}-\psi_{i-1,k}}{2\Delta z}, \qquad (3.45)
$$

and

$$
U_{i,k}=\sqrt{\left(u_{i,k}\right)^2+\left(w_{i,k}\right)^2}. \qquad (3.46)
$$

3.3 Temperature Field Discretization

Section 2.4.1 showed the development of the energy equation from its most basic

form. The purpose of energy equation development for characterizing ALM is to

determine the temperature profile of the water-filled tank during transducer operation.

This will show any heating that occurs in the fluid as a result of its being subjected to

nonlinear sound from the transducer. As a result, the following form of energy

conservation was determined valid for use[2]:

$$-\left(\frac{\partial^2 T}{\partial x^2}+\frac{\partial^2 T}{\partial z^2}\right)=-\left(\frac{\rho c_p}{\lambda}\right)\left[\frac{\partial T}{\partial t}+\left(\frac{\partial \psi}{\partial z}\right)\left(\frac{\partial T}{\partial x}\right)-\left(\frac{\partial \psi}{\partial z}\right)\left(\frac{\partial T}{\partial z}\right)\right]+$$
$$+\left(\frac{\mu}{\lambda}\right)\left[2\left(\frac{\partial^2 \psi}{\partial x \partial z}\right)^2+2\left(-\frac{\partial^2 \psi}{\partial x \partial z}\right)^2+\left(\frac{\partial^2 \psi}{\partial z^2}-\frac{\partial^2 \psi}{\partial x^2}\right)^2\right]\right] \qquad (3.47)$$

where the temporal term is

$$\frac{\partial T}{\partial t}=\frac{dT(\bar{r})}{dt}=\frac{\omega^2\mu\left(\frac{4}{3}+\frac{1-\gamma}{\mathrm{Pr}}\right)}{2\rho^3 c_f{}^4 C_T}\langle p(\bar{r})\rangle^2 \qquad (3.1)$$

as presented in section 2.2.4. Discretization of this relation gives

$$-\left(\frac{T_{i+1,k}-2T_{i,k}+T_{i-1,k}}{(\Delta x)^2}+\frac{T_{i,k+1}-2T_{i,k}+T_{i,k-1}}{(\Delta z)^2}\right)=\left\{-\left(\frac{\rho c_p}{\lambda}\right)\left[\frac{\partial T}{\partial t}\bigg|_{i,k}\right.\right.$$
$$+\left(\frac{\psi_{i,k+1}-\psi_{i,k-1}}{2\Delta z}\right)\left(\frac{T_{i+1,k}-T_{i-1,k}}{2\Delta x}\right)-\left(\frac{\psi_{i+1,k}-\psi_{i-1,k}}{2\Delta x}\right)\left(\frac{T_{i,k+1}-T_{i,k-1}}{2\Delta z}\right)\right]$$
$$+\left(\frac{\mu}{\lambda}\right)\left[4\left(\frac{\psi_{i+1,k+1}-\psi_{i-1,k+1}-\psi_{i+1,k-1}-\psi_{i-1,k-1}}{4\Delta x\Delta z}\right)^2\right.$$
$$+\left(\frac{\psi_{i,k+1}-2\psi_{i,k}+\psi_{i,k-1}}{(\Delta z)^2}-\frac{\psi_{i+1,k}-2\psi_{i,k}+\psi_{i-1,k}}{(\Delta x)^2}\right)^2\right]\right\} \qquad (3.48)$$

This equation is then solved for the temperature $T_{i,k}$:

---

[2] Note that this equation is assumed to be valid for both the Nyborg and the Lighthill streaming formulations. In Nyborg streaming, the subscript denoting the second-order nature of the terms is implied in the energy equation presented in this section.

$$
T_{i+1,k} = \left\{ \frac{T_{i+1,k} + T_{i-1,k}}{(\Delta x)^2} + \frac{T_{i,k+1} + T_{i,k-1}}{(\Delta z)^2} - \left(\frac{\rho c_p}{\lambda} \right) \left[\frac{\partial T}{\partial t} \right|_{i,k} \right.
$$

$$
+ \left(\frac{\psi_{i,k+1} - \psi_{i,k-1}}{2\Delta z} \right) \left(\frac{T_{i+1,k} - T_{i-1,k}}{2\Delta x} \right) - \left(\frac{\psi_{i+1,k} - \psi_{i-1,k}}{2\Delta x} \right) \left(\frac{T_{i,k+1} - T_{i,k-1}}{2\Delta z} \right) \right]
$$

$$
+ \left(\frac{\mu}{\lambda} \right) \left[4 \left(\frac{\psi_{i+1,k+1} - \psi_{i-1,k+1} - \psi_{i+1,k-1} - \psi_{i-1,k-1}}{4\Delta x \Delta z} \right)^2 \right.
$$

$$
\left. \left. + \left(\frac{\psi_{i,k+1} - 2\psi_{i,k} + \psi_{i,k-1}}{(\Delta z)^2} - \frac{\psi_{i+1,k} - 2\psi_{i,k} + \psi_{i-1,k}}{(\Delta x)^2} \right)^2 \right] \right\}
$$

$$
\times \left(\frac{1}{2} \right) \left(\frac{1}{(\Delta x)^2} + \frac{1}{(\Delta z)^2} \right)^{-1}
$$

$$
(3.49)
$$

Previously developed in 2.4.3 were the boundary conditions for energy considerations within the tank. For the case of constant wall temperatures, the discretized boundary conditions are simply

$$
T_{1,k} = T_{M,k} = T_{i,1} = T_{i,N} = T_{WALL} \tag{3.50}
$$

where T_{WALL} is the temperature at the tank walls. For the special case where heat dissipation from the transducer is considered, the boundary condition along the wall in the location of the transducer was previously determined to be

$$
-\lambda A \frac{dT}{dz} \bigg|_{z=0} = q. \tag{3.51}
$$

In order to have a useful form for a numerical solution, the above equation is discretized using the same dimensional iterations as used with the rest of the tank. Assuming that the power dissipation from the transducer is uniform over the wall surface at the location of the transducer, discretization is accomplished by breaking up the transducer length into

small increments equal to the grid spacing used for the fluid solution. Figure 3.3 shows a diagram of the transducer broken up into discrete sections to coincide with the tank meshing strategy.
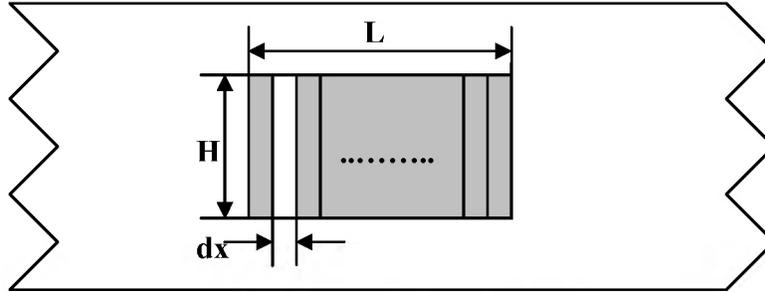

Figure 3.3 Transducer Discretization Scheme

As a result, the following equation is applicable to each element of the transducer:

$$ -\lambda H \Delta x \frac{dT}{dz}\bigg|_{z=0} = \frac{q}{L / \Delta x}. $$ (3.52)

In this equation, the product $H\Delta x$ is the area of one element and $q/(L/\Delta x)$ is the power to each individual element of the transducer. (Note that $L/\Delta x$ gives the number of elements used to partition the transducer for the numerical solution.) Although developed here, heat dissipation from the transducer was not actively pursued due to initial non-convergence of the subsequently developed code.

3.4 CFD Code

In order to determine the velocity, temperature, and pressure fields of the tank with a sound transducer producing the ALM phenomenon, the development of code to implement the discretized fundamental fluids equations was necessary. To simplify this process [mainly due to the fact that the author has limited knowledge of the variety of code languages], Matlab® was chosen as the program used to solve the fluid dynamics

and heat transfer portion of the ALM problem. This complemented the development of the ALM Program nicely since the ALM Program code was also written using Matlab®, and the CFD code was ultimately integrated with the ALM code.

3.4.1 Iteration Methodology

In order to calculate the velocity and temperature fields, the discretized equations were used in a Gauss-Siedel iterative manner of computation similar to that posed by Tannehill et al. (1997). Since the form of the Navier-Stokes equation used to calculate the velocity terms was decoupled from the energy equation (and thus did not depend on temperature as a driving factor, although temperature depended on velocity), the velocity and temperature fields were not calculated simultaneously, rather in sequence, beginning with the fluid dynamics equations. The following two sections outline the steps which are performed after the acoustic solution (radiation pressure, sound intensity) is obtained.

3.4.1.1 Velocity Field

The following steps outline the process taken to calculate the streaming velocity using a simple iteration schema.

(1) Each point in the vorticity and stream function fields is arbitrarily chosen to have an initial value of zero.

(2) The vorticity and stream function values at each point (i,k) are calculated based on the initial values within their respective fields for the $(i+1,k)$, $(i-1,k)$, $(i,k+1)$, and

$(i,k-1)$ locations.

(3) The errors for the dependent variables are calculated using the methodology

described next.

    a. **Stream Function:** The error in stream function is calculated as

$$\varepsilon_1 = \left| \psi_{i,k} - \psi_{i,k,OLD} \right|,$$
(3.53)

where ε_1 is the error in stream function for the current iteration, $\psi_{i,k}$ is the

value of the stream function calculated for the current iteration, and

$\psi_{i,k,OLD}$ is the value of the stream function calculated for the previous

iteration.

    b. **Vorticity:** The vorticity error is calculated as

$$\varepsilon_2 = \left| \zeta_{i,k} - \zeta_{i,k,OLD} \right|,$$
(3.54)

where ε_2 is the error in vorticity for the current iteration, $\zeta_{i,k}$ is the value

of vorticity calculated for the current iteration, and $\zeta_{i,k,OLD}$ is the value of

vorticity calculated for the previous iteration.

As the calculation process continues for each iteration step, the solution is

assumed to become more and more accurate, which is reflected in the reduction of

ε_1 and ε_2 in value.

(4) After the error in vorticity has reached the predetermined "convergence" value,

the iteration process for calculating vorticity ceases. Once the stream function

converges with a predetermined acceptable error, it will likewise cease iterating.

If the errors for either terms have values greater than the maximum allowed, the

steps 1 through 3 are repeated.

(5) Once the errors have reached the predetermined convergence value, the *x*- and *z*-components of velocity—as well as the velocity magnitude—for each grid point are calculated:

$$u_{i,k} = \frac{\psi_{i,k+1} - \psi_{i,k-1}}{2\Delta z},$$ (3.55)

$$w_{i,k} = -\left[\frac{\psi_{i+1,k} - \psi_{i-1,k}}{2\Delta x}\right],$$ (3.56)

and

$$U_{i,k} = \sqrt{(u_{i,k})^2 + (w_{i,k})^2}.$$ (3.57)

If the error calculated is smaller than or equal to some predetermined value, the solution is assumed to have converged. If the error is greater than the predetermined value, steps 1 through 3 are performed again.

3.4.1.2 Temperature Field

Once the velocity field is determined, the temperature field is calculated as follows.

(1) Each point in the temperature field is initially set to the ambient temperature of the tank.

(2) The temperature values at each point (*i,k*) are calculated based on the initial values within their respective fields for the (*i*+1,*k*), (*i*-1,*k*), (*i,k*+1), and (*i,k*-1) locations.

(3) The temperature error is calculated as

$$\varepsilon_3 = \left| T_{i,k} - T_{i,k,OLD} \right| \hspace{6cm} (3.58)$$

where ε_3 is the error in temperature for the current iteration, $T_{i,k}$ is the value of the temperature calculated for the current iteration, and $T_{i,k,OLD}$ is the value of temperature calculated during the previous iteration.

(4) Once the error in temperature reaches the predetermined "convergence" value, the iteration process for calculating temperature ceases. If the error is greater than the predetermined value, steps 1 through 3 are performed again.

3.5 Code Validation—Lid-Driven Cavity Problem

To determine the validity of the methodology described in this chapter, the lid-driven cavity problem was solved using a slight modification of the final code. This modified code removed the acoustically-induced body force and inserted a boundary condition at the maximum z-dimension of a steady velocity in the positive x-direction. Figure 3.4 through Figure 3.6 display results of a driven cavity calculation for a fluid in a one unit length by one unit length tank with a Reynolds number value of 400 and a lid velocity of one unit velocity. The results compare well with those produced by Pereira and Campos Silva (2005).
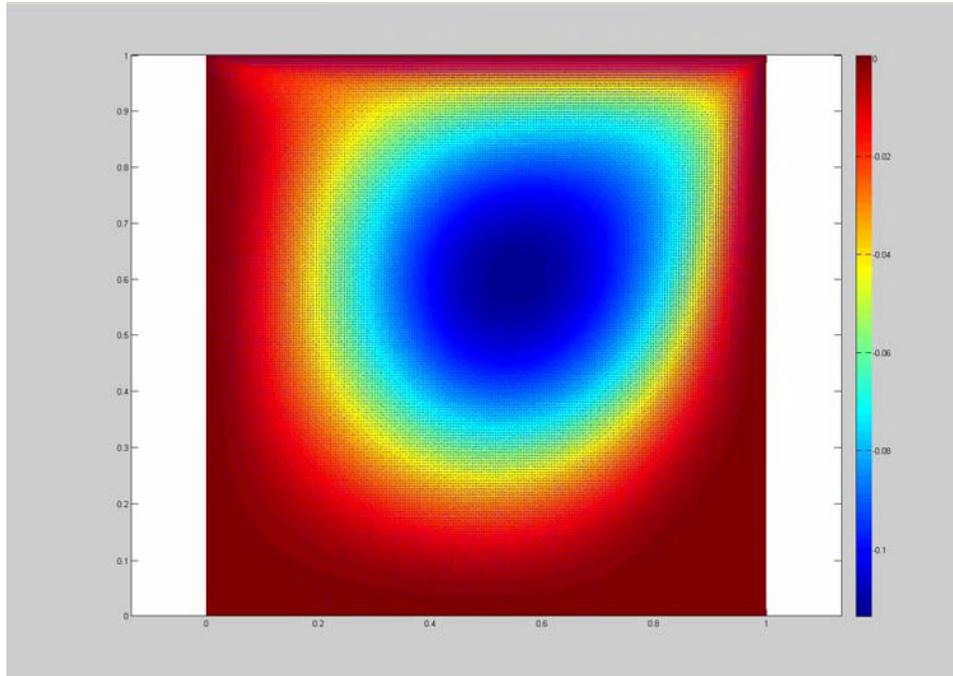
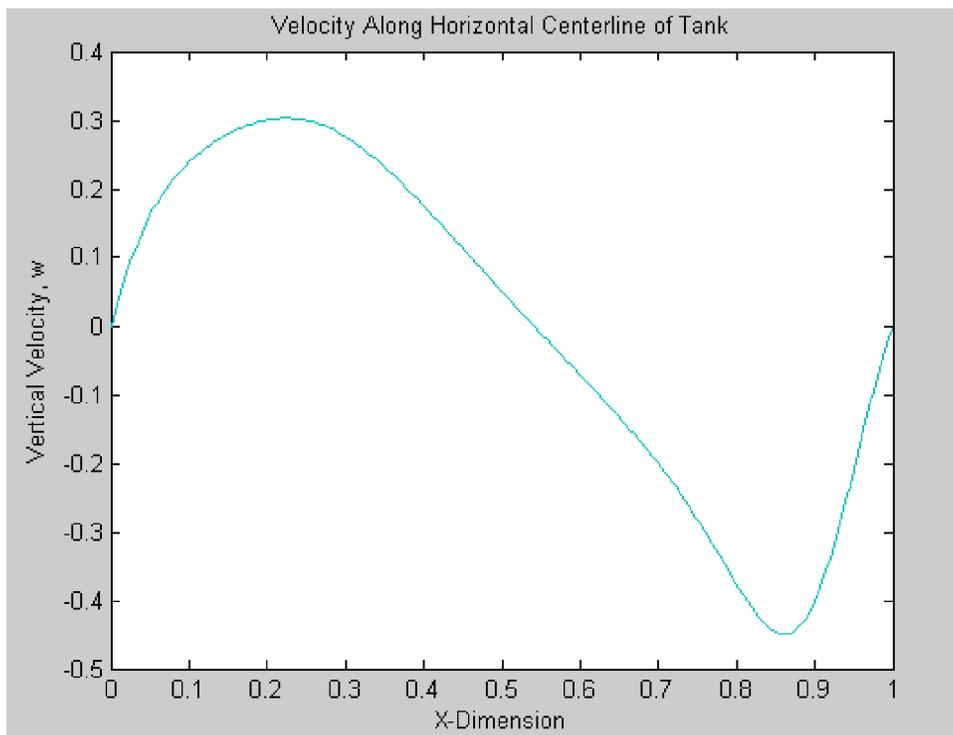**Figure 3.4 Results of Lid-Driven Cavity Flow Stream Function Using Code for Re = 400**

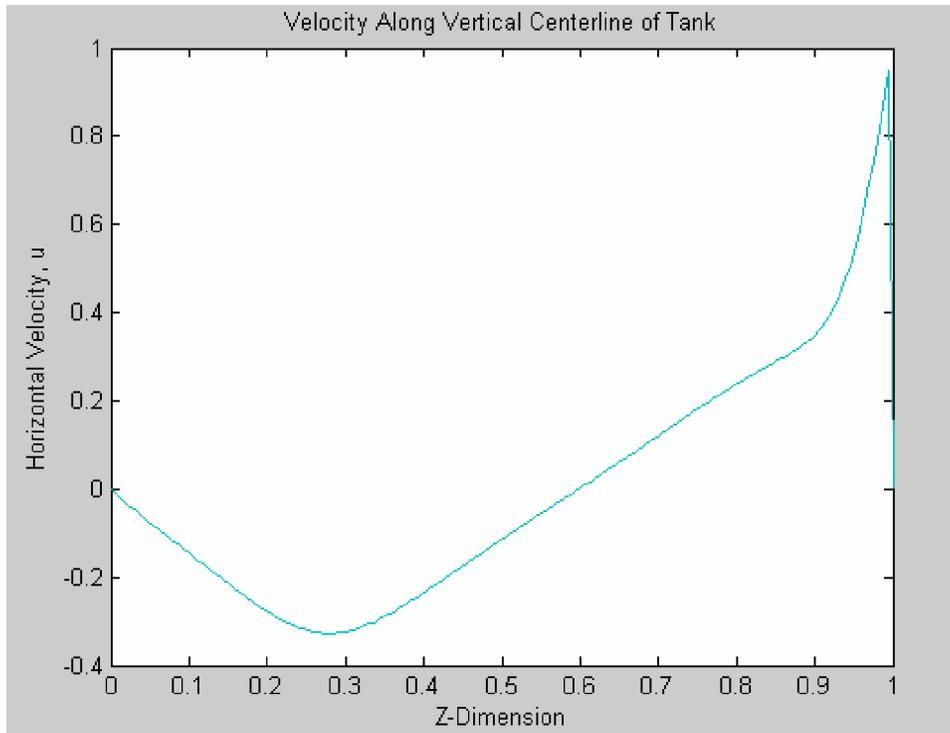**Figure 3.5 Vertical Velocity of Driven Cavity Along Horizontal Centerline**

Figure 3.6 Horizontal Velocity of Driven Cavity Along Vertical Centerline

3.6 Concluding Remarks

Although simple in nature, the finite differencing and subsequent iteration

methods presented in this chapter form the basis of code development for the solution of

the acoustic streaming problem. The appendix gives the finite difference code used

within Matlab® to implement the equations developed in this chapter. CHAPTER 4

presents the integration of the CFD code into the "ALM Program."

CHAPTER 4. "ALM PROGRAM" DEVELOPMENT

In order to efficiently calculate the effects of nonlinear sound on streaming and heating phenomena within a fluid medium using the simple geometric setup for which theoretical and numerical development presented in CHAPTER 2 and CHAPTER 3 was performed, a graphical user interface (GUI) integrating the nonlinear sound, streaming, and heating effects of ALM was created in the Matlab® environment. "ALM Program" was realized using Matlab® Student Version 6.0.0.42a Release 12 due to its preprogrammed codes and ease of implementation. The purpose of this program was to conduct the following ALM calculations:

- sound pressure,

- change in temperature over time,

- force on a bubble due to radiation pressure,

- velocity field, and

- temperature field.

These computations were performed using a three-step process:

(1) determine the fluid properties;

(2) calculate the acoustic solution (sound pressure, change in temperature, force on a bubble, and streaming force); and

(3) compute the velocity and temperature fields of the fluid using computational fluid dynamic code.

The remainder of this chapter is dedicated to a discussion of the highlights of "ALM Program," as well as a brief overview of how to use the program.

4.1 "ALM Program" Background

The "ALM Program" code was implemented using an existing Matlab® program created by Dr. Adin Mann. The original code utilized the acoustic solution relations for radiation pressure, change in temperature over time, streaming body force, and radiation pressure force on a bubble as presented in section 2.2. "ALM Program" was then expanded to perform CFD calculations to determine the streaming and temperature profiles of a rectangular tank. Other features included in the expanded version were a built-in database of various fluid properties for evaluation and instructions on how to use the property retrieval system. Although integrated with and vital to the program at hand, the details of the acoustic solution (section 2.2 material) are not discussed in this study.

4.2 "ALM Program" Description

As touched upon in the previous section, the CFD solution was integrated into the "ALM Program" using the framework which already existed for the original code. This allows the acoustic solutions—such as radiation pressure and streaming body force—to be saved and reused for the CFD solution during an analysis session. Additionally, the property values entered into or selected from the ALM Program GUI are retained and thus useful for the CFD calculations. Figure 4.1 shows the "ALM Program" in its startup state.

Figure 4.1 ALM GUI

4.2.1 ALM GUI Features

The ALM Program, although simple in nature, includes many features for simplifying the calculation of the acoustic, fluid, and thermal fields. These features are discussed in the following subsections

4.2.1.1 Fluid Property Retrieval

The fluid "Property Retrieval" feature has been added to the original ALM Program allow the user to select fluid properties for fluids common in a zero-gravity application—such as liquid hydrogen—as well as water for practical experimentation in a laboratory setting. In addition, a feature has been developed which allows manual entry of fluid properties.

4.2.1.1.1 Instructions

A set of instructions for usage of the ALM Program was developed in order to allow the user to obtain accurate results. These instructions are embedded in the program and can be accessed by clicking the left mouse button on the "Instructions" button. The instructions are shown in Figure 4.2.
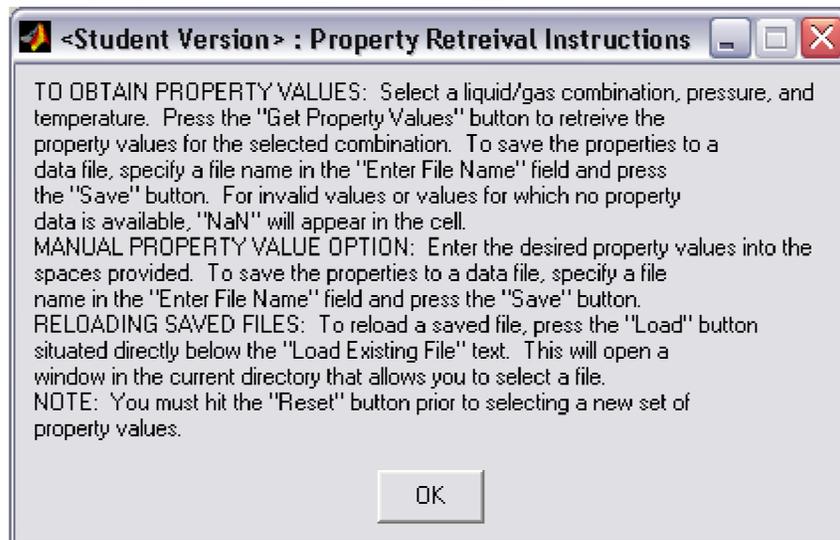
Figure 4.2 ALM GUI Instructions

4.2.1.1.2 Drop-Down Menu

Data "m" files containing fluid property information were written for each fluid/gas combination and have been stored in the ALM Program directory for recall on demand by the user. The following liquid/gas property combinations have been added to a drop-down menu in "Property Retrieval:"

- water/air;

- hydrogen/hydrogen vapor;

- hydrogen/helium gas;

- nitrogen/nitrogen vapor;

- nitrogen/helium gas;

- oxygen/oxygen vapor; and

- oxygen/helium gas.

Figure 4.3 shows the drop-down menu feature of "Property Retrieval."

Figure 4.3 Fluid/Gas Combination Selection

4.2.1.1.3 Manual Fluid Property Input

In addition to the fluid "Property Retrieval" feature implemented in the "ALM Program," an option was designed into the program to manually input fluid properties. When fluid properties are manually input (or input using the "Property Retrieval" menu as well), the properties may be saved as a ".mat" data file under a name of the user's choosing. The saved data file resides in the same directory as the program files and can be recalled using the "Load" button.

4.2.1.2 Solution Parameters

A section of the GUI was designed to input parameters of the transducer, tank, and bubble under scrutiny. These parameters are follows:

- transducer type (rectangular or disk);

- transducer size (x- and y-dimensions for the rectangular option, radius for the disk option);

- transducer frequency (in MHz);

- transducer power dissipated as heat;

- tank dimensions;

- number of grid points in the x- and z-directions; and

- bubble diameter.

4.2.2 Program Execution

Once all property values and solution parameters are chosen, "ALM Program" execution is accomplished in two phases:

1. execution of "ALM Program" and

2. execution of "CFD Solution."

This is accomplished by using a mouse to left click on the buttons corresponding to each. (Note that one must find the acoustic solution first, which requires activation of the "ALM Program" button as a primary step before activating the "CFD Solution" button.)

4.3 Results Presentation

The "ALM Program" was designed to effectively convey the calculated results using graphical methods. The pressure, fluid, and temperature fields were all plotted on two-dimensional grids.

4.3.1 ALM Calculations

Figure 4.4 gives an example of the results obtained for water at room temperature by executing the "Run ALM Program" feature. The solution sets calculated are for sound pressure, temperature change (dT/dt), fluid streaming body force (in the form of the streaming force divided by the density of the liquid), and force on a bubble for the chosen diameter. All values are given in SI units.
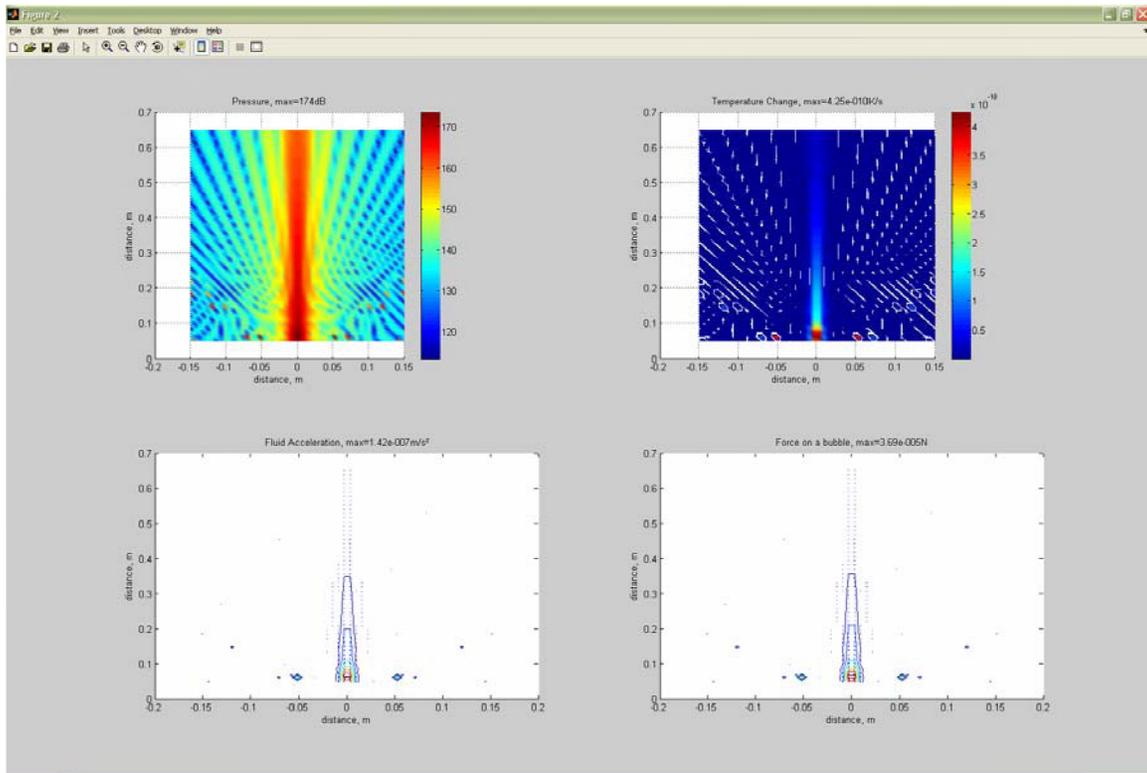
Figure 4.4 Example Solution of Acoustic Solution Displaying Sound Pressure, Temperature Change, Fluid Acceleration, and Force on a Bubble

4.3.2 CFD Solution

As articulated earlier in this chapter, once the acoustic solution is calculated, the CFD portion of ALM Program may be invoked to compute the velocity and temperature fields of a fluid during an ALM event. Figure 4.5 and Figure 4.6 show examples of the output expected for the streaming velocity and temperature solutions, respectively. Once again, units are SI.
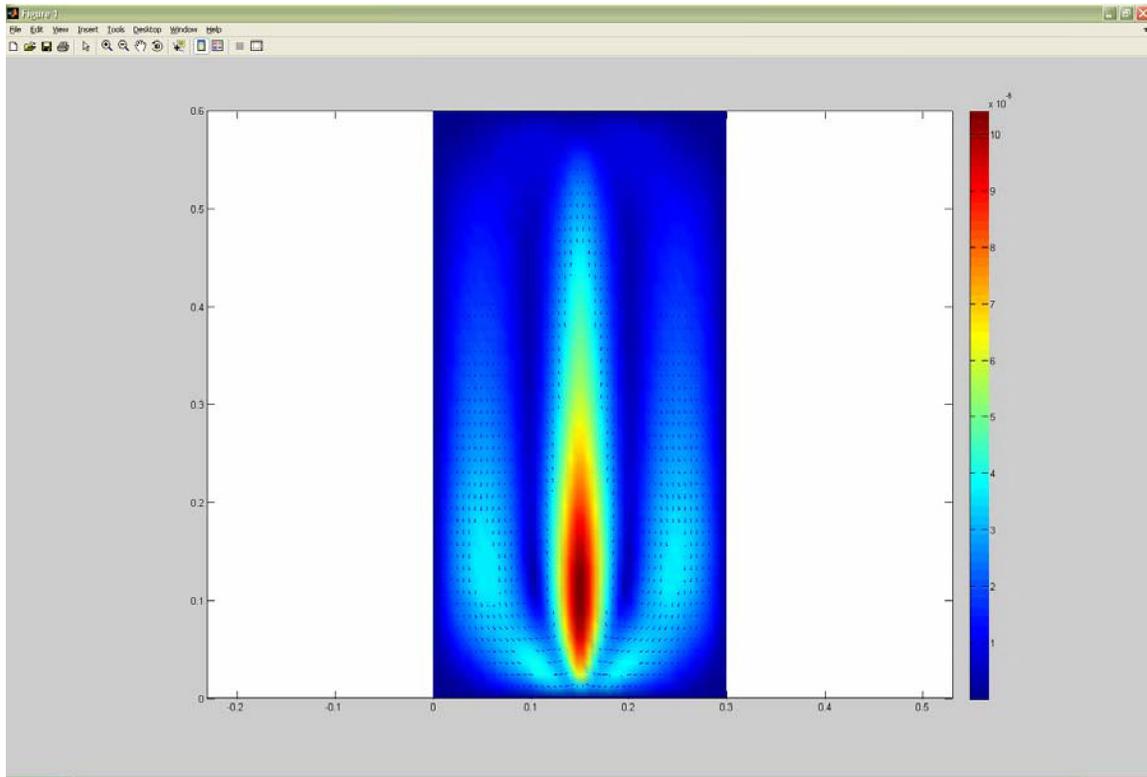
Figure 4.5 Example Velocity Profile of a Fluid During ALM Phenomenon

Note that the magnitude of velocity flow—as well as the flow stream—is depicted in the velocity profile plots.
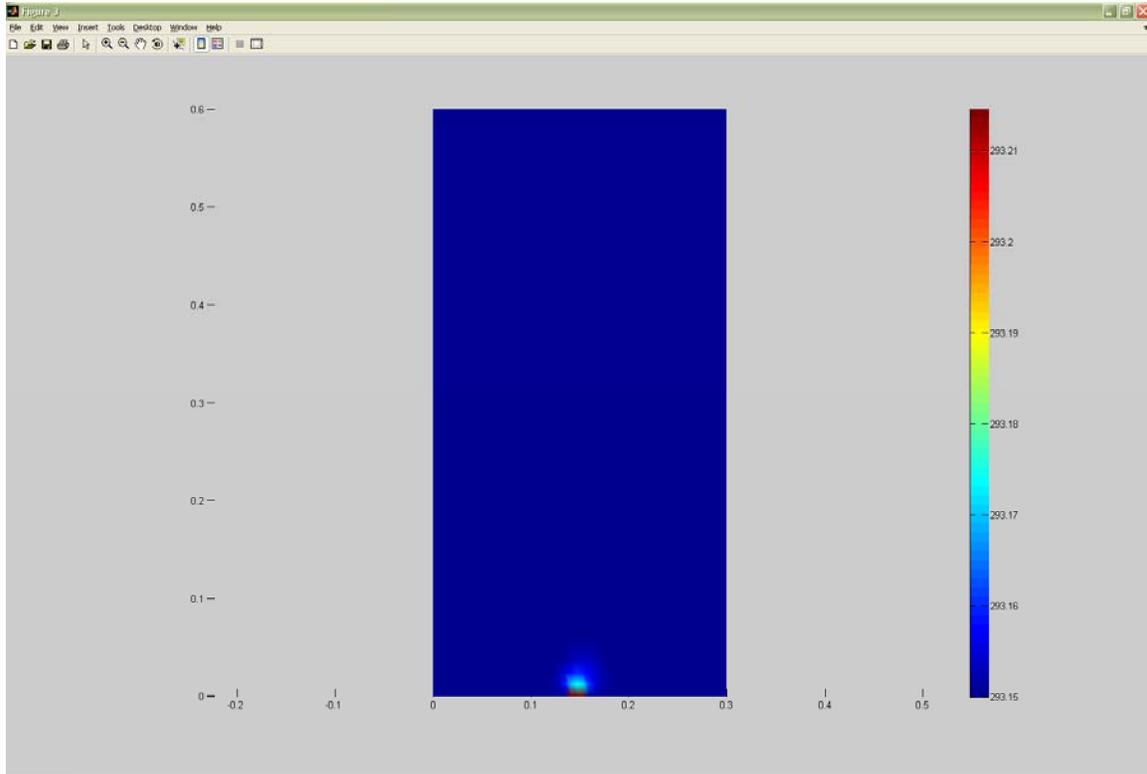
Figure 4.6 Example Temperature Profile of a Fluid During ALM Phenomenon

4.4 Comments on Use of "ALM Program"

The ALM Program is intended to be a useful tool for performing simple ALM calculations. As such, it has its limitations. One of the obvious restrictions regarding use of the code is that it currently only works for a fluid tank of rectangular geometry, although other geometry could easily be implemented in a future version. Another limiting factor (although later versions modified by Dr. J. Adin Mann have overcome this) is that the ALM Program in its current form only works for a single-source sound transducer, i.e., arrays cannot be considered during calculations. The code for calculating the acoustic solution would need to be updated based on later developments in order to implement an array solution. Another limitation of the ALM Program is that fluid property values are determined for discrete temperatures and pressures. This constrains

the user to the temperature and pressure values contained in the drop-down menus. Also, once calculations commence, property values are not adjusted to account for changes in pressure and/or temperature. One final major limitation of the ALM Program is the fact that assumptions levied on the model during development—such as incompressibility and constant properties (density, viscosity, etc.)—are levied upon each and every calculation made using the program. However, the code could be updated to change these restrictions in the future were a suitable model developed.

Despite all its drawbacks and disadvantages, the ALM Program has its high points. The property retrieval feature potentially saves the user time in researching property values, while the property value save feature allows the user to save the values for a particular run and recall them, allowing the user to recalculate a particular solution as needed. In addition, the acoustic and thermodynamic solutions are obtained by simply clicking a button.

Except where noted, the version of "ALM Program" described in this chapter is used to obtain simulation results in CHAPTER 5.

CHAPTER 5. SIMULATION AND EXPERIMENTAL

RESULTS

A number of cases were examined using the "ALM Program" CFD code to determine various effects on ALM. In addition, experiments were designed and performed at Iowa State University to characterize the physical effects of ALM. The empirical data was used to validate the ALM models under development. As a final attempt to characterize the phenomena of ALM, a number of cases were analyzed using the "ALM Program" where no experiment was performed for comparison. The primary goals of these analyses were to

- empirically determine the sound pressure, streaming velocity, and temperature profile of water in a tank excited by an ultrasonic transducer;

- compare "ALM Program" calculated ALM results with empirical data;

- compute the ALM phenomena for a transducer array;

- compare and contrast the CFD results obtained for the Nyborg and Lighthill streaming formulations;

- determine the effects of grid variation on the CFD results,

- calculate ALM results for cryogenic fluids (liquid hydrogen, nitrogen, and oxygen); and

- determine the effect of fluid parameter variation on ALM results.

All empirical results analyzed in this chapter—as well as corresponding model comparisons and simulations for transducer arrays—are taken from

"Analytical/Numerical Model of Fluid Phenomena Created by High Intensity Sound," by Mann et al.(2005).

5.1 Experimental Setup

The experimental setup constructed for ALM evaluation was designed to allow the development of a simple model for verification of ALM theory and code.[3] The equipment was designed to be amenable to three types of measurements: sound pressure level, fluid velocity, and fluid temperature. The following sections describe the general tank configuration and the experimental assemblages for sound, velocity, and temperature measurements.

5.1.1 General Description

ALM measurements were taken for a water-filled tank of the dimensions shown in Figure 5.1.
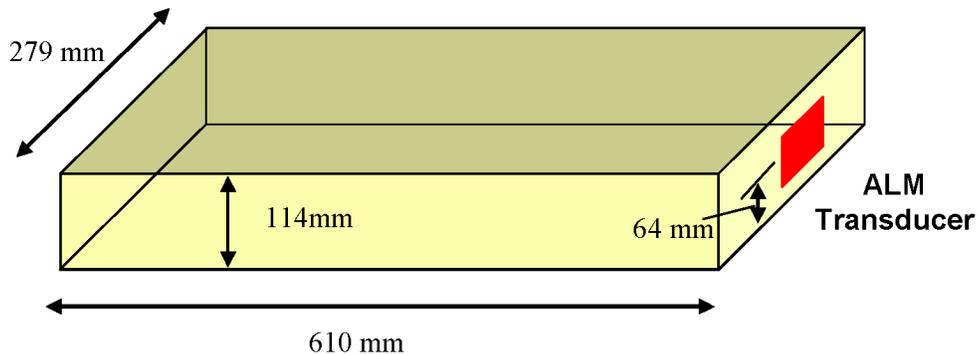
Figure 5.1 Diagram of Experimental Tank with Transducer

In an attempt to remove gravity from the experiment, the tank was oriented in such a manner that the streaming and radiation force would be primarily horizontal. The goal was to create an experiment which would allow the development and validation of a

---

[3] In essence, the theory and numerical development presented in CHAPTER 2 and CHAPTER 3 were developed based on the experimental setup presented in this section.

zero-gravity, two-dimensional model, which was realized and presented in CHAPTER 2 and CHAPTER 3.

The panels of the tank were constructed from clear Plexiglas® in order to facilitate the propagation of laser sheets used for particle image velocimetry (PIV) measurements through the water in the tank. Sound transducers were mounted at one end of the tank as shown in Figure 5.1. The top of the tank was open to allow ease of modification of the test setup and/or tank itself. Two transducer types were integrated into the setup—rectangular and disk (circular). Table 5.1 provides a description of the transducer parameters.

Table 5.1 Sound Transducer Parameters

Property	Transducer	
	Rectangular	**Disk**
Resonant Frequency	1.63 MHz	1.0 MHz
Dimensions	25.4 mm x 12.7 mm	25.4 mm Radius
Lens	No	Yes
Radius of Curvature	*NA*	*50 mm*
Center Thickness	*NA*	*10 mm*
Density	*NA*	*2,700 kg/m³*
Speed of Sound	*NA*	*6,240 m/s*

Sound was produced by the transducers by exciting them with a sinusoidal voltage source at their respective resonant frequencies. The voltage supply was produced by a function generator and stepped up in value using an amplifier to provide the needed power for transducer excitation. The transducers were excited using a variety of duty cycles—most commonly 10% (1 ms on, 9 ms off)—to modify the power output to the transducer. Figure 5.2 shows a simple schematic of the equipment setup needed for sound generation.
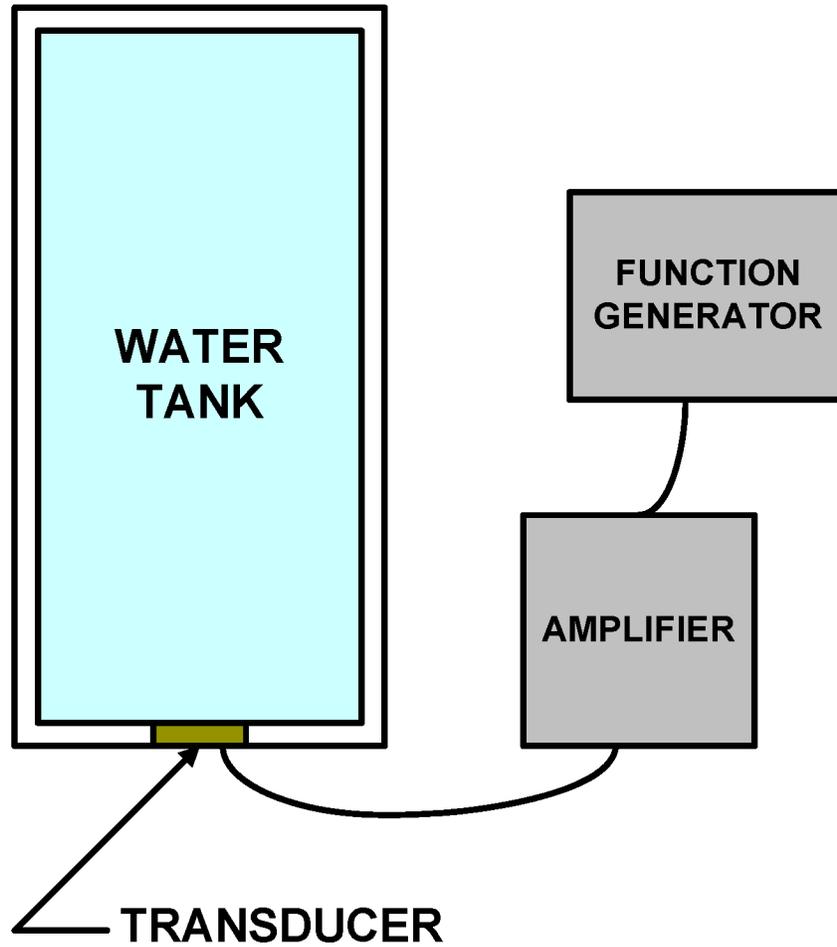
Figure 5.2 Schematic of Transducer Sound Generation Equipment (Top View of Tank)

5.1.2 Sound Measurements

Characterization of the sound effects of ALM was performed using the tank described in the previous section. The effect measured during sound characterizations was the sound pressure. A simple diagram of the experimental setup for sound measurements is given in Figure 5.3.
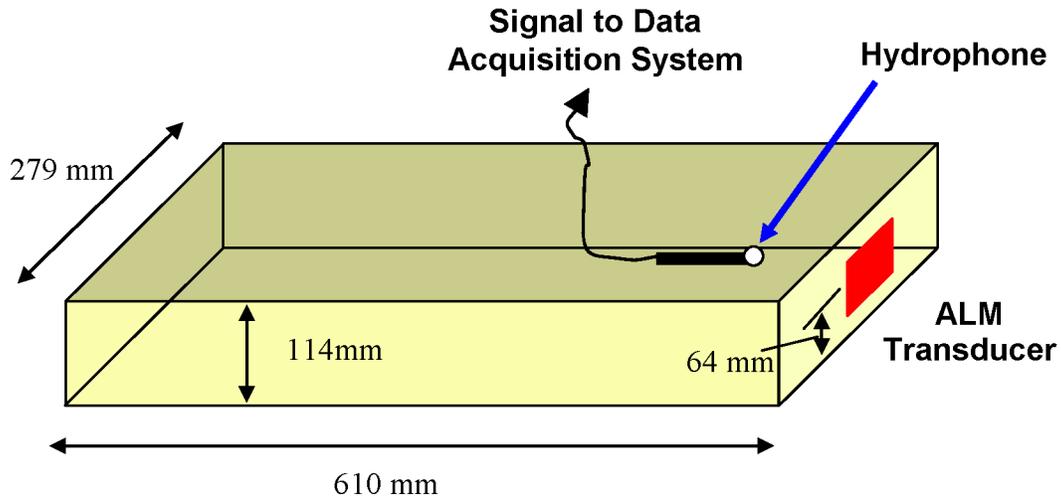
Figure 5.3 Three-Dimensional Diagram of Tank Setup for Sound Measurements

Sound was measured over the frequency range of 1-20 MHz using the equipment specified in Table 5.2.

Table 5.2 Sound Measurement Equipment

Measurement Component	Make and Model
Transducer	FORCE Institute MH28-10 Ultrasonic Hydraphone
Amplifier	FORCE Institute 250
Data Acquisition Card	National Instruments MI 6115
DAQ Software	Custom LabView Program

The sampling rate of the hydrophone was 5MHz for 131,072 points per sample to allow for greater than three tone burst cycle measurements (1.63 MHz x 3 = 4.89 < 5 MHz). A Fast Fourier Transform was employed with the data to plot the spectrum.

Figure 5.4 shows a diagram of the measurement increments within the tank used to obtain experimental results. The diagram gives a top view and shows sound measurement locations (represented by dark blue dots) relative to the sound transducer location.
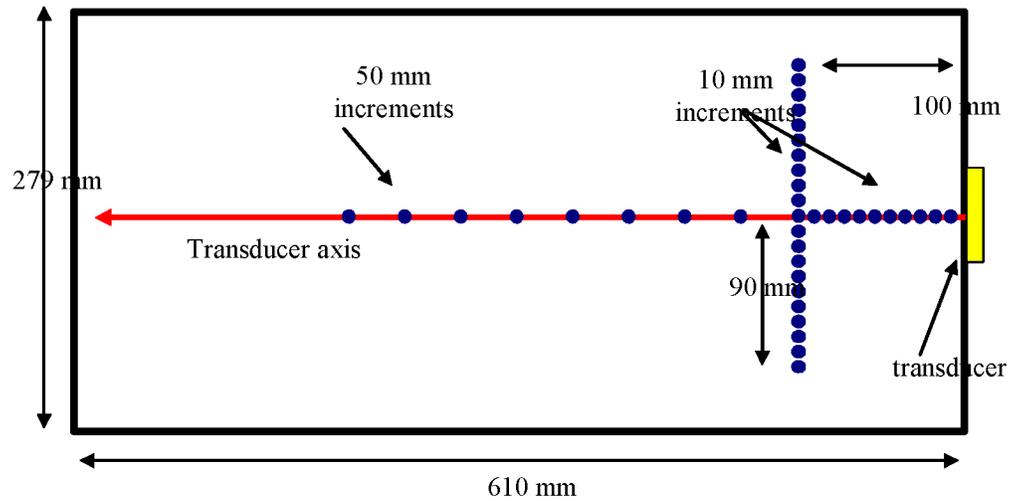
Figure 5.4 Diagram of Tank Showing Sound Measurement Locations

5.1.3 Fluid Velocity Measurements

Flow measurements were performed using the Particle Image Velocimetry (PIV) technique. Figure 5.5 and Figure 5.6 show photographs of the experimental setup used to measure the flow field of the tank during acoustic streaming.
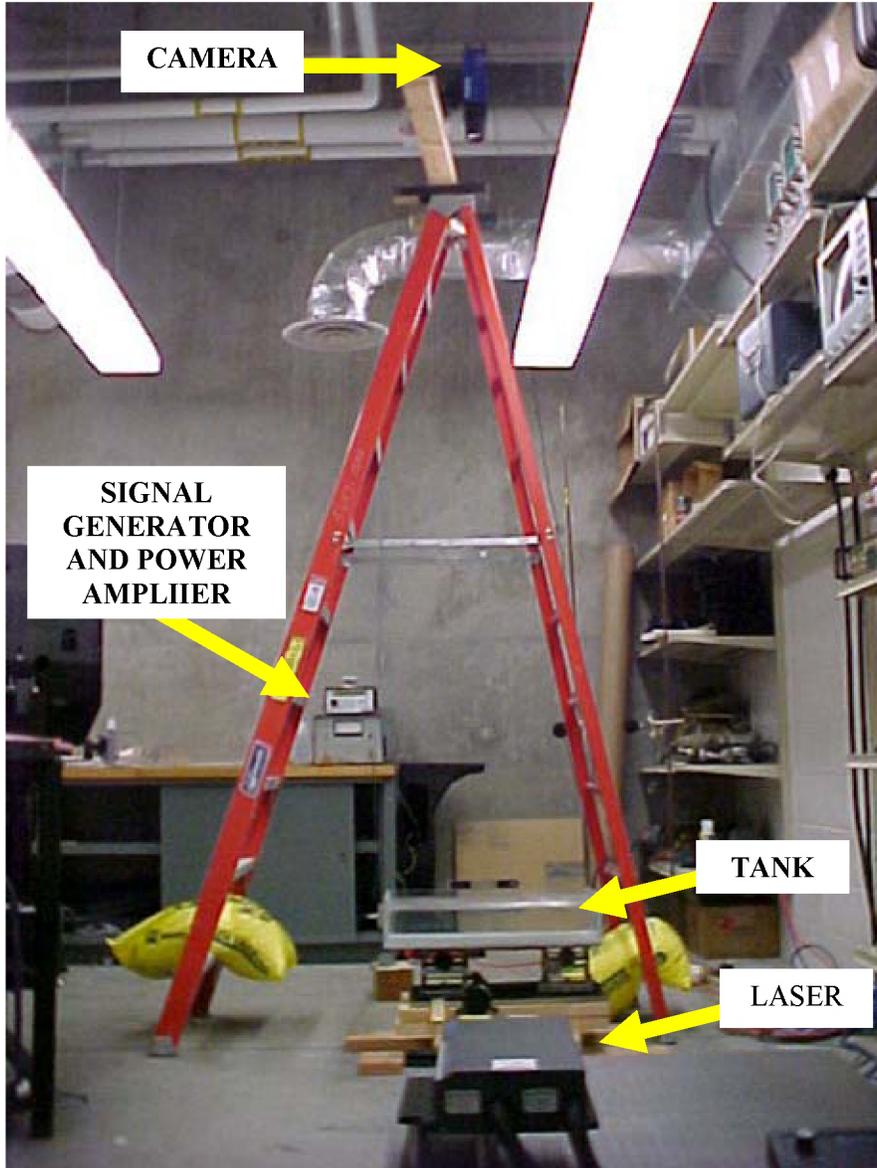
Figure 5.5 Flow Field Measurement Setup for PIV System
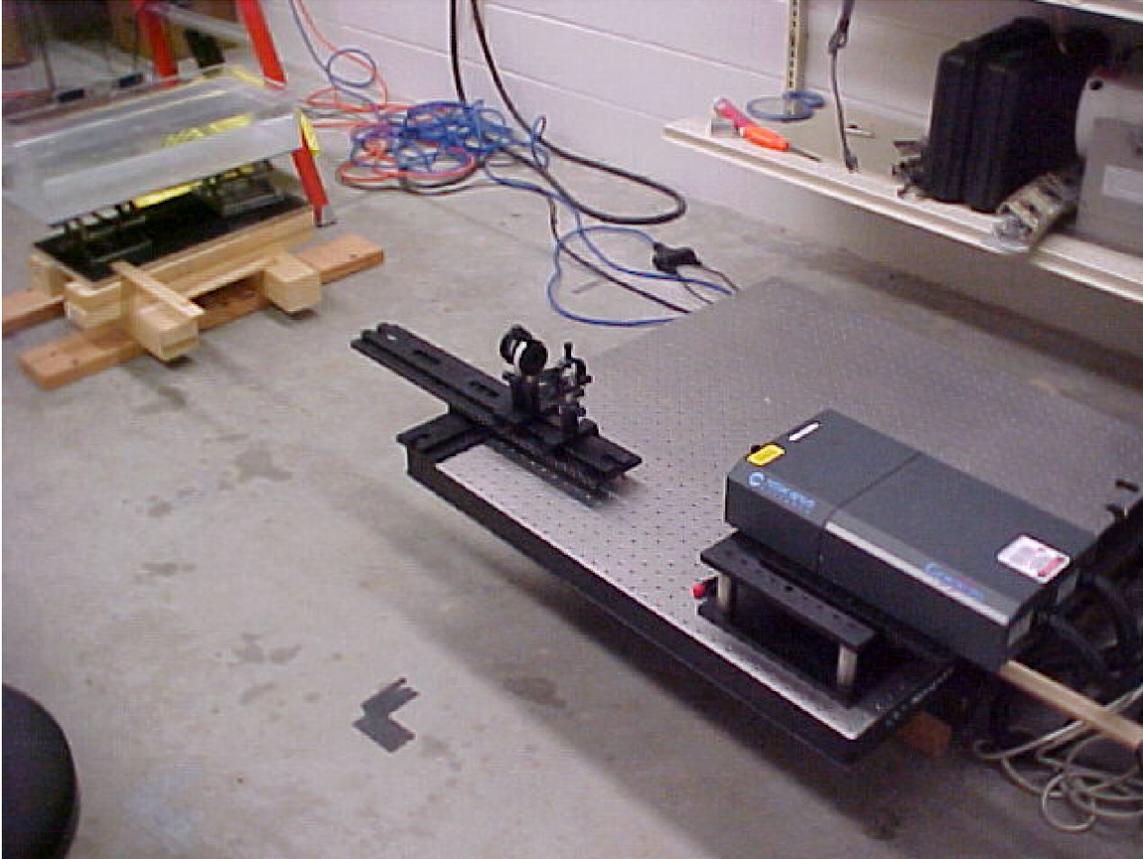
Figure 5.6 Flow Field Measurement Setup for PIV System

The tank water was filled with Sphericel hollow glass spheres of 11.7 micron nominal

diameter. The particles' low density—1.1s g/cm³, compared to 1.0 g/cm³ for water at

room temperature (Sphericel, 2001)—allowed them to remain suspended in the tank

water. A laser sheet was beamed through the right side wall of the tank parallel to the

open end of the tank and through the horizontal centerline of the transducer. This

allowed the camera mounted near the ceiling of the laboratory to take images of the tank

flow field.

5.1.4 Temperature Measurements

Temperature measurements were attempted for the fluid undergoing excitation from the sound transducers using a simple thermocouple and data acquisition setup. However, no discernible differences in temperature from the stagnant state were observed during excitation. Therefore, empirical temperature measurements are not elaborated upon in this thesis.

5.2 Single Transducer Results and Comparison

The ALM phenomena were empirically demonstrated for single transducer setups using the rectangular and disk transducers.

5.2.1 Sound Results

Again, although not credited to—or impacted by—this particular study, as with the theoretical formulation the sound results are presented in this section for thoroughness. The purpose for the review of these results is to highlight the fact that the accuracy of the streaming and heat solutions is directly tied into the accuracy of the acoustic solution.

Figure 5.7 shows a comparison of the measured and calculated data for sound level as measured normal to the rectangular transducer. Measurements were taken through the line normal to the transducer and across its horizontal and vertical center. The experimental and calculation transducers were of equal size—0.0254 meters by 0.0127 meters (1.0 inch by 0.5 inch). The measured sound pressure data is in dB relative to 20 μPa.
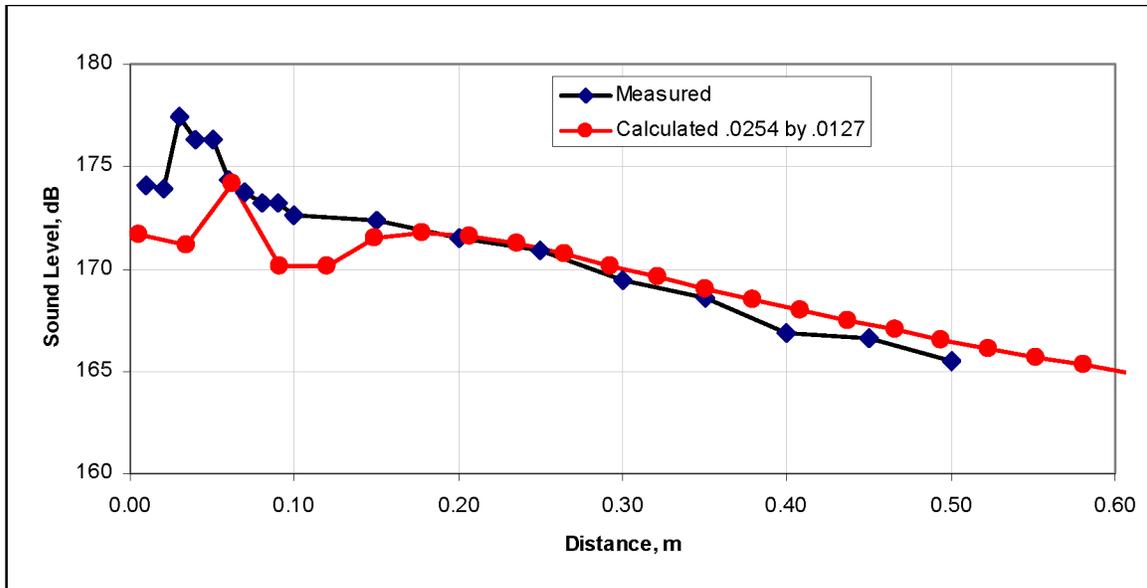
Figure 5.7 Sound Level Along Center Axis of Flow (Perpendicular to Face of Rectangular Transducer)

Note that the calculated solution is generally less in magnitude for distances 0.2 meters and less from the transducer. However, the solution is nearly identical to the measured sound level at distances greater than 0.2 meters from the transducer. As Mann et al. (2005) explain, reducing the effective size of the transducer to 0.02 meters by 0.01 meters more closely approximates the measured data (see Figure 5.8). As a result, the smaller transducer is used later for streaming calculations with the rectangular transducer for the remainder of this section.
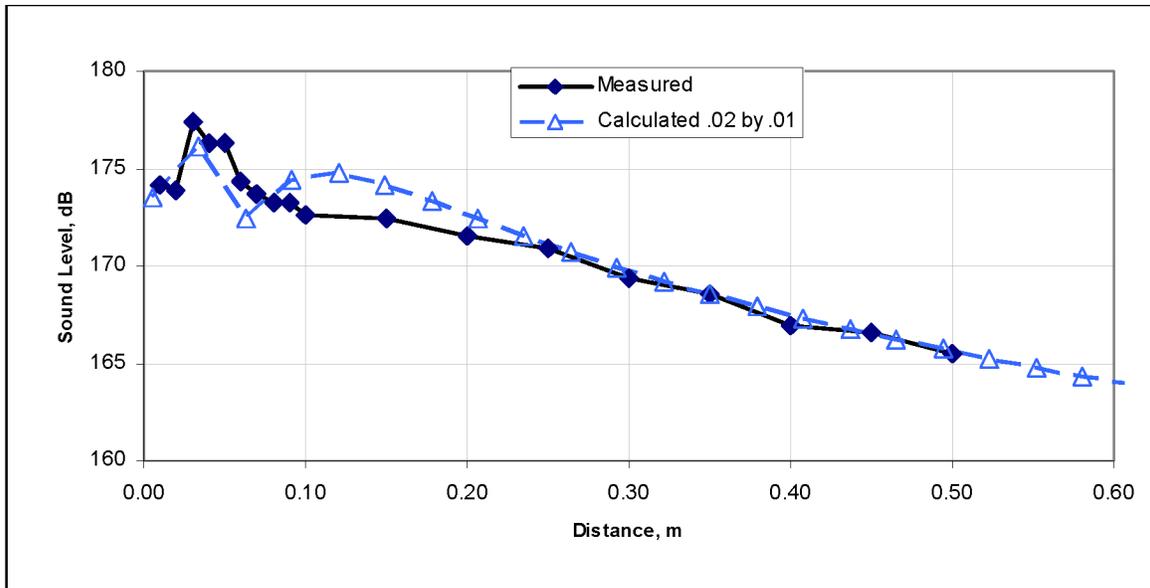
Figure 5.8 Sound Level Along Center Axis of Flow (Perpendicular to Face of Rectangular Transducer); Calculated Transducer Effective Size Reduced

Figure 5.9 shows a comparison of the measured and calculated data for sound level as measured parallel to and horizontally through the center of the transducer (refer to Figure 5.4). The experimental and calculation transducers were again of unequal size—0.0254 meters by 0.0127 meters (1.0 inch by 0.5 inch) for the measured data and 0.02 meters by 0.01 meters for the calculated data—to account for vibration effects with the aluminum tank wall. This effective transducer size again produced the best solution for the cases investigated.
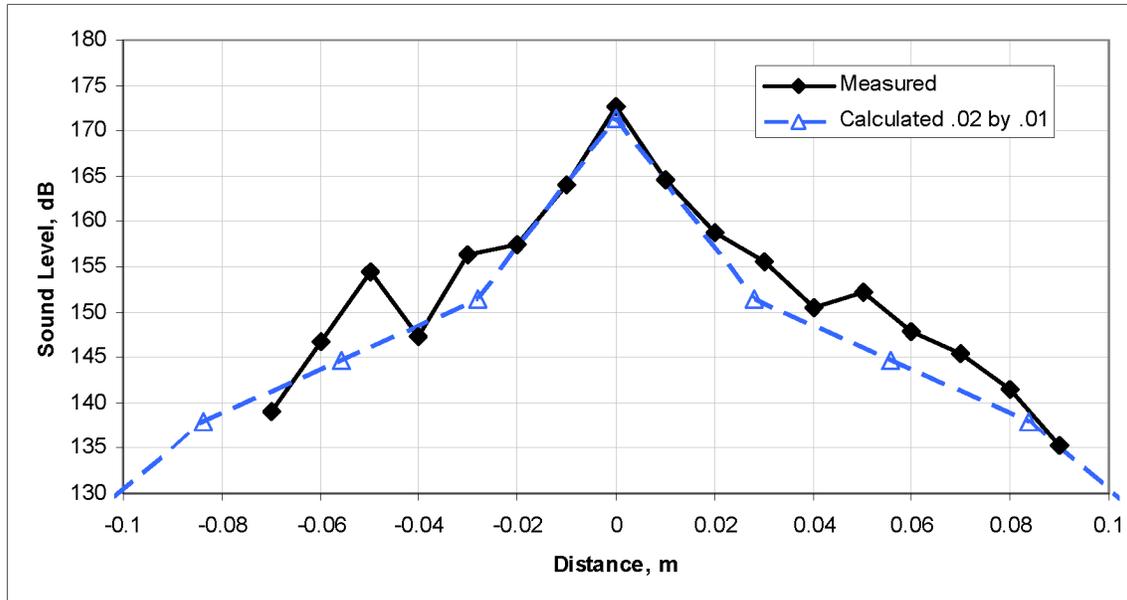
Figure 5.9 Sound Level Through Flow Along Centerline of and Parallel to Rectangular Transducer

The calculations prove to be very accurate within 0.02 meters on either side of the

centerline normal to the transducer.

5.2.2 Fluid Flow Results

Once the acoustic effects of ALM were measured, PIV was used to determine the

fluid flow properties of water at room temperature excided by the sound transducers.

For the rectangular transducer, Figure 5.10 shows a comparison between the

experimentally-determined flow field and the flow field calculated using the CFD code.

(Note that the plots are scaled to have the maximum 7.4×10^{-4} m/s.)
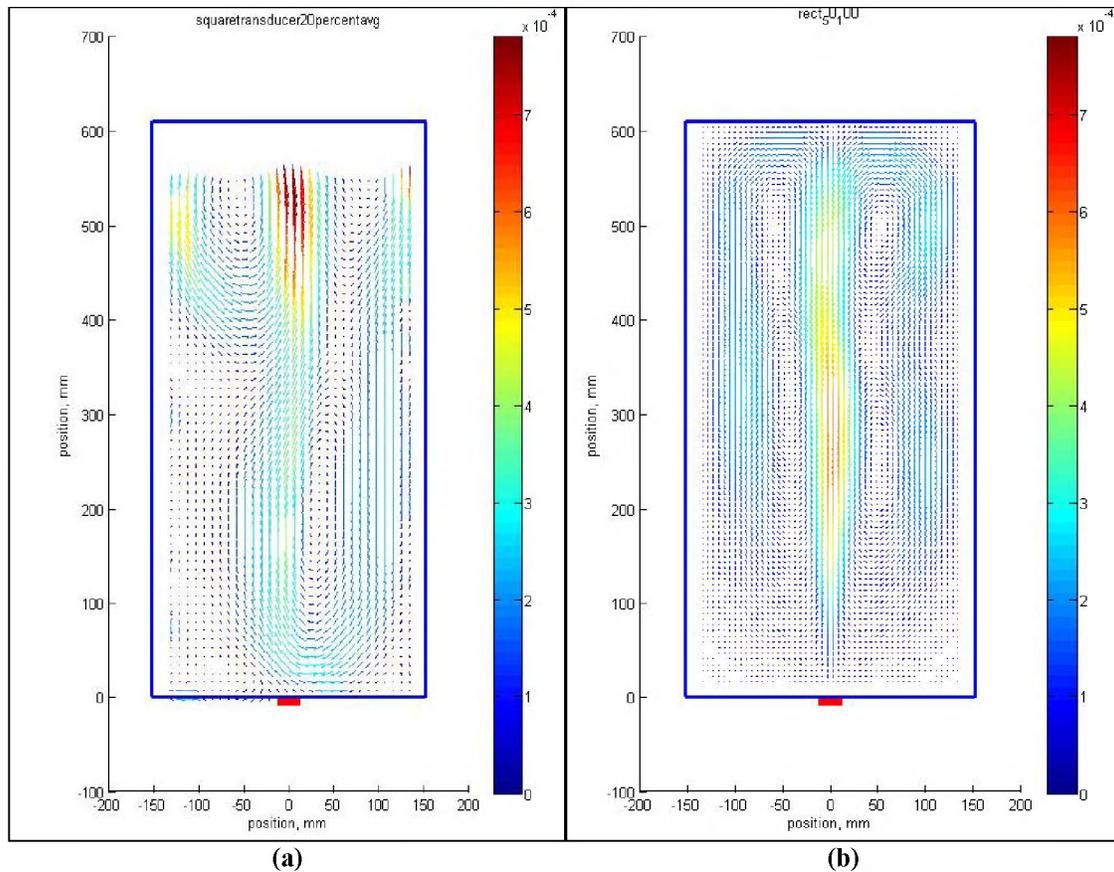
Figure 5.10 Comparison of Streaming Data Between (a) Experimental Data and (b) Computational Results for Rectangular Transducer

Also noteworthy is the fact that the measured flow field—although somewhat similar in direction and recirculation patterns—has higher intensity near the end of the tank opposite the transducer as opposed to the calculated solution, which has higher intensity at the center of the tank.

Figure 5.11 was plotted using the scaled PIV and CFD results for the rectangular transducer.
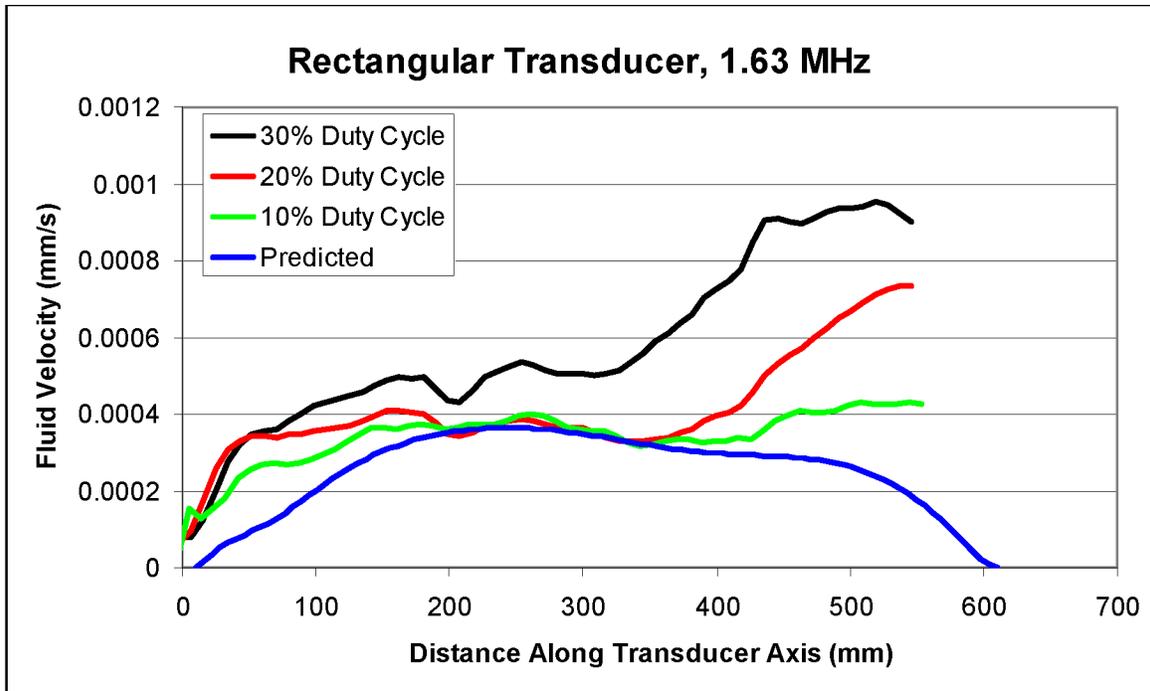
Figure 5.11 Rectangular Transducer Fluid Velocity Results (Along Beam Axis)

The predicted results for the rectangular transducer most closely matched the test data for

the experimental cases with 10% and 20% duty cycles.

(a)   **(b)**

Figure 5.12 gives the test and calculated fluid velocity results for the tank

configuration with the disk transducer.
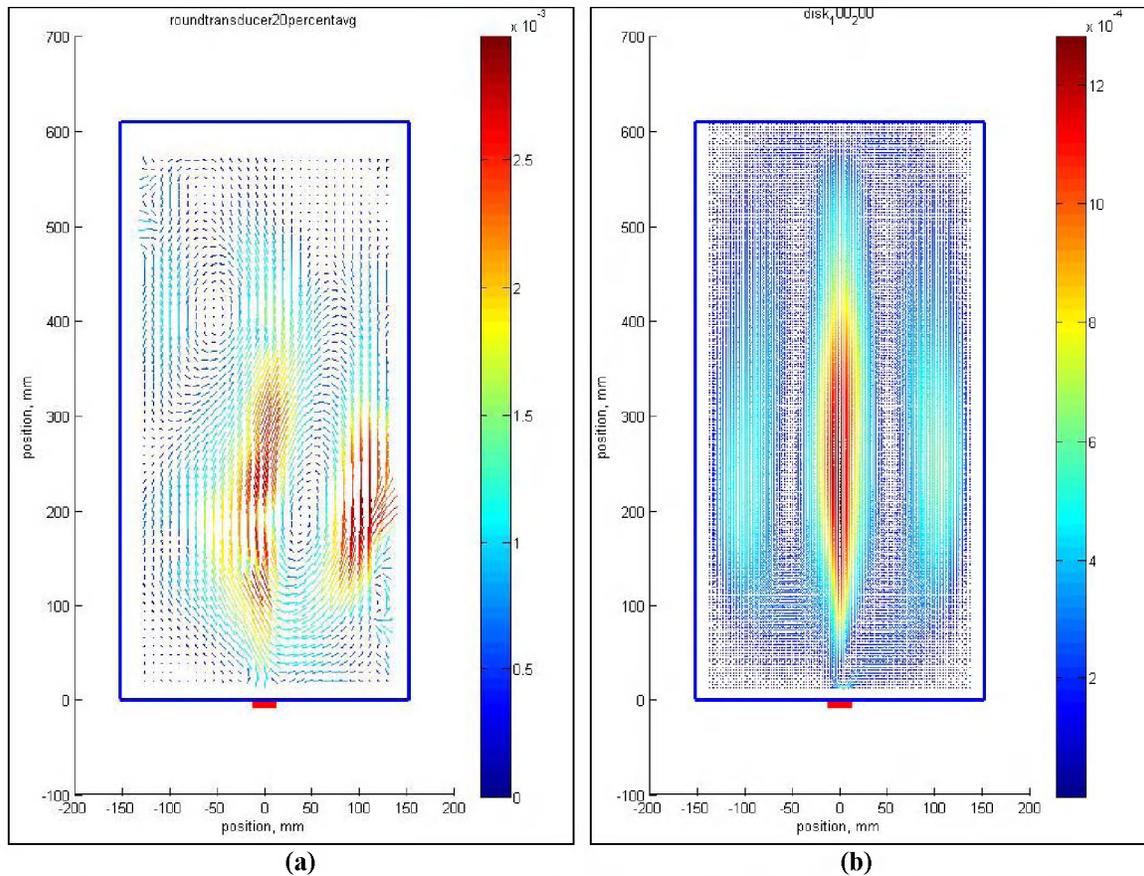
Figure 5.12 Comparison Between (a) Experimental and (b) Computational Results for Disk Transducer

As can be seen in **(a)**   **(b)**
Figure 5.12, the CFD code predicted a more accurate flow pattern for the fluid

excited by the disk transducer than for the rectangular transducer. Incongruence between

the experimental and computational results is likely due somewhat to the inability of the

experimenter to practically fabricate a symmetrical tank.

Again, a comparison plot was created for the disk transducer PIV and CFD results

(see Figure 5.13).
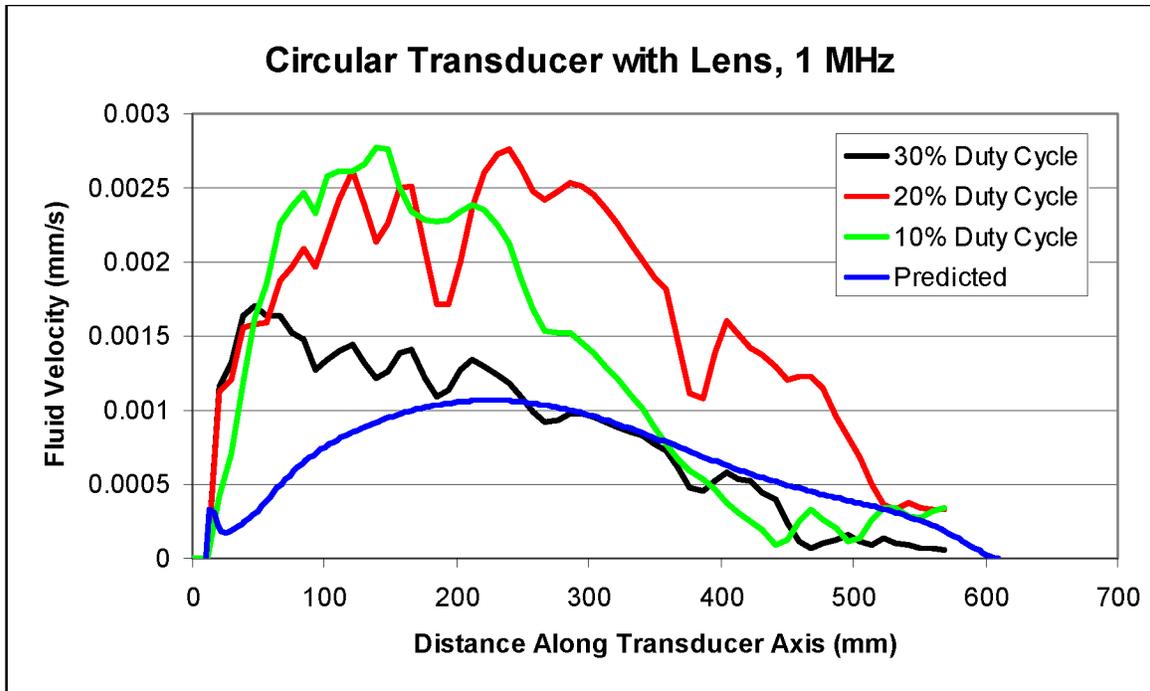
Figure 5.13 Disk Transducer Fluid Velocity Results (Along Sound Beam Axis)

Note that the predicted results for the disk transducer most closely matched the test data for a 30% duty cycle. Figure 5.14 shows the calculated solution for both the rectangular transducer at 1.63 MHz and the circular transducer at 1 MHz.
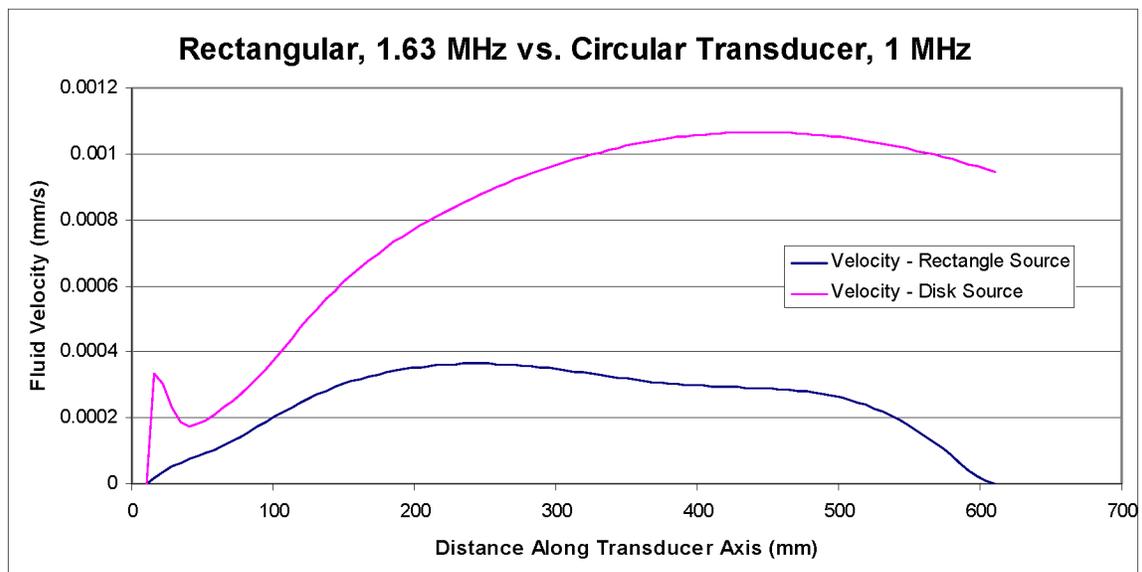
Figure 5.14 Comparison of Calculated Solutions for Rectangular and Disk Transducers

Note that the circular transducer predicted higher fluid velocity along the axis perpendicular to the transducer for the entire distance over which the fluid velocity was calculated.

5.3 Transducer Array Results

This section discusses the results obtained for the arrayed transducer analysis performed by Mann et al. (2005). Although determination of array phenomena was left unimplemented in the "ALM Program" presented in CHAPTER 4, the CFD code developed in this thesis was utilized in the cited work to determine the flow field and temperature profile for a water-filled tank of the parameters investigated experimentally. In addition, no experimental data was taken for arrayed transducers, driving the resulting discussion to involve only the calculations made using the ALM Program.

Figure 5.15 gives the results for a 1.0 MHz transducer array focused at x = -0.2 meters and z = 0.4 meters away from the center of the array.
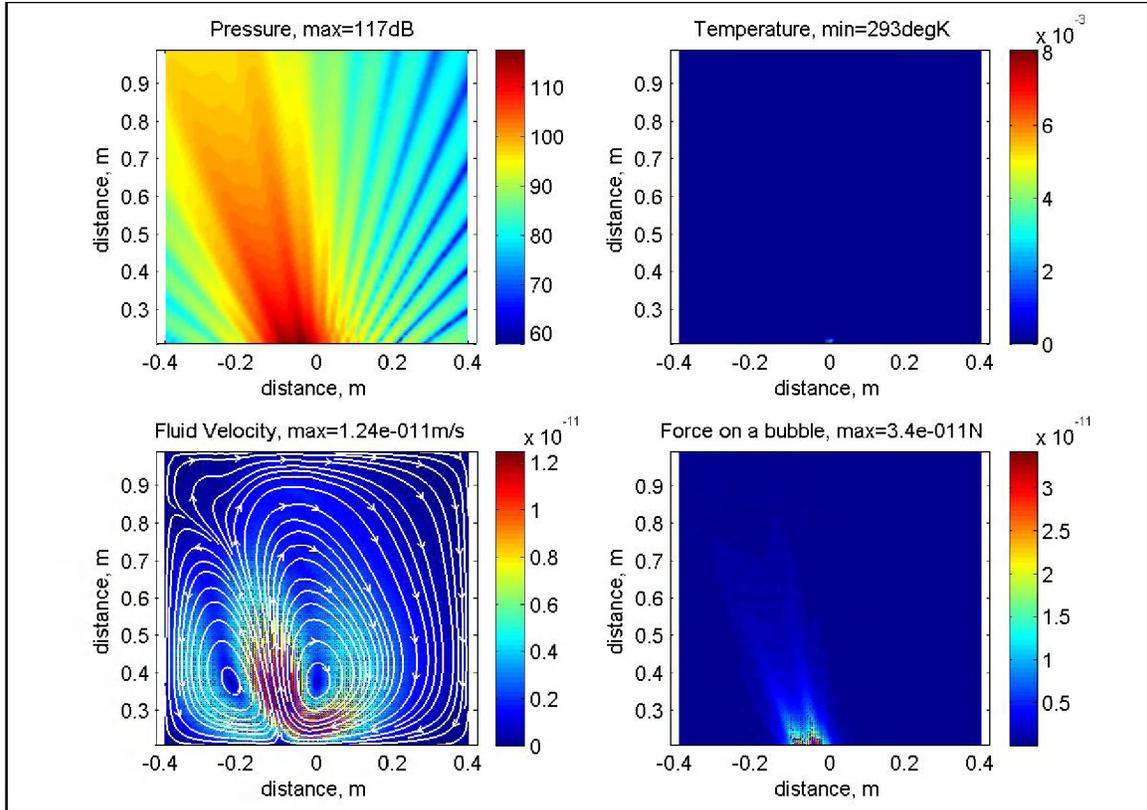
Figure 5.15 ALM Results for 1.0 MHz Array Focused at *x* = -0.2 m and *z* = 0.4 m

Note that the sound pressure and radiation force on a bubble have significantly greater magnitude in the general direction of the array focus. In addition, the streaming of the water in the tank follows a flow pattern in the direction of the focus and eventually begins a recirculation pattern near the far left corner of the tank. However, once again, no discernible temperature difference is shown to be the result of nonlinear sound from the transducers, as was seen with the single transducer setups. One significant observation is that the velocity magnitude was calculated to be on the order of 10^{-11} m/s. Although assumed to be incorrect, verification of this result would require the construction of a tank which uses a transducer array.

Figure 5.16 through Figure 5.20 present calculated array results for transducers

focused at x = 0.2 m and z = 0.4 m, x = 0.0 m and z = 0.4 m, x = -0.2 m and z = 0.4 m, x

= 0.2 m and z = 0.4 m, and x = 0.2 m and z = 0.4 m.
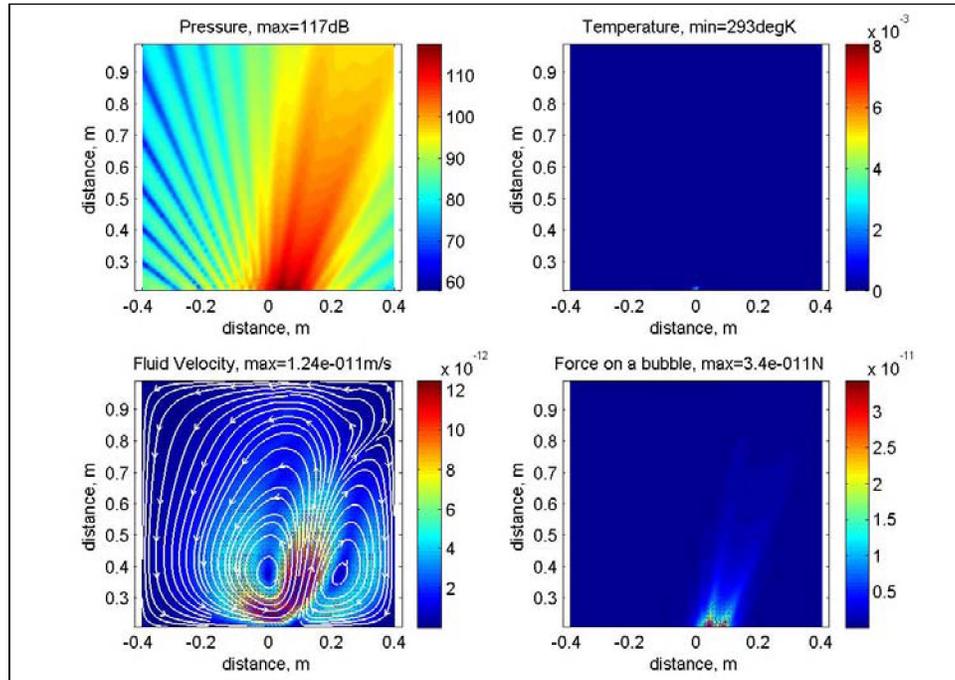
Figure 5.16 ALM Program Results for 1.0 MHz Array Focused at *x* = 0.2 m and *z* = 0.4 m
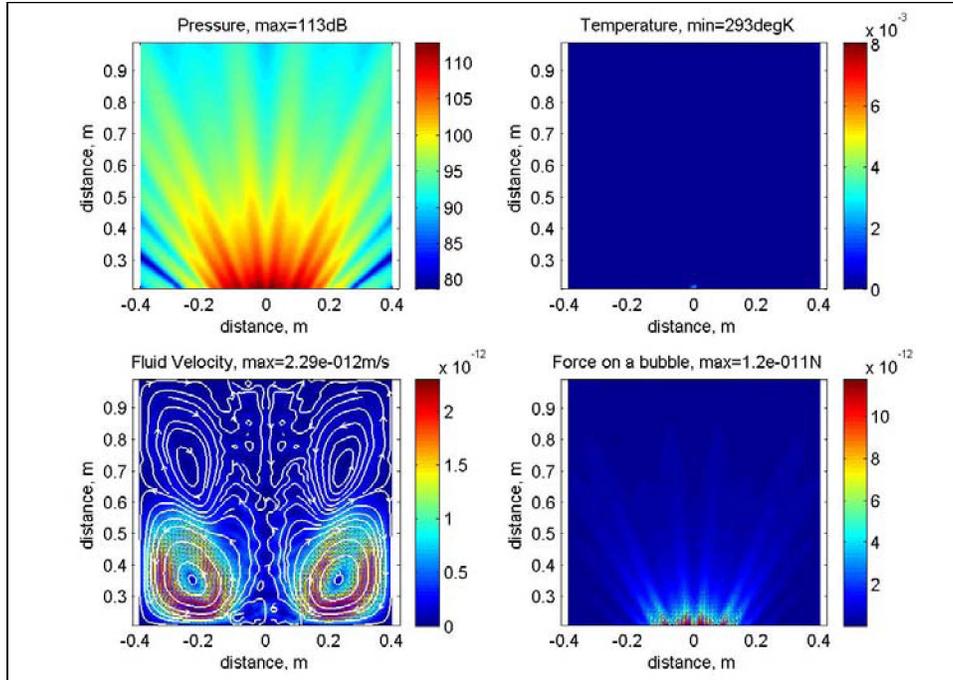
Figure 5.17 ALM Program Results for 1.0 MHz array focused at *x* = 0.0 m and z = 0.4 m
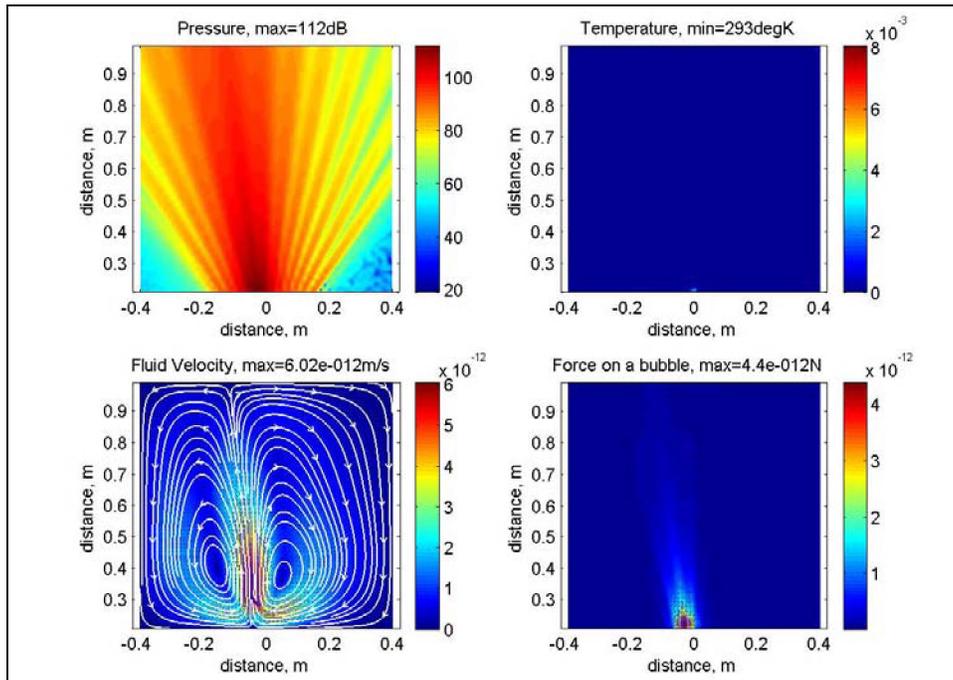
Figure 5.18 ALM Program Results for 1.5 MHz Array Focused at *x* = -0.2 m and z = 0.4 m
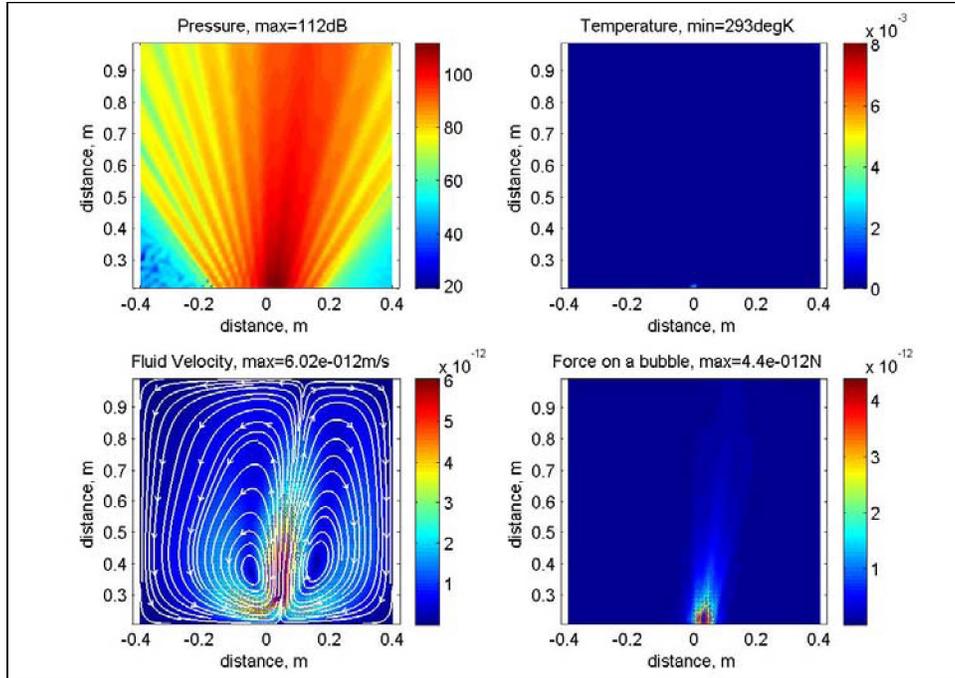
Figure 5.19 ALM Program Results for 1.5 MHz Array Focused at $x = 0.2$ **m and** $z = 0.4$ **m**
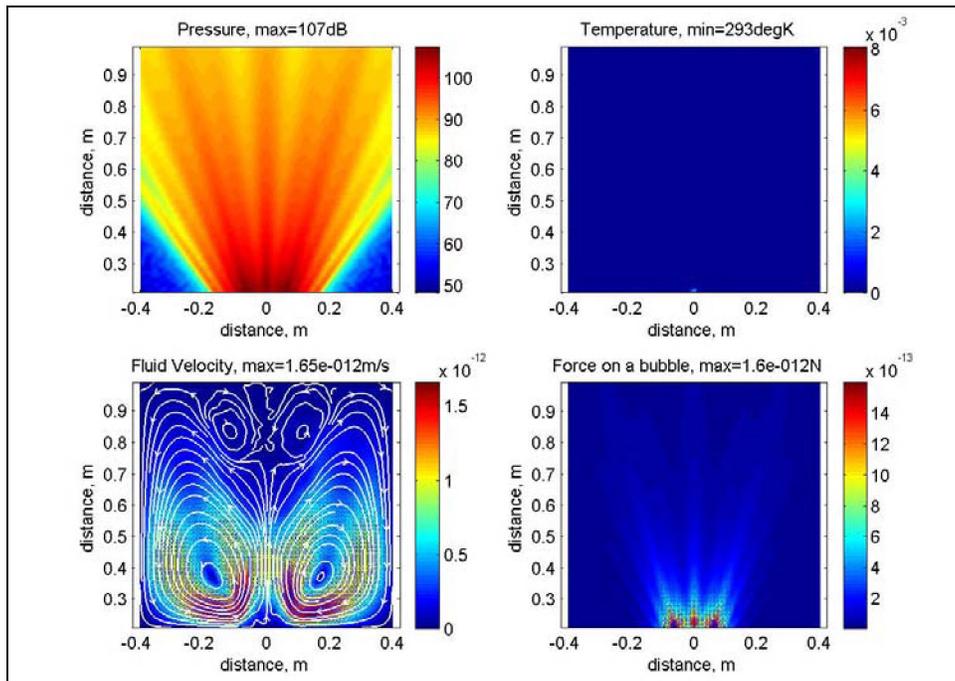
Figure 5.20 ALM Program Results for 1.5 MHz Array Focused at $x = 0.0$ **m and** $z = 0.4$ **m**

5.4 Nyborg Formulation Vs. Lighthill Formulation

One of the unanswered questions regarding the CFD code and one brought to interest during the theoretical development presented in CHAPTER 2 is "how do the results compare and contrast between the Nyborg and Lighthill formulations?" A comparison computation was performed with the CFD code using the experimental tank parameters with both the 0.0254 mm by 0.0127 mm rectangular transducer operating at 1.63 MHz and the 0.0254 meter diameter disk transducer operating at 1.0 MHz. Table 5.3 and Table 5.4 display comparisons of the results calculated for the rectangular transducer and disk transducer setups, respectively, using the Nyborg and Lighthill formulations. Figure 5.21 and Figure 5.22, and Figure 5.23 and Figure 5.24, display graphical representations of the results for the rectangular and disk transducers, respectively.

Table 5.3 Results of Comparison Between Nyborg and Lighthill Streaming Formulations (Rectangular Transducer)

Result	Maximum Value	
	Nyborg Formulation	**Lighthill Formulation**
Magnitude	$9.851 \times (10)^{-6}$ m/s	$9.800 \times (10)^{-6}$ m/s
x-Velocity	$3.819 \times (10)^{-6}$ m/s	$3.741 \times (10)^{-6}$ m/s
z-Velocity	$9.851 \times (10)^{-6}$ m/s	$9.800 \times (10)^{-6}$ m/s
Temperature	293.212 K	293.212 K

The variation between the overall velocity magnitudes is found to be about a half a percent. For the x- and z- velocities, the variation between the two methods is found to be approximately 0.5 and 2 percent. Note, however, that no discernible difference is found between the two methods for temperature.

Table 5.4 Results of Comparison Between Nyborg and Lighthill Streaming Formulations (Disk Transducer)

Result	Maximum Value	
	Nyborg Formulation	**Lighthill Formulation**
Magnitude	3.549 x (10)$^{-6}$ m/s	3.543 x (10)$^{-6}$ m/s
x-Velocity	1.092 x (10)$^{-6}$ m/s	1.082 x (10)$^{-6}$ m/s
z-Velocity	3.549 x (10)$^{-6}$ m/s	3.543 x (10)$^{-6}$ m/s
Temperature	293.209 K	293.209 K

Again, a comparison between the Nyborg and Lighthill solutions shows almost no differences in results. The variation between the overall velocity magnitudes is found to be about a fifth of a percent. For the x- and z- velocities, the variation between the two methods is found to be approximately 0.2 and 1 percent. Note, however, that no discernible difference is found between the two methods for temperature.

(a) **(b)**
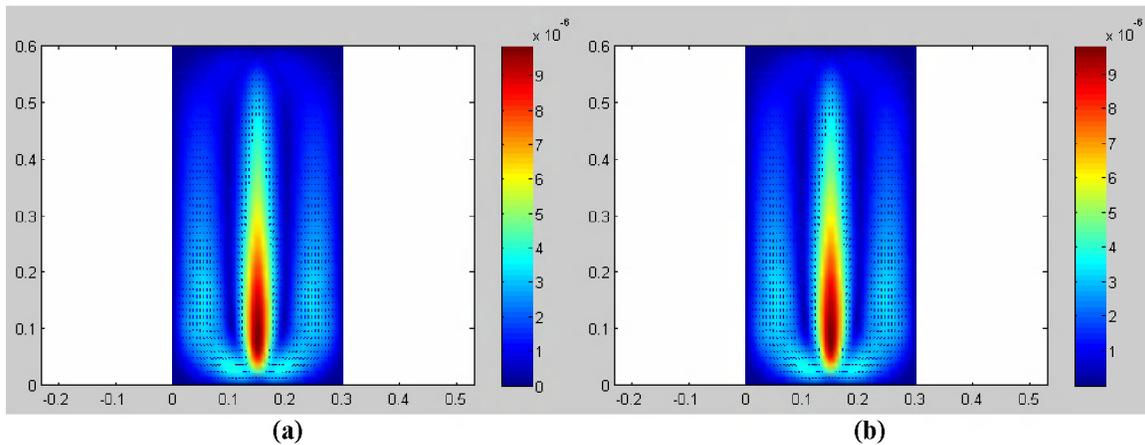
Figure 5.21 Velocity Field Using Experimental Parameters for (a) Nyborg Solution and (b) Lighthill Solution (Rectangular Transducer)
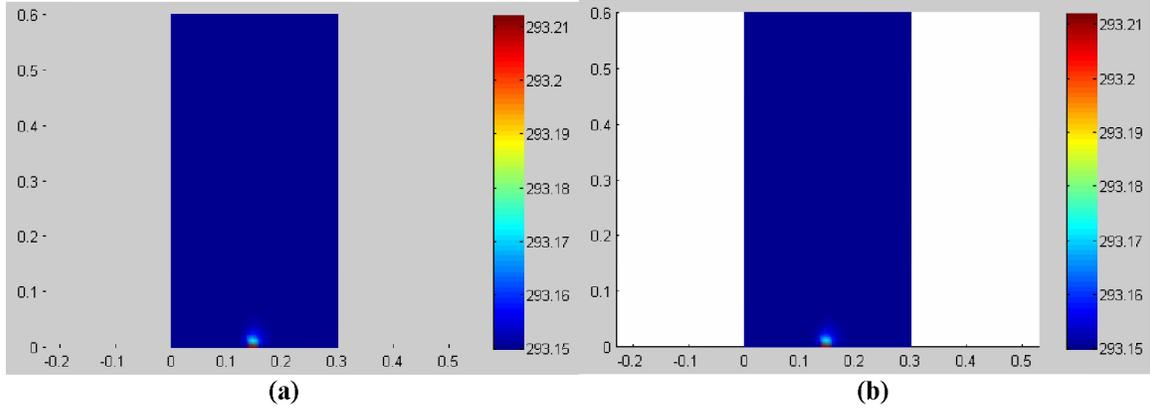
Figure 5.22 Temperature Field Using Experimental Parameters for (a) Nyborg Solution and (b) Lighthill Solution (Rectangular Transducer)
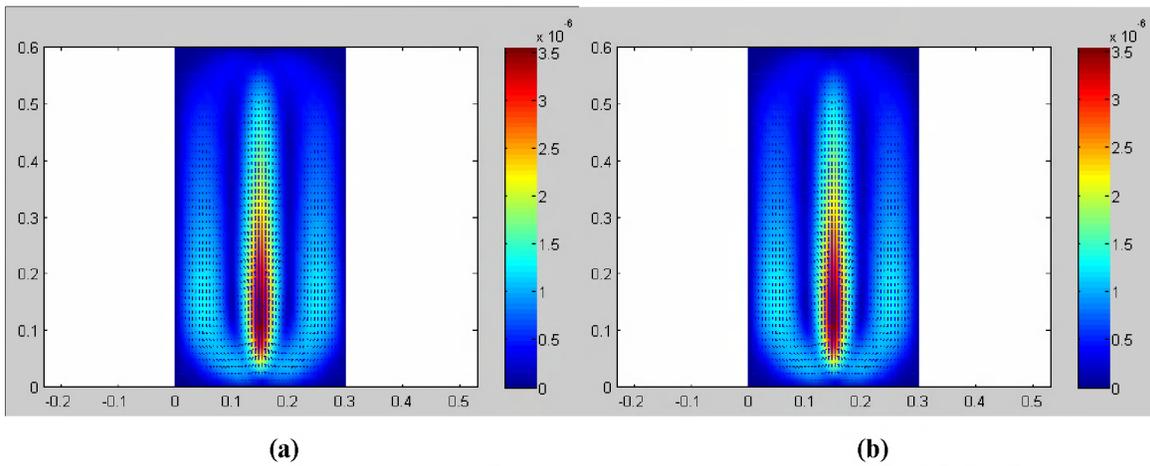
Figure 5.23 Velocity Field Using Experimental Parameters for (a) Nyborg Solution and (b) Lighthill Solution (Disk Transducer)
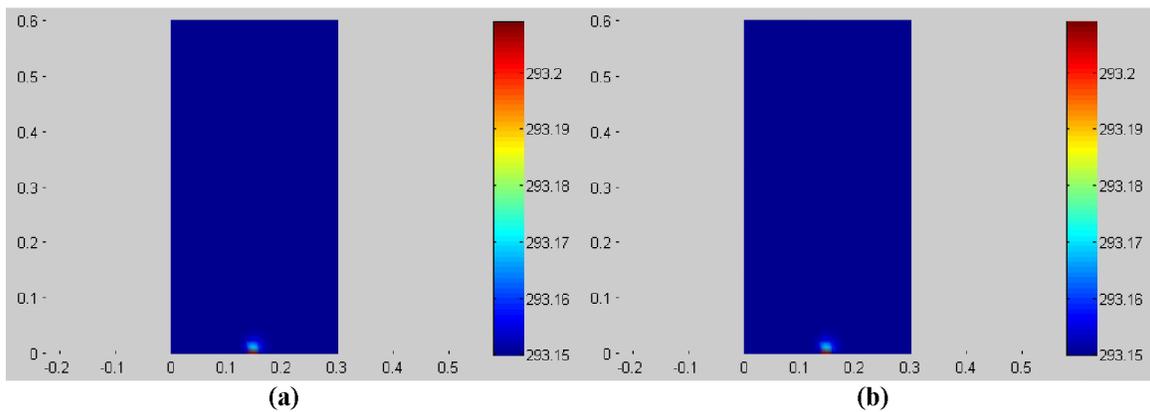
Figure 5.24 Temperature Field Using Experimental Parameters for (a) Nyborg Solution and (b) Lighthill Solution (Disk Transducer)

5.5 Effect of Grid Size on CFD Results

One disadvantage to the CFD code developed during this study is that the number of grid points must be arbitrarily chosen. This results in a trial and error methodology for choosing optimizing the balance between accuracy and computation time. The purpose of this section is to report on the effects of variation in grid size.

To demonstrate the effect of grid size selection on ALM calculations, a test case was performed for the rectangular transducer in water at room temperature and pressure (20°C and 1 bar). The results are shown in Table 5.5.

Table 5.5 Effect of Grid Size on ALM Results

Result	Maximum Value for Varied Viscosity				
	25 x 50	50 x 50	50 x 100	100 x 100	100 x 200
Pressure	174 dB	173 dB	173 dB	177 dB	177 dB
Temperature Change	$2.38 \times (10)^{-10}$ K/s	$2.05 \times (10)^{-10}$ K/s	$2.05 \times (10)^{-11}$ K/s	$4.9 \times (10)^{-10}$ K/s	$4.88 \times (10)^{-10}$ K/s
Body Force/Density	$7.91 \times (10)^{-8}$ m/s²	$6.83 \times (10)^{-8}$ m/s²	$6.84 \times (10)^{-9}$ m/s²	$1.63 \times (10)^{-7}$ m/s²	$1.63 \times (10)^{-7}$ m/s²
Force on Bubble	$4.13 \times (10)^{-5}$ N	$3.56 \times (10)^{-5}$ N	$3.56 \times (10)^{-5}$ N	$8.51 \times (10)^{-5}$ N	$8.48 \times (10)^{-5}$ N
Magnitude	$9.841 \times (10)^{-6}$ m/s	$9.800 \times (10)^{-6}$ m/s	$9.334 \times (10)^{-6}$ m/s	$9.949 \times (10)^{-6}$ m/s	$9.847 \times (10)^{-7}$ m/s
x-Velocity	$2.871 \times (10)^{-6}$ m/s	$3.741 \times (10)^{-6}$ m/s	$3.733 \times (10)^{-7}$ m/s	$3.572 \times (10)^{-6}$ m/s	$3.600 \times (10)^{-8}$ m/s
z-Velocity	$9.841 \times (10)^{-6}$ m/s	$9.800 \times (10)^{-6}$ m/s	$9.334 \times (10)^{-6}$ m/s	$9.949 \times (10)^{-6}$ m/s	$9.847 \times (10)^{-7}$ m/s
Temperature	NA[4]	293.212 K	293.196 K	293.175 K	293.166 K

As can be seen from the data, the calculated ALM values fluctuated a fair amount for different grid sizes. In addition, for the 25 x 50 grid, the temperature solution produced no results, rather the following error was incurred: "Attempted to access T(12.5,2); index

[4] Temperature solution did not converge for a grid size of twenty-five by fifty cells in the x- and z-directions, respectively.

must be a positive integer or logical." Also note that trends were not very consistent—pressure, temperature change, force, and velocity values did not tend to increase only or decrease only as the grid size was increased. However, the calculated temperature did tend to decrease as the grid size was improved.

5.6 Results for Cryogenic Fluids

Three extremely low-temperature liquids were investigated for ALM effects: hydrogen, nitrogen, and oxygen. In order to compare the results of the three fluids—as well as those for water at room temperature—the solution for each fluid was obtained at a pressure of one bar.

5.6.1 Liquid Hydrogen

Computational ALM results were computed for liquid hydrogen at a temperature of 18 K. Table 5.6 gives the maximum values obtained for the fluid while Figure 5.25 and Figure 5.26 present plots of the acoustic, streaming, and heating solutions.

Table 5.6 ALM Results for Liquid Hydrogen at 18 K and 1 bar

Result	Value
Pressure	175 dB
Temperature Change	$2.24 \times (10)^{-5}$ K/s
Body Force/Density	$2.95 \times (10)^{-5}$ m/s²
Force on Bubble	$2.2 \times (10)^{-4}$ N
Magnitude	0.8406 m/s
x-Velocity	0.3069 m/s
z-Velocity	0.8406 m/s
Temperature	18 K
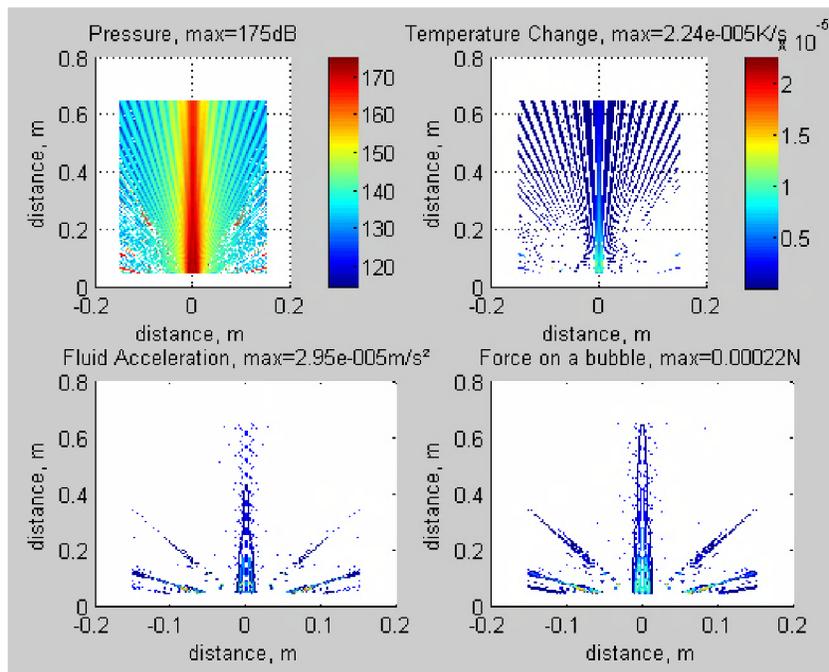
Figure 5.25 Acoustic Results for Liquid Hydrogen at 18 K and 1 bar
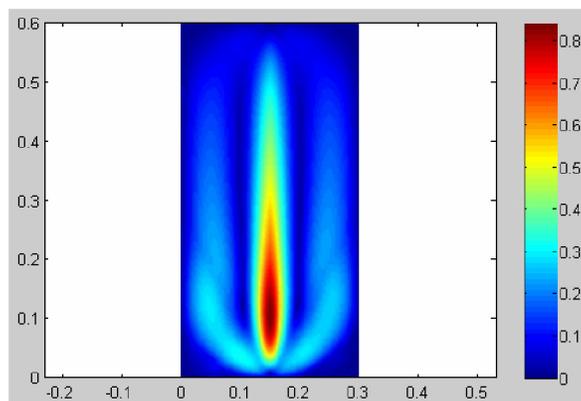
Figure 5.26 Streaming Results for Liquid Hydrogen at 18 K and 1 bar (Temperature did not Plot)

The results show that "ALM Program" predicts fluid velocities at nearly 1 m/s in the

region of greatest flow. However, no temperature rise was computed.

5.6.2 Liquid Nitrogen

For liquid hydrogen, the temperature was set to 18 K. Table 5.7 gives the

maximum values obtained for the fluid.

Table 5.7 ALM Results for Liquid Nitrogen at 75 K and 1 bar

Result	Value
Pressure	173 dB
Temperature Change	$2.76 \times (10)^{-4}$ K/s
Body Force/Density	0.00126 m/s²
Force on Bubble	$3.29 \times (10)^{-5}$ N
Magnitude	0.5780 m/s
x-Velocity	0.2080 m/s
z-Velocity	0.5780 m/s
Temperature	75.0001 K

Figure 5.27 and Figure 5.28 give the plots obtained from "ALM Program."
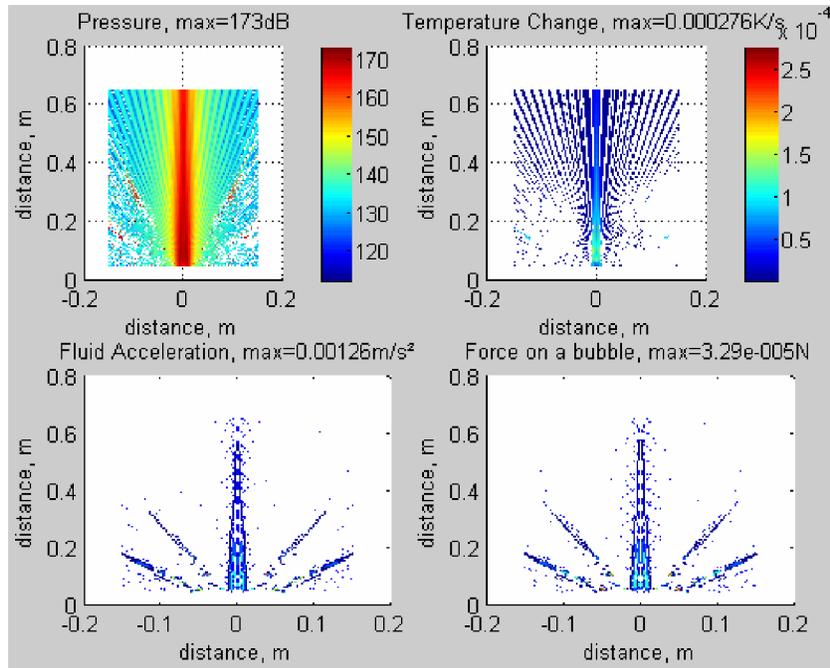
Figure 5.27 Acoustic Results for Liquid Nitrogen at 90 K and 1 bar

(a)   (b)
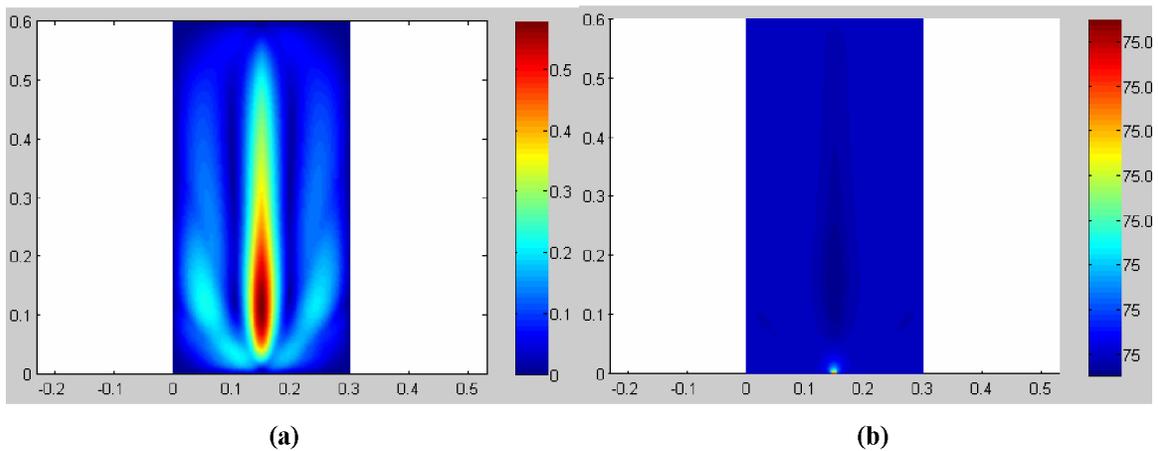
Figure 5.28 (a) Streaming and (b) Temperature Results for Liquid Nitrogen at 90 K and 1 bar

For nitrogen, the fluid speeds are roughly half those seen for hydrogen. In addition, the temperature rise is small enough to be considered negligible, although the plot for temperature may indicate the path of heating were it to increase in magnitude.

5.6.3 Liquid Oxygen

The final cryogenic fluid calculated was oxygen at a temperature 90 K. The

maximum magnitudes for the ALM solution are presented in Table 5.8.

Table 5.8 ALM Results for Liquid Oxygen at 90 K and 1 bar

Result	Value
Pressure	173 dB
Temperature Change	0.0493 K/s
Body Force/Density	0.212 m/s²
Force on Bubble	$3.14 \times (10)^{-5}$ N
Magnitude	91.917 m/s
x-Velocity	34.792 m/s
z-Velocity	91.916 m/s
Temperature	90.0000 K

Figure 5.29 and Figure 5.30 give plots of the ALM solutions.
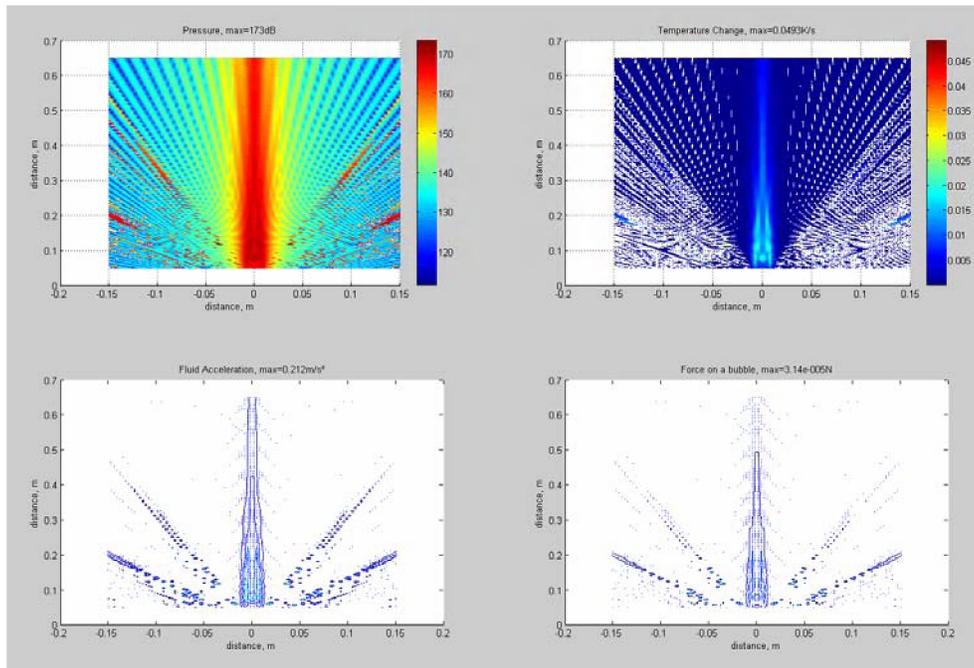
Figure 5.29 Acoustic Results for Liquid Oxygen at 90 K and 1 bar
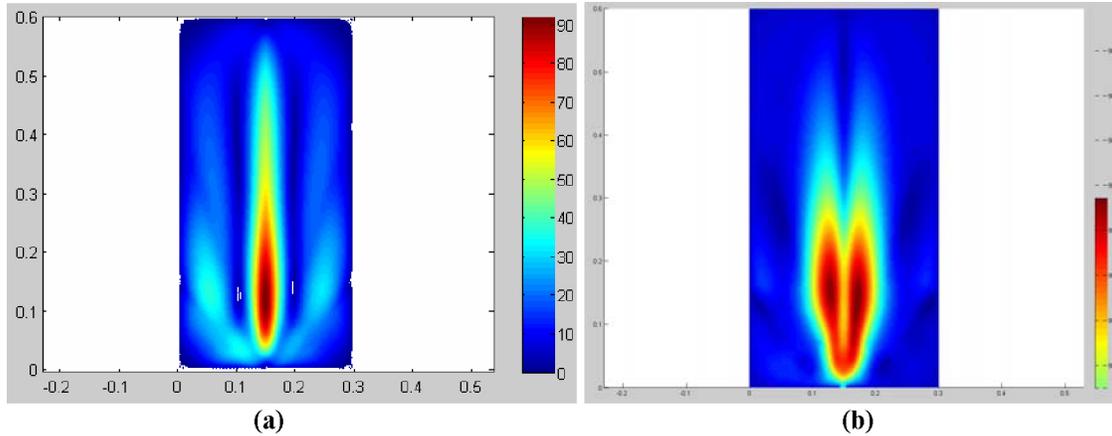
Figure 5.30 (a) Streaming and (b) Temperature Results for Liquid Oxygen at 90 K and 1 bar

For liquid oxygen, speeds are seen to be roughly two orders of magnitude greater than those for hydrogen and helium. Also, the temperature rise paths are seen to take a different form than for the other fluids, although the magnitudes are nearly negligible.

5.6.4 Comments on Computations for Cryogenic Fluids

The solutions for cryogenic liquids proved to be very difficult to obtain. Since the properties were vastly different from those of liquid water, adjustments had to be made in the code. In order to facilitate "accurate" results, the grid spacing were changed to 100 x-dimension cells and 200 z-dimension cells. This resulted in a total "ALM Program" convergence time of roughly an hour. Also, one interesting observation was that the Lighthill streaming formulation tended not to converge for the case of liquid oxygen. Therefore, the results presented were calculated using the Nyborg streaming formulation.

5.7 Effect of Property Value Variation on ALM

One final corollary investigated for this research of ALM was the influence of property variation on the calculated ALM results. In particular, solutions were calculated for varying values of the fluid viscosity, density, and attenuation terms. To obtain

solution sets, properties were adjusted one at a time prior to running the ALM Program.

The method used for analyzing property variation is highly oversimplified and

empirically unverifiable. For example, one cannot actually change viscosity and expect

density to remain the same, etc. However, in a general sense, to ascertain the effects of

density and viscosity on ALM results, each fluid property was independently modified

and computations performed. These variations were executed for water and both the

rectangular and disk transducers in a 20°C ambient for the experimental tank parameters

were considered. As with many of the previous computations, the 0.0254 meter by

0.0127 meter rectangular transducer was assumed to perform at a frequency of 1.63 MHz

while the 0.0254 meter diameter disk transducer was evaluated at 1.0 MHz. For

consistency, all results shown were calculated using the Lighthill formulation.

5.7.1 Viscosity Variation

Table 5.9 presents a result comparison for viscosity variation with the rectangular

transducer setup. The viscosity values for each successive calculation were increased by

a factor of two.

Table 5.9 Results of Viscosity Variation for Rectangular Transducer (Reference 0.0010015 kg/m-s)

Result	Maximum Value for Varied Viscosity			
	μ	$2\,\mu$	$4\,\mu$	$8\,\mu$
Pressure	173 dB	173 dB	173 dB	173 dB
Temperature Change	$2.05 \times (10)^{-10}$ K/s	$4.1 \times (10)^{-10}$ K/s	$8.19 \times (10)^{-10}$ K/s	$1.64 \times (10)^{-9}$ K/s
Body Force/Density	$6.83 \times (10)^{-8}$ m/s^2	$1.37 \times (10)^{-7}$ m/s^2	$2.73 \times (10)^{-7}$ m/s^2	$5.47 \times (10)^{-7}$ m/s^2
Force on Bubble	$3.56 \times (10)^{-5}$ N	$3.56 \times (10)^{-5}$ N	$3.56 \times (10)^{-5}$ N	$3.56 \times (10)^{-5}$ N
Magnitude	$9.800 \times (10)^{-6}$ m/s	$9.827 \times (10)^{-5}$ m/s	$9.839 \times (10)^{-6}$ m/s	$9.845 \times (10)^{-6}$ m/s
x-Velocity	$3.741 \times (10)^{-6}$ m/s	$3.780 \times (10)^{-6}$ m/s	$3.799 \times (10)^{-6}$ m/s	$3.809 \times (10)^{-6}$ m/s
z-Velocity	$9.800 \times (10)^{-6}$ m/s	$9.827 \times (10)^{-5}$ m/s	$9.839 \times (10)^{-6}$ m/s	$9.845 \times (10)^{-6}$ m/s
Temperature	293.212 K	293.176 K	293.163 K	293.156 K

The results show that for the range of viscosity increases examined, the temperature change, body force, and velocity tend to increase, while the overall fluid temperature decreases. However, the rates at which these values change are drastically different. Figure 5.31 shows plots for selected results.
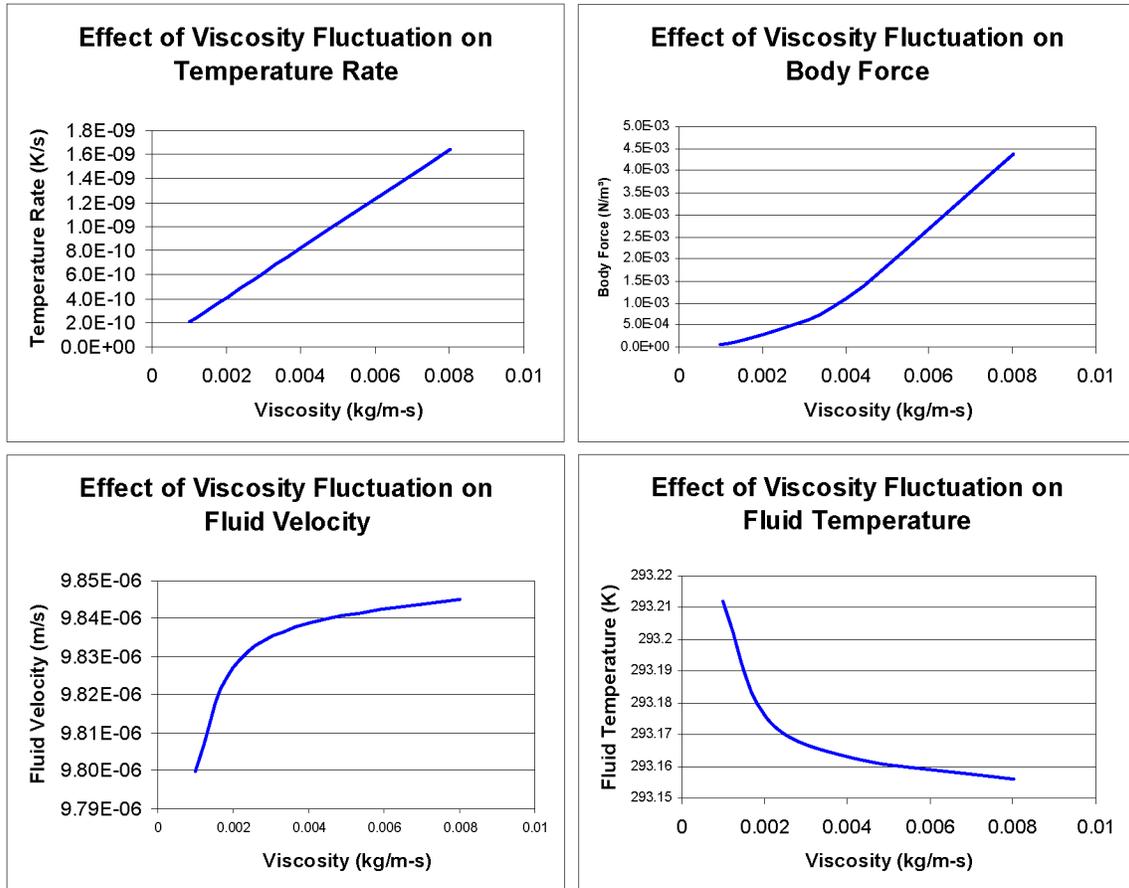
Figure 5.31 Effect of Viscosity Variation on ALM Results (Rectangular Transducer)

As can be seen in Figure 5.31, only temperature rate increases linearly. Viscosity

increases tend to increase the body force present within the fluid media at an ever faster-

growing pace. The fluid velocity also tends to increase, albeit with significant

exponential decay as the viscosity becomes larger. Finally, the fluid temperature actually

tends to decrease with increasing viscosity.

Table 5.10 and Figure 5.32 display the results of viscosity variation for the disk

transducer.

Table 5.10 Results of Viscosity Variation for Disk Transducer (Reference 0.0010015 kg/m-s)

Result	Maximum Value for Varied Viscosity			
	μ	2μ	4μ	8μ
Pressure	172 dB	172 dB	172 dB	172 dB
Temperature Change	$5.84 \times (10)^{-11}$ K/s	$1.17 \times (10)^{-10}$ K/s	$2.34 \times (10)^{-10}$ K/s	$4.67 \times (10)^{-10}$ K/s
Body Force/Density	$1.95 \times (10)^{-8}$ m/s²	$3.9 \times (10)^{-8}$ m/s²	$7.8 \times (10)^{-8}$ m/s²	$1.56 \times (10)^{-7}$ m/s²
Force on Bubble	$5.59 \times (10)^{-6}$ N	$5.59 \times (10)^{-6}$ N	$5.59 \times (10)^{-6}$ N	$5.59 \times (10)^{-6}$ N
Magnitude	$3.543 \times (10)^{-6}$ m/s	$3.546 \times (10)^{-6}$ m/s	$3.548 \times (10)^{-6}$ m/s	$3.549 \times (10)^{-6}$ m/s
x-Velocity	$1.082 \times (10)^{-6}$ m/s	$1.087 \times (10)^{-6}$ m/s	$1.089 \times (10)^{-6}$ m/s	$1.090 \times (10)^{-6}$ m/s
z-Velocity	$3.543 \times (10)^{-6}$ m/s	$3.546 \times (10)^{-6}$ m/s	$3.548 \times (10)^{-6}$ m/s	$3.549 \times (10)^{-6}$ m/s
Temperature	293.209 K	293.176 K	293.163 K	293.156 K
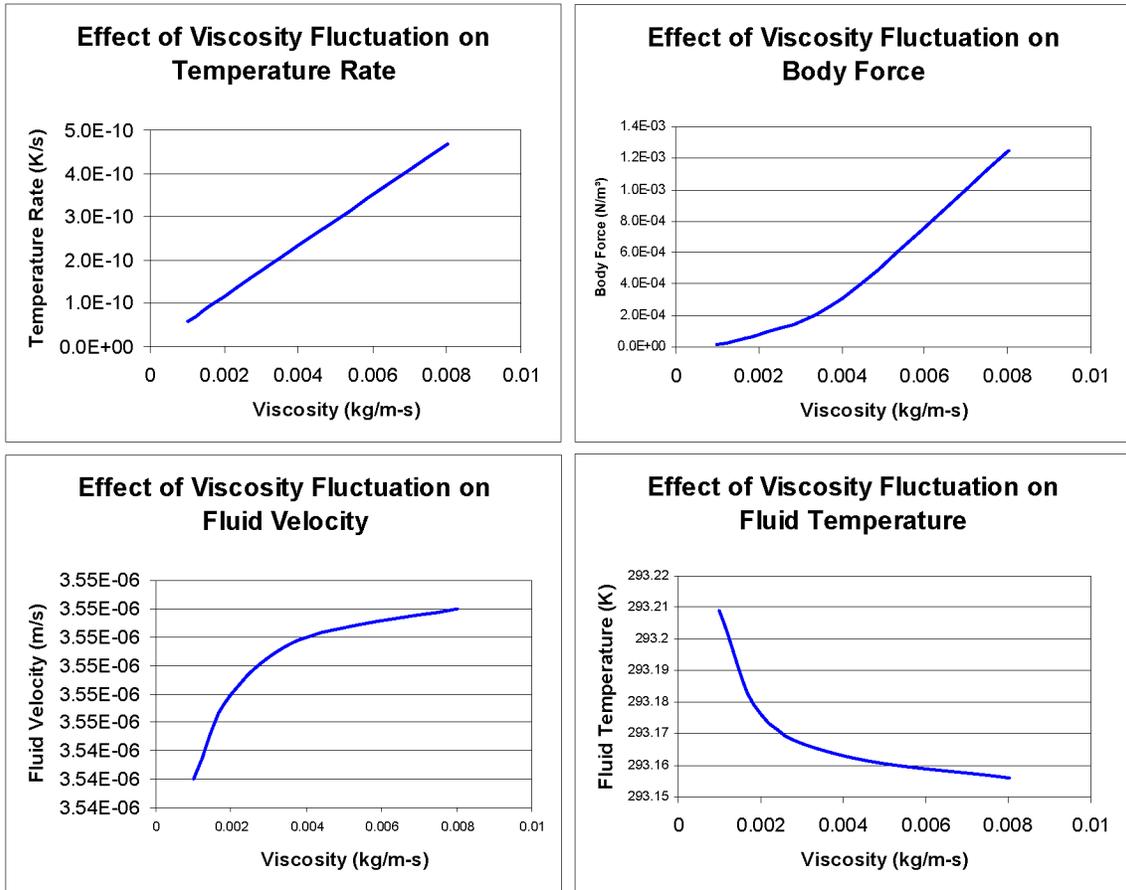
Figure 5.32 Effect of Viscosity Variation on ALM Results (Disk Transducer)

The same general trends are once again encountered here as for the rectangular transducer.

5.7.2 Density Variation

Table 5.11 gives results comparison for density variation with the rectangular transducer setup. As with viscosity, the density values for each successive calculation were increased by a factor of two.

Table 5.11 Results of Density Variation for Rectangular Transducer (Reference 1000 kg/m³)

Result	Maximum Value for Varied Viscosity			
	ρ	2ρ	4ρ	8ρ
Pressure	173 dB	173 dB	173 dB	173 dB
Temperature Change	$2.05 \times (10)^{-10}$ K/s	$2.56 \times (10)^{-11}$ K/s	$3.2 \times (10)^{-12}$ K/s	$4 \times (10)^{-13}$ K/s
Body Force/Density	$6.83 \times (10)^{-8}$ m/s²	$8.54 \times (10)^{-9}$ m/s²	$1.07 \times (10)^{-9}$ m/s²	$1.33 \times (10)^{-10}$ m/s²
Force on Bubble	$3.56 \times (10)^{-5}$ N	$1.19 \times (10)^{-5}$ N	$3.23 \times (10)^{-6}$ N	$8.22 \times (10)^{-7}$ N
Magnitude	$9.800 \times (10)^{-6}$ m/s	$2.457 \times (10)^{-6}$ m/s	$6.149 \times (10)^{-7}$ m/s	$1.538 \times (10)^{-7}$ m/s
x-Velocity	$3.741 \times (10)^{-6}$ m/s	$9.449 \times (10)^{-7}$ m/s	$2.3745 \times (10)^{-7}$ m/s	$5.952 \times (10)^{-8}$ m/s
z-Velocity	$9.800 \times (10)^{-6}$ m/s	$2.457 \times (10)^{-6}$ m/s	$6.149 \times (10)^{-7}$ m/s	$1.538 \times (10)^{-7}$ m/s
Temperature	293.212 K	293.210 K	293.209 K	293.209 K

As expected, an increase in overall mass tends to decrease the rate temperature change, body force per unit density, and velocity of the fluid. However, as with the increase in viscosity, an increase in density also tends to decrease the overall fluid temperature. These phenomena are quite visible in Figure 5.33.
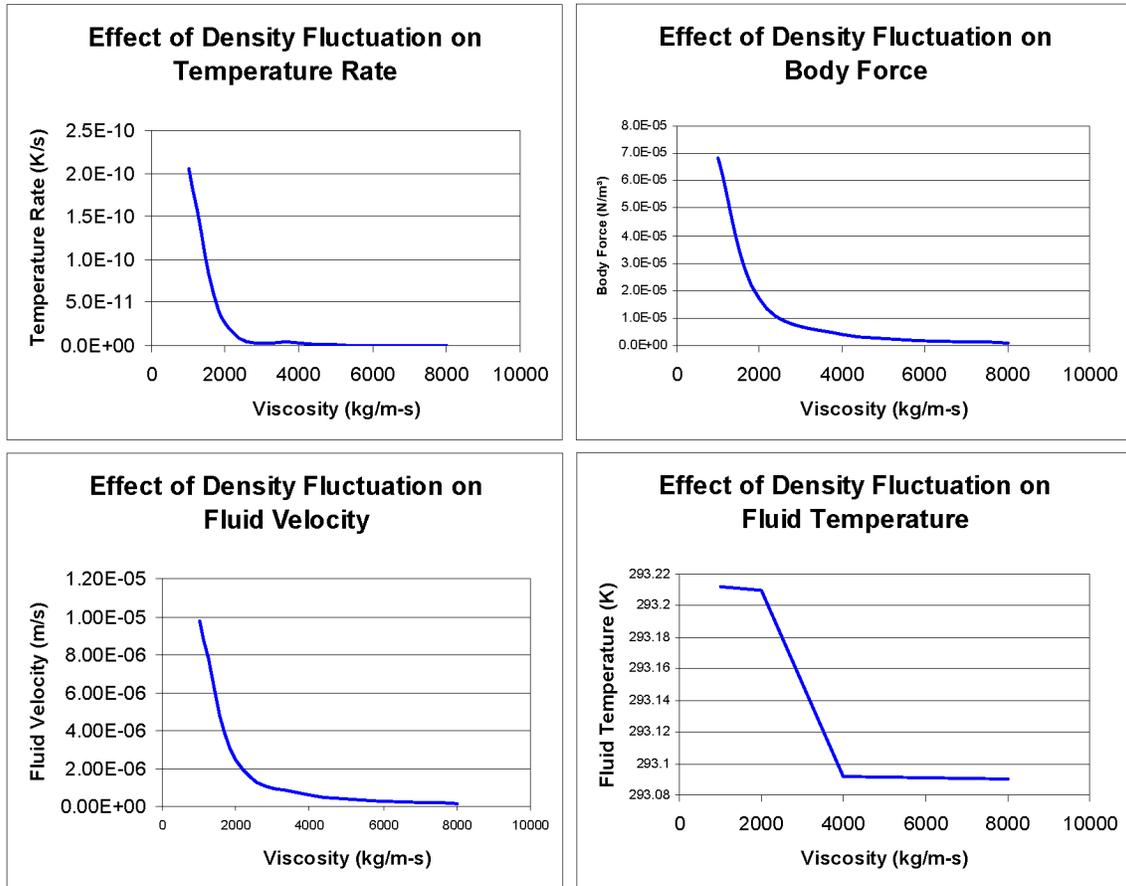
Figure 5.33 Effect of Density Variation on ALM Results (Rectangular Transducer)

Note that—for the most part—increasing the value of density has a completely different effect on ALM results from that seen with viscosity changes. This time, an initially rapid decrease is seen for temperature rise, body force, fluid velocity, and fluid temperature in the form of an initial sharp decrease in value followed by a decay in the decrease after density has doubled.

Table 5.12 shows the results of density variation for the disk transducer.

Table 5.12 Results of Density Variation for Disk Transducer (Reference 1000 kg/m³)

Result	Maximum Value for Varied Viscosity			
	ρ	2ρ	4ρ	8ρ
Pressure	172 dB	172 dB	172 dB	172 dB
Temperature Change	$5.84 \times (10)^{-11}$ K/s	$7.3 \times (10)^{-12}$ K/s	$9.12 \times (10)^{-13}$ K/s	$1.14 \times (10)^{-13}$ K/s
Body Force/Density	$1.95 \times (10)^{-8}$ m/s²	$2.44 \times (10)^{-9}$ m/s²	$3.05 \times (10)^{-10}$ m/s²	$3.81 \times (10)^{-11}$ m/s²
Force on Bubble	$5.59 \times (10)^{-6}$ N	$1.42 \times (10)^{-6}$ N	$3.55 \times (10)^{-7}$ N	$8.86 \times (10)^{-8}$ N
Magnitude	$3.543 \times (10)^{-6}$ m/s	$8.865 \times (10)^{-7}$ m/s	$2.217 \times (10)^{-7}$ m/s	$5.545 \times (10)^{-8}$ m/s
x-Velocity	$1.082 \times (10)^{-6}$ m/s	$2.717 \times (10)^{-7}$ m/s	$6.807 \times (10)^{-8}$ m/s	$1.704 \times (10)^{-8}$ m/s
z-Velocity	$3.543 \times (10)^{-6}$ m/s	$8.865 \times (10)^{-7}$ m/s	$2.217 \times (10)^{-7}$ m/s	$5.545 \times (10)^{-8}$ m/s
Temperature	293.209 K	293.209 K	293.209 K	293.209 K

Again, results were similar to those obtained for the rectangular transducer setup, except that the fluid temperature showed no discernible change for the different density values investigated. The various phenomena calculated are plotted in Figure 5.34.
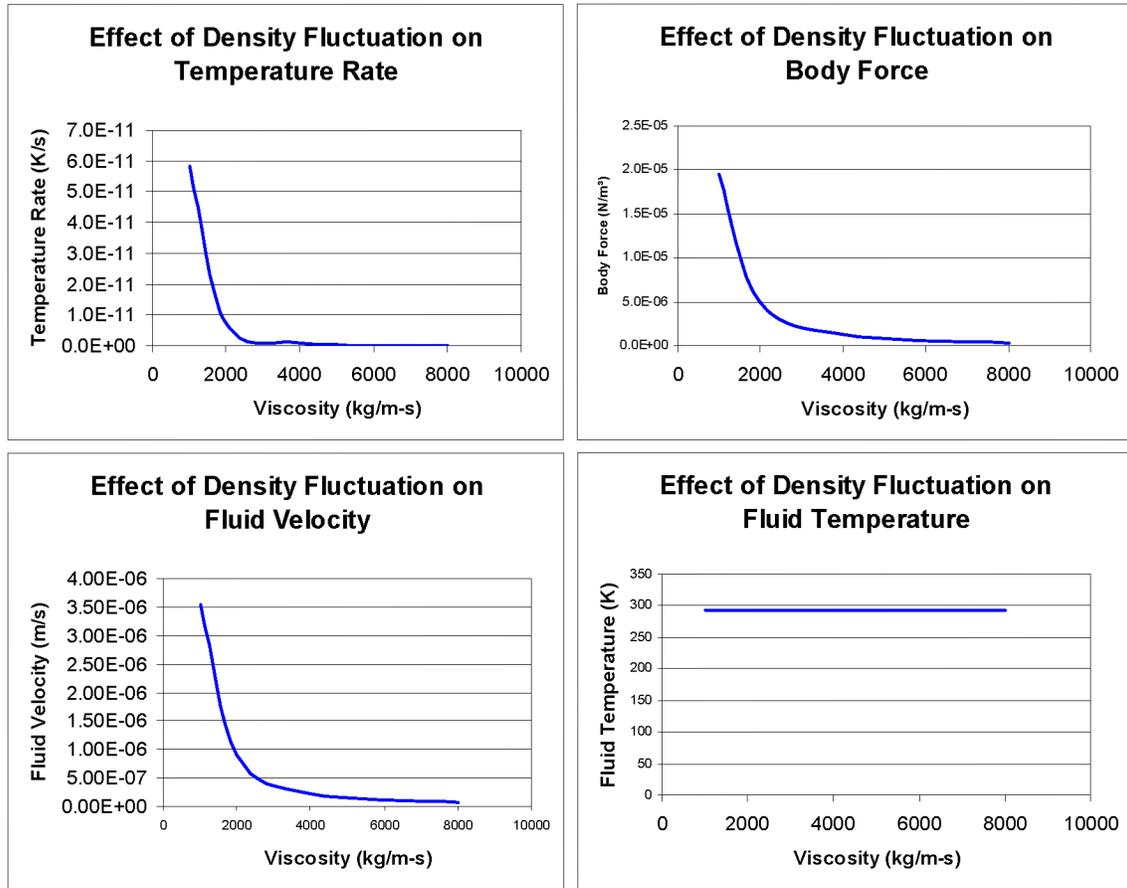
Figure 5.34 Effect of Density Variation on ALM Results (Disk Transducer)

In addition, comparisons for property variation were made between the Nyborg and Lighthill streaming formulations. These are presented in Table 5.10, Table 5.11, and Table 5.12 for 8x increases in density, viscosity, and both density and viscosity for the rectangular transducer.

Table 5.13 Results of Comparison Between Nyborg and Lighthill Streaming Formulations for 8x Increased Density (Rectangular Transducer)

Result	Maximum Value	
	Nyborg Formulation	**Lighthill Formulation**
Magnitude	$1.539 \times (10)^{-5}$ m/s	$1.538 \times (10)^{-7}$ m/s
x-Velocity	$5.967 \times (10)^{-6}$ m/s	$1.1871 \times (10)^{-8}$ m/s
z-Velocity	$1.539 \times (10)^{-5}$ m/s	$1.538 \times (10)^{-7}$ m/s
Temperature	293.209 K	293.209 K

F

Table 5.14 Results of Comparison Between Nyborg and Lighthill Streaming Formulations for 8x Increased Viscosity (Rectangular Transducer)

Result	Maximum Value	
	Nyborg Formulation	**Lighthill Formulation**
Magnitude	$9.851 \times (10)^{-6}$ m/s	$9.845 \times (10)^{-6}$ m/s
x-Velocity	$3.819 \times (10)^{-6}$ m/s	$3.809 \times (10)^{-6}$ m/s
z-Velocity	$9.851 \times (10)^{-6}$ m/s	$9.845 \times (10)^{-6}$ m/s
Temperature	293.156 K	293.156 K

As with the case where density was greatly increased, when viscosity increases the velocity is seen to be slightly larger with the Nyborg formulation.

Table 5.15 Results of Comparison Between Nyborg and Lighthill Streaming Formulations for 8x Increased Density and Viscosity (Rectangular Transducer)

Result	Maximum Value	
	Nyborg Formulation	**Lighthill Formulation**
Magnitude	$1.539 \times (10)^{-7}$ m/s	$1.539 \times (10)^{-7}$ m/s
x-Velocity	$5.967 \times (10)^{-8}$ m/s	$5.965 \times (10)^{-7}$ m/s
z-Velocity	$1.539 \times (10)^{-7}$ m/s	$1.539 \times (10)^{-7}$ m/s
Temperature	293.156 K	293.156 K

Note that now that both property values have increased, virtually no difference is seen between the Nyborg and Lighthill formulations.

5.7.3 Attenuation Variation

The final parameter varied for this thesis was the attenuation coefficient. The attenuation coefficient was varied (independently of other parameters, such as viscosity and density) in order to determine the effect on ALM results, particularly the velocity solution. Table 5.16 gives the ALM maximum results for attenuation coefficients varying from 0.001α to 1000α for the rectangular transducer.

Table 5.16 Effect of Variation in Attenuation Coefficient on ALM Results for Rectangular Transducer (Reference 0.0213 m^{-1})

Result	Maximum Value for Varied Attenuation Coefficient						
	$0.001\,\alpha$	$0.01\,\alpha$	0.1α	α	10α	100α	1000α
Pressure	173 dB	173 dB	173 dB	173 dB	173 dB	173 dB	173 dB
Temperature Change	2.05 x $(10)^{-13}$ K/s	2.05 x $(10)^{-12}$ K/s	2.05 x $(10)^{-11}$ K/s	2.05 x $(10)^{-10}$ K/s	2.05 x $(10)^{-9}$ K/s	2.05 x $(10)^{-8}$ K/s	2.05 x $(10)^{-7}$ K/s
Body Force/Density	6.83 x $(10)^{-11}$ m/s^2	6.83 x $(10)^{-10}$ m/s^2	6.83 x $(10)^{-9}$ m/s^2	6.83 x $(10)^{-8}$ m/s^2	6.83 x $(10)^{-7}$ m/s^2	6.83 x $(10)^{-6}$ m/s^2	6.83 x $(10)^{-5}$ m/s^2
Force on Bubble	3.56 x $(10)^{-5}$ N	3.56 x $(10)^{-5}$ N	3.56 x $(10)^{-5}$ N	3.56 x $(10)^{-5}$ N	3.56 x $(10)^{-5}$ N	3.56 x $(10)^{-5}$ N	3.56 x $(10)^{-5}$ N
Magnitude	9.851 x $(10)^{-9}$ m/s	9.851 x $(10)^{-8}$ m/s	9.846 x $(10)^{-7}$ m/s	9.800 x $(10)^{-6}$ m/s	9.141 x $(10)^{-5}$ m/s	4.719 x $(10)^{-4}$ m/s	Did Not Converge
x-Velocity	3.819 x $(10)^{-9}$ m/s	3.818 x $(10)^{-8}$ m/s	3.811 x $(10)^{-7}$ m/s	3.741 x $(10)^{-6}$ m/s	3.095 x $(10)^{-5}$ m/s	3.887 x $(10)^{-4}$ m/s	Did Not Converge
z-Velocity	9.851 x $(10)^{-9}$ m/s	9.851 x $(10)^{-8}$ m/s	9.846 x $(10)^{-7}$ m/s	9.800 x $(10)^{-6}$ m/s	9.141 x $(10)^{-5}$ m/s	4.546 x $(10)^{-4}$ m/s	Did Not Converge
Temperature	293.196 K	293.196 K	293.196 K	293.212 K	293.229 K	Did Not Converge	Did Not Converge

Figure 5.35 plots the results shown in Table 5.16.
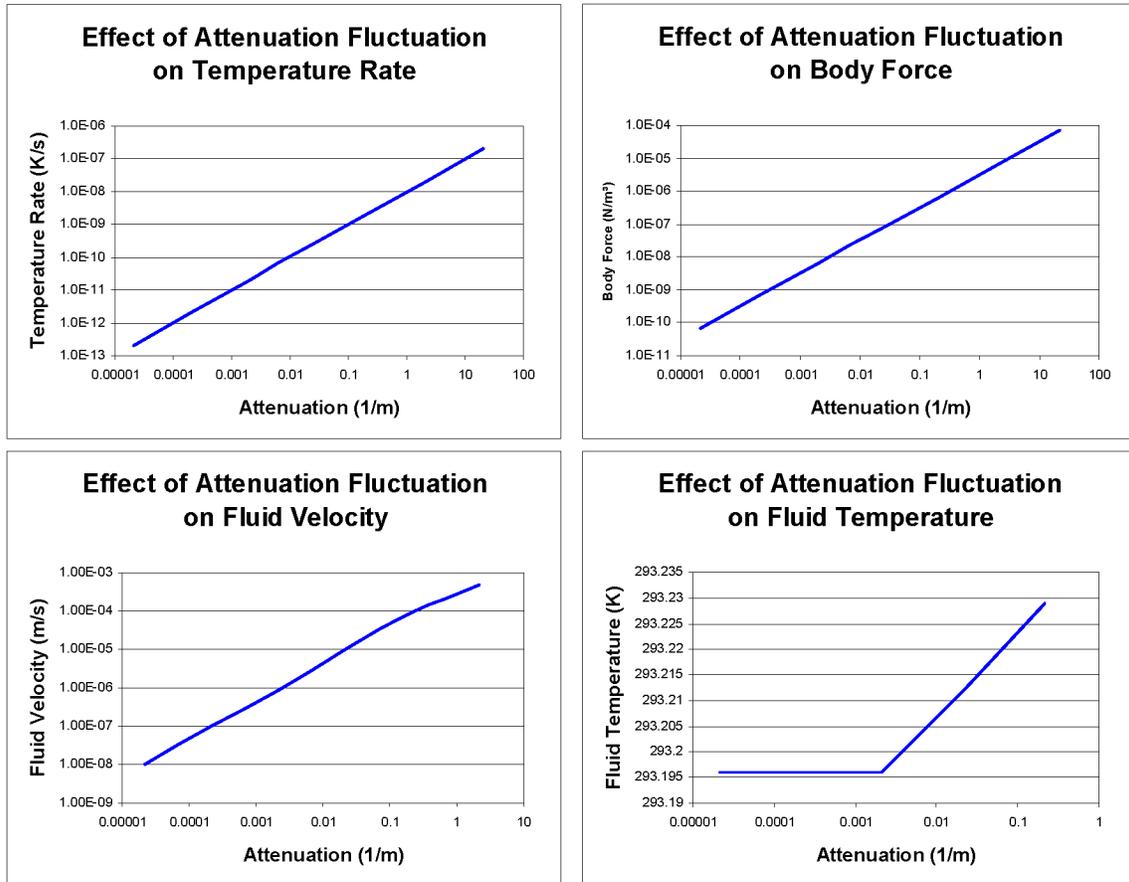
Figure 5.35 Effect of Attenuation Fluctuation on ALM Results (Rectangular Transducer)

As can be seen from the data, attenuation fluctuation tends to cause a linear increase in temperature rate and body force, and velocity. For fluid temperature, the increase also appears to be somewhat linear. However, the first few data points show negligible change, rather constant temperature.

Results for the disk transducer are presented in Table 5.17 and Figure 5.36.

Table 5.17 Effect of Variation in Attenuation Coefficient on ALM Results for Disk Transducer (Reference 0.0213 m^{-1})

| Result	Maximum Value for Varied Attenuation Coefficient						
	0.001 α	0.01 α	0.1α	α	10α	100α	1000α
Pressure	172 dB	172 dB	172 dB	172 dB	172 dB	172 dB	172 dB
Temperature Change	5.84 x (10)$^{-14}$ K/s	5.84 x (10)$^{-13}$ K/s	5.84 x (10)$^{-12}$ K/s	5.84 x (10)$^{-11}$ K/s	5.84 x (10)$^{-10}$ K/s	5.84 x (10)$^{-9}$ K/s	5.84 x (10)$^{-8}$ K/s
Body Force/Density	1.95 x (10)$^{-11}$ m/s^2	1.95 x (10)$^{-10}$ m/s^2	1.95 x (10)$^{-9}$ m/s^2	1.95 x (10)$^{-8}$ m/s^2	1.95 x (10)$^{-7}$ m/s^2	1.95 x (10)$^{-6}$ m/s^2	1.95 x (10)$^{-5}$ m/s^2
Force on Bubble	5.59 x (10)$^{-6}$ N	5.59 x (10)$^{-6}$ N	5.59 x (10)$^{-6}$ N	5.59 x (10)$^{-6}$ N	5.59 x (10)$^{-6}$ N	5.59 x (10)$^{-6}$ N	5.59 x (10)$^{-6}$ N
Magnitude	3.549 x (10)$^{-9}$ m/s	3.549 x (10)$^{-8}$ m/s	3.549 x (10)$^{-7}$ m/s	3.543 x (10)$^{-6}$ m/s	3.484 x (10)$^{-5}$ m/s	2.251 x (10)$^{-4}$ m/s	Did Not Converge
x-Velocity	1.092 x (10)$^{-9}$ m/s	1.091 x (10)$^{-8}$ m/s	1.091 x (10)$^{-7}$ m/s	1.082 x (10)$^{-6}$ m/s	9.959 x (10)$^{-6}$ m/s	1.592 x (10)$^{-4}$ m/s	Did Not Converge
z-Velocity	3.549 x (10)$^{-9}$ m/s	3.549 x (10)$^{-8}$ m/s	3.549 x (10)$^{-7}$ m/s	3.543 x (10)$^{-6}$ m/s	3.484 x (10)$^{-5}$ m/s	2.200 x (10)$^{-4}$ m/s	Did Not Converge
Temperature	293.196 K	293.196 K	293.196 K	293.196 K	293.197 K	Did Not Converge	Did Not Converge
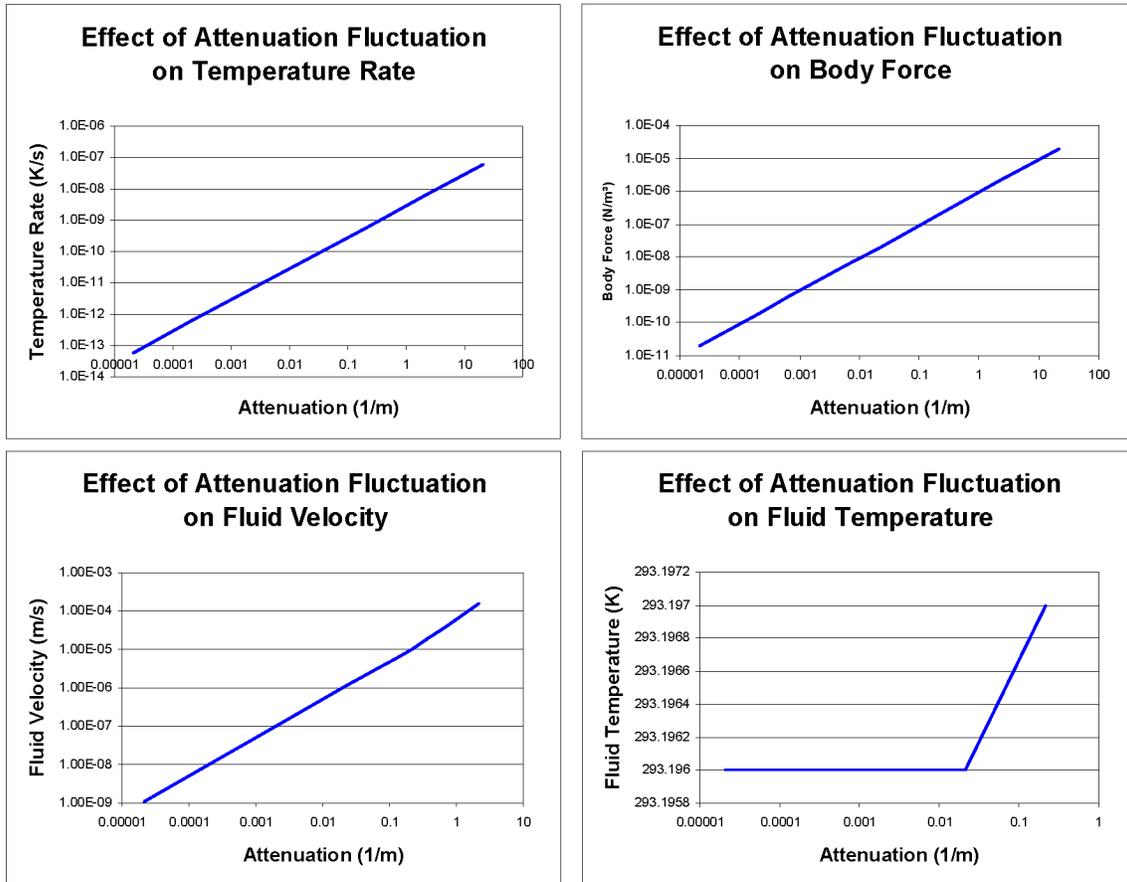
Figure 5.36 Effect of Attenuation Fluctuation on ALM Results (Disk Transducer)

As can be seen from the data, attenuation fluctuation results in similar patterns for temperature rate, body force, and fluid velocity. However, the overall fluid temperature appears to increase nearly linearly with an increase in temperature

CHAPTER 6. CONCLUSIONS

As stated in the opening words of this thesis, the primary objective for performing this study of ALM effects was to develop a CFD model which would predict the steady streaming velocity and temperature of a fluid field due to the effects of nonlinear sound. The work undertaken for this study has served as only one piece of a larger study by Iowa State University in conjunction with NASA Glenn Laboratory and has been primarily built around the acoustic models developed by Richard Oeftering of NASA, Dr. Adin Mann of Iowa State University, and the Master's thesis of LeAnn Faidley. In addition, prior studies of steady streaming by leading academics such as Nyborg, Lighthill, Riley, and countless others were called upon for insight into the mechanisms through which ALM is realized and can be modeled.

CHAPTER 2 began with a presentation of ALM theory previously developed by Faidley (2001) and Mann et al. (2005). This included relations for the sound pressure, force on a buoyant object (specifically, on a bubble), streaming body force, and rate of change in temperature—all due to high-frequency, nonlinear sound. This prior groundwork laid the foundation for the development of a streaming model based on the Navier-Stokes equations. Models based on two different assumptions were posited and explained. The final model chosen for subsequent CFD code development (except for the case of cryogenic fluids) was based on what has been referred to in this paper as the "Lighthill streaming formulation." The method employed by Sir James Lighthill in his Journal of Sound and Vibration Article entitled simply "Acoustic Streaming" (1978) and implemented in the present study employed a time-averaged Reynolds stress, which was subtracted from the viscous side of the Navier-Stokes equations. In contrast, the "Nyborg

Streaming Formulation" broke all components of the fluid equations into terms of like order and concluded that the streaming body force can basically be approximated as a second-order convection relation (again, a time-averaged Reynolds stress) composed of first-order velocity terms. Regardless of the formulation philosophy, the resultant forms of the Navier-Stokes equations derived were transformed into an appropriate form of the vorticity transport equation. This allowed the two "vector" equations—the x- and z-expressions of the conservation of momentum equation—to be combined into one equation, which later simplified implementation of the CFD code.

In addition to the vorticity transport equation, a tailored energy equation was derived and utilized the temperature change term presented by Mann et al. (2005). The energy equation relied upon a mix of terms, which included the stream function and vorticity.

Due to its simplicity of implementation, the finite difference method of solution for partial differential equations was chosen and implemented as explained in CHAPTER 3. The methodology utilized was based on a five-point grid which was broken into cells of Δx width by Δz length. A presentation using a generic variable, $g(x)$, was given to outline the Taylor series expansions used to formulate terms for first and second derivatives, as well as mixed second derivatives of a variable. Once this was accomplished, the Nyborg and Lighthill versions of the vorticity transport equations—as well as the energy equation—were transformed using appropriate numerical approximations.

CHAPTER 4 briefly described the "ALM Program" which was further developed from earlier versions created by Dr. Mann. The primary function of the Matlab® code

was to allow an ALM investigator to calculate the effects of ALM for simple geometries while allowing the selection or designation of various fluid properties, transducer specifications, and tank geometries. The "ALM Program" was designed to include a built-in fluid property selector and file save function, as well as functions by which the sound, fluid, and temperature solutions are implemented. The CFD code developed by this study was integrated into the latest version of "ALM Program" to allow the user simple access to flow and temperature field predictions.

CHAPTER 5 commenced with a presentation and comparison of simulation data with empirical test data. The experimental setup designed and results obtained at Iowa State University and presented in "Analytical/Numerical Model of Fluid Phenomena Created by High Intensity Sound" (Mann et al., 2005) were drawn upon for a comparison of the CFD model with measured data. In addition to comparisons with the experimental data, a number of unverified situations were explored in order to examine the effects of changes in the model. For example, a set of calculations were performed in order to discern any differences in results between the Nyborg and Lighthill streaming methods. In addition, various solution sets were calculated to determine the general nature of fluid flows for low-temperature liquids, such as would be utilized in microgravity environments (hydrogen, oxygen, etc.). Finally, the effects of viscosity and subsequently density changes on the different ALM phenomena were predicted using the "ALM Program."

A number of interesting observations and conclusions were noted throughout the model development process and data comparison. These are explained in section 6.1.

The final section of this thesis—6.2—posits a number of areas which might be explored in order to fine tune the model and overall streaming research.

6.1 Discussion of Simulated and Experimental of Results

A summary discussion of the results and conclusions arising from the data presented in CHAPTER 5 is presented in this section.

6.1.1 Comparison Between Empirical and Computational Flow

As with any computational endeavor, correlation with experimental data not only validates or invalidates a mathematical model, but it also allows the researcher insight into the subtle and not-so-subtle errors inherent within the methodologies used. This thesis was no exception. As will be explained during the remainder of this section, many discrepancies and similarities were discovered when comparing and contrasting the empirical and computational results.

6.1.1.1 Velocity Magnitude Discrepancy

One very noteworthy and disappointing result found with the computational results of this study was the extremely low magnitude of velocity the CFD code calculated. Although the flow fields found with the CFD solutions were fairly close to those seen experimentally, the magnitudes calculated were oftentimes two to three orders of magnitude smaller than those measured with the PIV system. Also seen through array calculations were velocity predictions in the order of 10^{-11} to 10^{-12} m/s. Although many hours were spent investigating several possible causes, this discrepancy has not yet been pinpointed. However, one primary parameter was found to affect the magnitude of

velocity. As the attenuation coefficient was increased, the computed velocities were seen to increase. In section 5.7.3, plots were created for the effects of attenuation variation on maximum velocity magnitude. The data showed a fairly linear relationship between the attenuation coefficient and velocity. As such, an attempt was made to quantify this relationship. The resulting equations for the rectangular and disk transducers are as follows (where U is the magnitude of velocity and α is the attenuation coefficient).

- **Rectangular Transducer**

$$U = 0.00045\alpha \qquad\qquad (6.1)$$

- **Disk Transducer**

$$U = 0.00016\alpha \qquad\qquad (6.2)$$

The implications of these results are that, for the rectangular transducer, a magnitude of attenuation which would give a calculated result approximately the same value as the empirical data—0.74 mm/s—would be 1.6 m^{-1}, while an attenuation value of approximately 19 m^{-1} would be required to give a calculated velocity for the disk transducer of nearly

3 mm/s, which was found experimentally. Since drastically different values for attenuation appear to be required when looking at the rectangular transducer versus the disk transducer, the likelihood that modification of the attenuation coefficient alone would cause the accuracy of the flow solution to increase is minimal. However, one must consider that fluctuation of this parameter has a significant effect on the streaming results.

6.1.1.2 Flow Patterns

One very encouraging observation of the fluid velocity calculations was that the flow fields tended to look very similar for the CFD and experimental results. In particular, the experimental results tended to validate the flow patterns predicted by the code for the disk transducer. As mentioned by Mann et al. (2005), the slight differences in the flow patterns may be due to the fact that the experimental setup was not perfectly symmetrical.

6.1.2 Nyborg vs. Lighthill Streaming Formulations

For the case of water in room temperature, the Nyborg and Lighthill streaming formulations provided nearly identical results when computed using the developed CFD code, showing less than four percent variation. However, for other calculations, the choice of formulation was critical to convergence of a solution (although convergence is not necessarily an indicator of accuracy). For example, the simulation run with liquid oxygen as the fluid did not converge for the Lighthill streaming implementation of the CFD code but did provide a flow field of similar pattern to that for water at room temperature when computed with the Nyborg streaming philosophy. Obviously, much work needs to be done to determine the appropriateness and validity of each formulation for each situation in which a velocity field calculation is desired. In addition, more experimental work needs to be performed with various fluids over various temperature ranges to compare both methods with empirical data to discern the applicability and limitations of each method.

6.1.3 Cryogenic Fluids

One extremely interesting investigation produced highly unpredicted results. When examining the computational flow fields for cryogenic fluids, the outcome appeared to be opposite that for water at room temperature. Whereas the aqueous calculations produced extremely low flow rates (on the order of 10^{-4} to 10^{-6} m/s), the cryogenic fluid calculations showed flow speeds on the order of 10^{0} to 10^{2} m/s.

6.1.4 Fluid Property Variation

Another facet of the ALM code studied was a qualitative analysis of property variation effects on ALM phenomena. For this portion of the study, the effects of density and viscosity variation were independently examined for the case of water at room temperature. The results showed that an increase in viscosity tended to increase the temperature rate and body force, and fluid viscosity while decreasing the overall fluid temperature. In addition, increasing the fluid density tended to decrease all four results. While the methodology employed produced mythical results (i.e., property variation almost always occurs for more than one property at a time), the results indicate that general preliminary analysis could be performed and compared with water when selecting a fluid to undergo ALM effects.

6.1.5 Temperature Results Discussion

An interesting result of the CFD calculations was that almost no thermal effect was seen within the fluid due to nonlinear sound. This was also true for the simple measurements taken in the laboratory.

One possibility for the low values, however, is that the extremely low velocities calculated for the tank resulted in an extremely low temperature profile due to little viscous heat dissipation. The validity of the temperature results needs to be evaluated in light of the velocity results since the temperature calculations directly depend on the outcome of the flow field calculations.

6.2 Future Work

Since this thesis was focused first and foremost on the CFD calculations of ALM phenomena with the assumption that the sound pressure and fluid body force/density theory has matured, the recommendations provided herein are primarily directed toward improvements to the fluid and heat transfer theory and code. With that in mind, much headway has yet to be made to strengthen the CFD code developed for the ALM program. Investigations into such improvements as grid refinements, irregular meshing, and simulations using commercial CFD codes are warranted and are briefly discussed in this section.

6.2.1 Bulk Viscosity and Incompressibility

During model development, the incompressibility argument eliminated the bulk viscosity term from the Navier-Stokes equations. As a result (perhaps incorrectly), this fluid property was left from consideration during the entire model development. However, according to Tannehill et al. (1997) and Schlichting and Gersten (2000), the bulk viscosity is often considered when sound absorption is present. Pierce (1981) gives the following form of the attenuation coefficient, which considers bulk viscosity:

$$\alpha' = \frac{\omega^2 \mu}{2\rho c^3} \left[\frac{4}{3} + \frac{\mu_B}{\mu} + \frac{(\gamma - 1)}{\mathrm{Pr}} \right], \tag{6.3}$$

where ω is the circular frequency of the sound, m is the fluid viscosity, μ_B is the fluid bulk viscosity, γ is the specific heat ratio of the fluid, Pr is the Prandtl number of the fluid, ρ is the fluid density, and c is the speed of sound through the fluid medium. Since the bulk viscosity would only increase the attenuation coefficient, one can observe from Figure 5.35 or Figure 5.36 that the velocity will correspondingly increase. Future work should include the bulk viscosity term with the attenuation coefficient for comparison with the model presented in this thesis.

In addition, a model which utilizes compressibility should be developed for evaluation. Such a model would prove to be more complex and would include the bulk viscosity term, as well as the stream function developed in section 2.3.2.2.2.

6.2.2 CFD Code Improvements

A number of options should be explored for CFD code improvement, working both within and outside of the assumption framework set for this investigation into the ALM phenomenon. A subset of these is talked about in the following paragraphs.

6.2.2.1 Convergence Improvements

Convergence parameters for the CFD solution were chosen rather arbitrarily, as can be seen in the discussion of equation discretization in CHAPTER 3. The Navier-Stokes equations developed were steady-state, and thus fall into the classification of "equilibrium problems." As such, the method chosen for computations was iterative (or "relaxation"). However, only the basic form of the discretized equations was used. One

improvement to the convergence of the code would be to use the successive

overrelaxation (SOR) method. As Tannehill et al. (1997) show, an arbitrary correction

could be made to the calculated velocity value between iterations as follows:

$$u_{i,k}{}^{(l+1)'} = u_{i,k}{}^{l'} + \chi\left(u_{i,k}{}^{l+1} - u_{i,k}{}^{l'}\right), \qquad (6.4)$$

where $u_{i,k}{}^{l'}$ is the corrected velocity for the previous iteration, $u_{i,k}{}^{l+1}$ is the calculated

velocity for the current iteration, and $u_{i,k}{}^{(l+1)'}$ is the corrected velocity for the current

iteration. Note that when $\chi = 1$, the calculated and corrected velocity terms for the

current iteration are the same, thus giving a SOR solution for this case an identical value

as that for the original code developed in CHAPTER 3.

Since the fluid tank under study is for a rectangular geometry and Dirichlet

boundary conditions are applied, the following calculations can be made to find the

optimal value for χ:

$$\sigma = \frac{1}{1 + (\Delta x / \Delta z)^2} \left[\cos\left(\frac{\pi}{p}\right) + (\Delta x / \Delta z)^2 \cos\left(\frac{\pi}{q}\right) \right] \qquad (6.5)$$

and

$$\chi_{OPTIMUM}\, \frac{2}{1 + \left(1 - \sigma^2\right)^{1/2}} \qquad (6.6)$$

where Δx is the grid size in the x-direction, Δz is the grid size in the z-direction, p is the

number of grid spacing in the x-direction, and q is the number of grid spacing in the z-

direction. Utilizing the SOR method could drastically improve the computational time—

Tannehill et al. (1997) claim that convergence times have even been reduced by over

thirty times.

While other methodologies, such as coloring schemes, block-iterative methods, alternating direction implicit (ADI) methods could be employed (Tannehill et al., 1997), the simplicity of the SOR scheme should accompany a first-choice decision to reduce the computational time of the CFD code.

6.2.2.2 Mesh Improvements

Another area for which improvements could be sought is in the area of grid generation and meshing. A number of different areas could be explored for improving the mesh over which the ALM computations are performed, such as implementing alternatives to the five-point finite differencing formula and utilization of irregular meshes.

6.2.2.2.1 Nine-Point Formula

One potential solution for improving the accuracy of the CFD calculations is to use a nine-point formulation based on the grid shown in Figure 6.1.
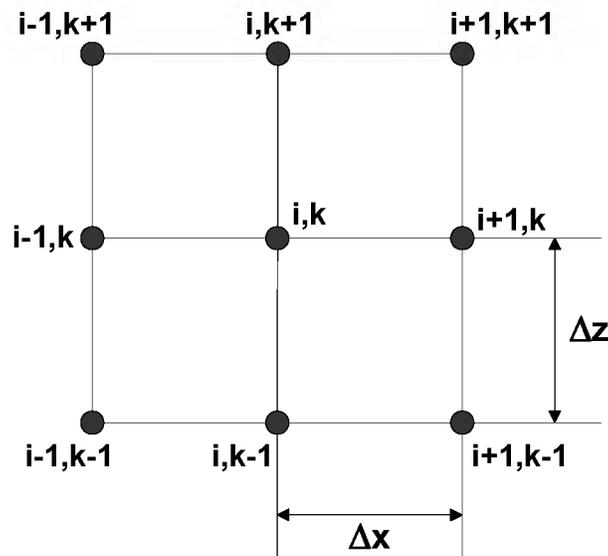

Figure 6.1 Grid for Nine-Point Formulation

Beginning with fourth-order Taylor series and utilizing methods similar to those employed in section 3.1, the following value for the stream function is derived (see Li, Tang, & Fornberg, 1995, or Lynch and Rice, 1978, for a starting point):

$$
\psi_{i,j} = \left[\frac{1}{(\Delta x)^2} + \frac{1}{(\Delta x)^2}\right] \frac{\left(8\zeta_{i,j} + \zeta_{i+1,j} + \zeta_{i-1,j} + \zeta_{i,j+1} + \zeta_{i,j-1}\right)}{20}
$$
$$
+ \left[\frac{-(\Delta x)^2 + 5(\Delta z)^2}{(\Delta x)^2 + (\Delta z)^2}\right] \frac{\left(\psi_{i+1,j} + \psi_{i-1,j}\right)}{10}
$$
$$
+ \left[\frac{5(\Delta x)^2 - (\Delta z)^2}{(\Delta x)^2 + (\Delta z)^2}\right] \frac{\left(\psi_{i,j+1} + \psi_{i,j-1}\right)}{10}
$$
$$
+ \frac{\left(\psi_{i+1,j+1} + \psi_{i-1,j+1} + \psi_{i+1,j-1} + \psi_{i-1,j-1}\right)}{20}
$$

$$(6.7)$$

Although the equation utilized is derived using the fourth order, making it attractive as a more precise methodology, Tannehill et al. (1997) warn that it may not improve the accuracy of the result.

6.2.2.2.2 Irregular Mesh Generation

Another possible improvement to the CFD code would be to implement an irregular mesh which would exploit a finer grid near the areas determined to have greater flow values, i.e., through the jet created by the sound transducer and near the tank boundaries. This would allow for an optimization of the number of equations required for calculating the velocity and temperature fields by creating coarse grid areas in the predicted regions of small values while increasing the granularity of the grid at the locations of interest. For the tank setup studied in this thesis, a structured grid scheme could be developed to realize optimal grid spacing. Tannehill et al. (1997) classify

structured grid generation methods into three categories: complex variable methods, algebraic methods, and differential equation methods.

In addition to creating an optimized number of equations, irregular meshes could be implemented in future codes to determine flow in irregularly-shaped structures, such as pipes, circular tanks, etc. These would likely be created using an unstructured grid strategy, such as point insertion schemes, advancing front methods, or domain composition methods (Tannehill et al., 1997).

6.2.2.3 Primitive Variable Approach

During the initial stages of CFD code development for ALM phenomena, a primitive variable approach was attempted and implemented. The resulting preliminary code was used to solve the two-dimensional lid-driven cavity problem. However, in order to reduce the number of equations for CFD calculation (and thus the computation time), this was abandoned for the vorticity-stream function approach presented in CHAPTER 2. Still, this philosophy for determining the streaming velocity and temperature solutions should be re-explored and compared with the vorticity transport methodology presented in this thesis.

6.2.2.4 Parameter Scaling

Another potential methodology for improving the CFD code lies with the scaling of Navier-Stokes parameters. The modeling tactic presented in the main body of this thesis assumed dimensional parameters. However, nondimensionalization may present opportunities to increase the accuracy of the code by allowing the parameters utilized to be similar in order of magnitude.

6.2.3 Commercial CFD Software

An alternative approach to improving the CFD solution of acoustic streaming (and one touched upon by Mann et al., 2005) is to explore the possibilities for inputting the streaming body force into a commercially-available numerical program, such as Fluent or ANSYS CFX, among others. This would minimize the risk of inaccuracies by allowing the acoustic streaming investigator to utilize an established CFD code with advanced meshing and convergence parameters. In addition, a commercial CFD code would allow the researcher to analyze streaming flow fields in three dimensions using complex geometries provided the acoustic streaming body force could be calculated for such a situation.

6.2.4 Further Experimentation

One undeniable result of this study is the find that much more experimentation is necessary to improve the ALM models. A number of improvements could be made to existing experiments, as well as additions of more experiments. The following suggestions for future experimental work are presented from the point of view of "what kind of testing would be useful for increasing the accuracy of the CFD code?"

- *A variety of fluids should be tested.* Initially, more experimentation should be performed with water. However, other Newtonian fluids, such as alcohol, should be measured for ALM effects. Performing these tests would allow a more comprehensive look into the discrepancies between the model and measured data and present greater opportunities for model correction.

- *Tests should be performed over a variety of conditions (temperature, ambient pressure).* Where practical, this should be performed for all the same reasons as testing a variety of fluids.

- *More precise temperature measurements should be made.* Equipment with tight tolerances regarding temperature measurements should be utilized to evaluate the flow field heat effects.

- *Experiments should be performed using transducer arrays.*

- *Tests should be performed with different tank geometries.*

- *Microgravity tests should be expanded.* The work of the Iowa State University undergraduate team consisting of May et al. (2003) proved interesting and useful but a greater variety of microgravity experiments should be designed.

- *Improvements on 2-dimensional setup.* If at all practicable, additional effort should be made to improve the tank setup such that all asymmetries and imperfections are minimized. This would allow for the CFD code to more accurately predict flow within the tank boundaries.

Although not comprehensive, the preceding list gives a number of suggestions which could be followed for enhancing the effectiveness of empirically testing ALM phenomena.

6.3 Closing Remarks

This study of ALM effects—particularly acoustic streaming—has proven to be an interesting topic. The area has many potential uses, such as enhanced fluid flow in microgravity, improvements in manufacturing processes (such as electroplating), and—in the author's opinion—enhanced convective heat transfer replacing complex mechanical

components (i.e., fans). It is the hope of the author that the topic of ALM receives much

more attention—not only in academia, as seems to be the case regarding the vast majority

of research discovered and cited within this thesis—but also in industry, where a strong

interest base could fully develop the usefulness of the phenomena.

REFERENCES

[1] Amari, M., Joly, N., & Gusev, V. (2003). *Acoustic streaming development in annular resonators.* Le Mans, France: Authors.

[2] Anderson, M. J., Budwig, R. S., Line, K. S., & Frankel, J. G. (2002). Use of acoustic radiation pressure to concentrate small particles in air flow, *2002 IEEE Ultrasonics Symposium* (pp. 481-484).

[3] Faidley, L. E (2001). *Thesis.*

[4] Hoffelner, J., Landes, H., & Lerch, R. Calculation of acoustic streaming velocity and radiation force based on finite element simulations of nonlinear wave propagation, *2000 IEEE Ultrasonics Symposium,* (pp. 585-588).

[5] Huang, J., Holt, R. G., Cleveland, R. O., and Roy, R. A. (2004). Experimental validation of a tractable numerical model for ultrasound heating in flow-through tissue phantoms. *Journal of the Acoustical Society of America,* 116 (4), 2451-2458.

[6] Incropera, F. P. & DeWitt, D. P. (2002). *Fundamentals of heat and mass transfer* (5th ed.). New York: John Wiley and Sons.

[7] Jenkins, D. A. (2003). Free surface shape for an ultrasonic nebuliser. *ANZIAM J44E* (pp. 464-478).

[8] Li, M., Tang, T., & Fornberg, B (1995). A compact fourth-order finite difference scheme for the steady incompressible Navier-Stokes equations. *International Journal for Numerical Methods in Fluids,* 20, 1137-1151.

[9] Lighthill, J. (1978). Acoustic streaming. *Journal of Sound and Vibration,* 61(2), 391-418.

[10]   Lynch, R. & Rice, J. (1978). High accuracy finite difference

approximation to solutions of elliptic partial differential equations. *Applied*

Mathematical Sciences, 75(6), 2541-2544.

[11]   Mann, J., Faidley, L, Morfeld, M, & Kopp, M. (2000). *Numerical model*

of the excess pressure created by a phased array for acoustic liquid manipulation.

Ames, IA: Iowa Space Grant Consortium.

[12]   Mann, J. (2003). *Analytical/numerical modeling of fluid phenomena*

created by high intensity sound: Research proposal to Rich Oeftering at the

National Aeronautics Space Administration Glenn Research Center. Ames, IA:

Author.

[13]   Mann, J., Clinkinbeard, N. Laage, J., Olsen, M., & Subramaniam, S.

(2005). *Analytical/numerical model of fluid phenomena created by high intensity*

sound. Ames, IA: Authors.

[14]   May, A., Clemens, J., Sullivan, T., White, A., Rehn, K., & Bernstein, J.

(2003). *Acoustic manipulation of bubbles in a fluid flow.* Ames, IA: Authors.

[15]   Mitome, H. (1990). Study of the generation mechanism of an acoustic jet

through visualization experiments, *Proceedings of 11th Symposium on Ultrasonic*

Electronics (60-62). Kyoto, Japan: Japanese Journal of Applied Physics.

[16]   Munson, B., Young, D., & Okiishi, T. (2002). *Fundamentals of fluid*

mechanics (4th ed.). New York: John Wiley and Sons.

[17]   Nightengale, K. & Trahey, G. E. (2000). A finite element model for

simulating acoustic streaming in cystic breast lesions with experimental validation.

IEEE Transactions on Ultrasonics, Ferroelectrics, and Frequency Control, 47(1), 210-215.

[18]   Nyborg, W. (1997). Acoustic streaming. In M. Hamilton and D. Blackstock, *Nonlinear Acoustics* (207-228). San Diego: Academic Press.

[19]   Oeftering, R. (1999). Acoustic liquid manipulation, *IEEE Ultrasonics Symposium* (675-678). Tahoe, NV: Caesars.

[20]   Oeftering, R., Chato D., & Mann, J. Liquid propellant manipulated acoustically. (2003). [On-line]. http://www.grc.nasa.gov/WWW/RT2002/7000/7715oeftering.html

[21]   Pierce, A. (1981). *Acoustics: An introduction to its physical principles and applications.* New York: McGraw-Hill.

[22]   Pereira, V. & Campos Silva, J. (2005). Simulations of incompressible fluid flows by a least squares finite element method. *Journal of the Brazilian Society of Mechanical Sciences and Engineering,* 27(3), 274-282.

[23]   Riley, N. (1998). Acoustic streaming. *Theoretical Computational Fluid Dynamics,* 10, 349-356.

[24]   Riley, N. (2001). Steady streaming. *Annual Review of Fluid Mechanics,* 33, 43-65.

[25]   Schlichting, H. & Gersten, K. (2000). *Boundary layer theory (8th ed.).* New York: Springer.

[26]   Tannehill, J., Anderson D., & Pletcher, R. (1997). *"Computational fluid mechanics and heat transfer (2nd ed.).* Philadelphia: Taylor and Francis.

[27]   Trinh, E. H. (1998). Acoustic streaming in microgravity: flow stability and heat transfer enhancement. *Microgravity Fluid Physics & Transport Phenomena Conference, 4th, Proceedings* (pp. 497-502). Cleveland.

[28]   Wan, Q. & Kuznetsov, A. *Numerical efficiency comparison of heat transfer enhancement between two parallel beam by acoustic streaming induced by standing and traveling waves.* Raleigh, NC: Authors.

[29]   Wan, Q. & Kuznetsov, A. (2003). Streaming in a channel bounded by an ultrasonically oscillating beam and its cooling efficiency. *Numerical Heat Transfer, Part A,* 45, 21-27.

[30]   Wang, T. (1997). Radiation pressure and acoustic levitation. In M. Hamilton and D. Blackstock, *Nonlinear Acoustics* (177-203). San Diego: Academic Press.

[31]   Yu, H. & Kim, E. S. (2003). Micropropulsion of air and liquid by acoustic streaming. *Proceedings IEEE Sixteenth Annual International Conference on Micro Electro Mechanical Systems* (pp. 76-79). Kyoto, Japan.

[32]   Yu, H. & Kim, E. S. (2004) Ultrasonic underwater thruster. *Proceedings of the Seventeenth IEEE International Conference on Micro Electro Mechanical Systems* (pp. 486-489). Maastricht, the Netherlands.

[33]   Zauhar, G., Starritt, S. A., & Duck, F. A. (1998). Studies of acoustic streaming in biological fluids with an ultrasound Doppler technique. *The British Journal of Radiology,* 71(843) 297-302.

[34]   Zhu, X., Zhao, X., & Du, G. (1998). Theory of acoustic streaming

generated by ultrasonic lamb waves. *Journal of the Acoustical Society of*

America, 104(1), 86-90.

[35]   Potters Industries, Incorporated. Sphe014el® hollow glass spheres. (2001).

[On-line]. Available: http://www.pottersbeads.com/markets/polySphericel.asp

[36]   WordReference.com. Radiation pressure. (2006). [On-line].

http://www.wordreference.com/definition/acoustic+radiation+pressure

BIOGRAPHICAL SKETCH

Nicholus Ryan Clinkinbeard was born July 20, 1978, in Des Moines, Iowa. He received the bachelor in science in Mechanical Engineering from Iowa State University in 2002 and expects to receive the Master of Science in Mechanical Engineering from Iowa State University in 2006. While pursuing his degrees at ISU, he served as a Research Assistant in the departments of Mechanical Engineering and Aerospace Engineering from 2002 to 2003. He worked for Rockwell Collins Government Systems Division in Cedar Rapids, Iowa, from 2000 to 2006—first as a Mechanical Engineering Cooperative Education student and subsequently as a Mechanical Engineer. He currently serves as Dynamicist in the Rockwell Collins Environmental Effects Engineering department.